2021

Laboratory Measurements of Bed Shear Stress in Open Channel Flow and Soil Erosion Rate in Cohesive Soils

Gunnar Schurmann Kern
South Dakota State University

LABORATORY MEASUREMENTS OF BED SHEAR STRESS IN OPEN CHANNEL FLOW AND SOIL EROISION RATE IN COHESIVE SOILS

By:

GUNNAR SCHURMANN KERN

A thesis submitted in partial fulfillment of the requirement for the

Master of Science

Major in Civil and Environmental Engineering

South Dakota State University

2021

THESIS ACCEPTANCE PAGE

Gunnar Kern

This thesis is approved as a creditable and independent investigation by a candidate for the master's degree and is acceptable for meeting the thesis requirements for this degree. Acceptance of this does not imply that the conclusions reached by the candidate are necessarily the conclusions of the major department.

Francis Ting
Advisor Date

Nadim Wehbe
Department Head Date

Nicole Lounsbery, PhD
Director, Graduate School Date

This thesis is dedicated to my grandfather, D. Patrick Kern, who has inspired me to pursue my dream of becoming an engineer.

ACKNOWLEDGEMENTS

I would like to express my sincere gratitude to South Dakota State University and the Jerome J. Lohr College of Engineering, Civil and Environmental Engineering Department, for allowing me to fulfill my Master of Science Degree and thesis study. The completion of this study could not have been possible without the expertise of Dr. Francis Ting, thesis advisor and committee chair, who has an exceptional attitude and experience for engineering research. I would like to thank Dr. Suzette Burckhard and Dr. Rhoda Burrows for being a part of my thesis committee and taking the time to read and listen to my thesis. A thank you is also owed to Dr. Allen Jones for guiding me in the Geotechnical Engineering Laboratory on experimental methods and procedures. I would also like to thank my parents, Jeffrey and Shelly Kern, Fiancée, Rebecca, and the rest of my family for supporting me during my engineering studies.

Funding for this study was provided by the United States Department of Transportation (USDOT) to the Mountain-Plains Consortium (MPC). The support of the MPC is gratefully acknowledged.

TABLE OF CONTENTS

ABBREVIATIONS

a = Straight-line fit slope;

A, B = integration constants in log-law;

b = Channel width;

b = Straight-line fit y-intercept;

CI = Confidence Interval;

cm = centimeter;

C_u = Estimated Shear Strength from Q_u;

D = particle diameter (uniform grain);

D_0 = Initial diameter of soil cylinder;

d_r = grain diameter with r % of particles finer;

f = bulk friction factor;

f_b = bed-related friction factor;

ft = feet;

ft^3/s = feet cubed per second;

f_w = sidewall-related friction factor;

g = Acceleration due to gravity;

G = Specific Gravity of soil particles;

G_1 =Specific Gravity of liquid corrected for the temperature;

h = Measured flow depth;

h_0 = Initial height of soil sample cylinder;

H_0 = Initial height of soil sample;

h_e = Effective flow depth;

Hz = Hertz (/sec.);

in = inch;

K = constant depending on the temperature of the suspension and specific gravity of the soil sample, Table 3 in ASTM D 422;

k = Factory calibrated orifice discharge coefficient for A-8 Hydraulic Channel;

k = von Kármán constant;

k_s = Equivalent grain roughness

L = Effective Depth, found from Table 2, ASTM D 422;

l = length soil sample was eroded;

L = Liter;

L_0 = Initial Length;

LED = Light Emitting Diode;

L_i = Length at time;

LL = Liquid Limit;

ln( ) = Natural Log;

log-law = logarithmic law

m = meter;

$M_{0, Dry}$ = Mass of dry soil sample before erosion test;

$M_{0, Wet}$ = Mass of wet soil sample before erosion test;

M_c = Mass of container;

M_{cs} = Mass of Container plus dry soil;

M_{cws} = Mass of Container plus wet soil;

$M_{f, Dry}$ = Mass of dry soil sample after erosion test;

$M_{f, Wet}$ = Mass of wet soil sample after erosion test;

mm = millimeter;

mm/hr = millimeters per hour

mm/pixel = millimeters per pixel;

n = Porosity of sediment;

N/m^2 = Newtons per square meter = Pa = Pascal;

^oC = Degrees Celsius;

P = Percentage of soil remaining in suspension at the level the hydrometer measured the density of the suspension;

PI = Plasticity Index;

PIV = Particle Image Velocimetry;

PL = Plastic Limit;

psi = pounds per square inch;

Q = Discharge rate;

Q_u = Unconfined Compressive Strength;

R = Hydrometer Reading;

R^2 = Coefficient of determination;

r_b = R_b = bed-related hydraulic radius;

Re = Reynolds number;

R_h = Bulk hydraulic radius;

RMSE = Root-Mean-Square-Error;

r_w = sidewall-related hydraulic radius;

S = Channel slope;

SA = Surface Area;

t = time elapsed during erosion test;

t = Time from the beginning of sedimentation to the recorded reading;

u = Mean velocity;

u* = Friction velocity;

V = flow velocity;

v = kinematic viscosity;

V_1 = Depth-average velocity estimated from the PIV measured velocity profile;

W = Mass of Dry Soil for Hydrometer experiment;

w = moisture content;

W = oven-dry mass of soil sample recorded before hydrometer test;

w = water (moisture) content of soil;

x = Horizontal Coordinate;

y = Vertical coordinate;

y_0 = Displacement height (virtual bottom);

y_1 = Actual location of sediment bed;

y_2 = Approximate location of free surface;

Y_{Avg} = Average water depth;

$Y_{downstream}$ = Downstream of test area water depth;

$Y_{test\ area}$ = Water depth immediately above channel bed of test area ;

$Y_{upstream}$ = Upstream of test area water depth;

$z = (y - y_0)$;

Δh = Differential pressure head measured by transducer;

ΔL = Deflection length;

ε = Effective roughness of bed;

ε = Unit Strain;

μm = Micro-meter;

μs = Micro-second;

ρ = Density of water;

τ_0 = Estimated bed shear stress from PIV measurements;

τ_b = bed-related shear stress;

τ_{b1} = Estimated bed shear stress from measured flow depth and channel slope;

τ_{b2} = Estimated bed shear stress from logarithmic law;

τ_w = sidewall-related shear stress;

$\dot{z}$ = Average erosion rate;

LIST OF TABLES

Appendix B

LIST OF FIGURES

Chapter 3

Appendix D

ABSTRACT

LABORATORY MEASUREMENTS OF BED SHEAR STRESS IN OPEN CHANNEL FLOW AND SOIL EROISION RATE IN COHESIVE SOILS

GUNNAR SCHURMANN KERN

2021

The relationship between soil erosion rate and bed shear stress is an important problem in sediment transport and scour. However, reliable measurements of the soil erosion function are challenging, both in the field and in the laboratory. The objective of this study is to investigate an experimental setup for conducting bed shear stress and soil erosion rate measurements using an open channel flume with a rough bed.

These experiments were performed in an A-8 Hydraulic Channel with a fixed gravel bed. The flow discharge was kept constant at 0.158 ft.^{3}/s, and bed shear stress was varied by changing the channel slope. A soil specimen was placed in a circular cutout in the gravel bed. Soil samples with a range of unconfined compressive strengths were prepared by changing the water content. The soil erosion rate was found from the difference in the mass of the sample before and after the test.

Two different methods were used to estimate bed shear stress: from the measured velocity profile using the logarithmic law, and from the measured flow depth and channel slope. The velocity profiles were measured using the Particle Image Velocimetry (PIV) technique. The measured data showed that the equivalent grain roughness correlated well with the size of the large grains in the gravel bed. The equivalent grain roughness decreased with the flow-depth-to-grain-diameter ratios (h/d_{90}). The bed shear stress in

the sediment recess was not significantly different from the bed shear stress on the surrounding gravel bed. It was also found that the measured soil erosion rate correlated well with the unconfined compressive strength or water content.

Chapter 1

Introduction

1.1 Definitions

Erosion occurs in rivers and streams when the bed shear stress produced by the flow exceeds the critical shear stress the soil bed can resist. The erosion rate is a measurement of the amount of soil lost over a specific period. Previous studies have utilized Erosion Function Apparatus (EFA) devices to measure soil erosion rate and bed shear stress. Bed shear stress is defined as the force of friction from a fluid acting on an area of soil. The critical shear stress is the friction force needed to initiate erosion. Among other soil properties, the unconfined compressive strength has been used to predict the critical shear stress of clay soils. The unconfined compressive strength is the maximum axial compressive stress that a cylindrical sample can withstand under unconfined conditions.

Two techniques were used in this study to estimate the bed shear stress. The first method uses the measured flow depth and channel slope and accounts for side-wall effect Cheng (2011).

$$\tau_b = \rho g R_b S \tag{1.1}$$

where ρ = the density of water (kg/m^3); g = acceleration due to gravity (m/s^2); R_b = bed-related hydraulic radius (m); and S = Slope of hydraulic channel (m/m). The second method uses a measured velocity profile and the logarithmic law to estimate a friction velocity (Middleton and Southard, 1984):

$$\frac{u}{u^*} = A * ln\left(\frac{y-y_0}{k_s}\right) + B \tag{1.2}$$

where u = time-averaged velocity at a distance y from the reference level; y_0 = displacement height; u* = friction velocity; A = 1/k (k-value ≈ 0.4 is the von Kármán constant); k_s = equivalent grain roughness; and B is a constant which value depends on the nature of the bed surface. A value of 8.5 for B was obtained by Nikuradse (1933) for uniform, close-packed sand grains in fully developed turbulent flow over a hydraulically rough bed.

1.2 Motivation

This study is concerned with Erosion Function Apparatus (EFA) type devices. Existing EFA type devices use an open-channel flume or water tunnel to recirculate water. Because these devices typically have smooth walls, the local shear stress developed over the soil sample can be much higher than the wall shear stress computed based on a smooth surface. The bed shear stress also varies with the height of soil protrusion into the flow. When the soil surface is eroding non-uniformly the configuration of the soil protrusion is constantly changing. Therefore, a constant and uniform shear stress cannot be maintained over the soil surface, making it difficult to establish a reliable relationship between soil erosion rate and bed shear stress. Various sensing devices have been developed and employed by researchers to monitor the position of the eroding surface and automatically advance the soil sample without the need for operator intervention, with varying degrees of success.

1.3 Objectives and Scope of Work

The present study investigates a different design for the EFA to measure the erosion-rate-versus-shear-stress curve. Instead of the smooth wall used in existing devices, a

layer of gravel was glued to acrylic sheets and installed in a tilting flume to produce fully developed turbulent flow over a rough surface. A circular cutout was made in the gravel bed to accommodate a circular soil sample. It is hypothesized that the erosive action of the flowing water in this experimental arrangement would be controlled primarily by the boundary-layer turbulence generated upstream, and thus less sensitive to the surface roughness and configuration of the soil surface as the erosion progresses. The specific objectives of the experimental study are to:

1. Determine the effect of soil erosion depth on the bed shear stress in the experimental setup described above.
2. Measure the erosion-rate-versus-shear-stress curves of Nora Moody Clay to investigate the effect of unconfined compressive strength and water content on the soil critical shear stress and erosion rate.

The turbulent velocity field over the gravel bed and clay sample was measured separately under steady, uniform flow conditions using the Particle Image Velocimetry (PIV) technique. The flow depth in the flume and the channel slope were also measured. The bed shear stress was obtained from the measured data using two different methods: (1) from the measured flow depth and channel slope, and (2) by fitting the logarithmic law (log-law) to the measured velocity profile. The results were used to examine the effect of erosion depth on the fluid velocity field over the soil sample and the local bed shear stress. Test samples of Nora Moody Clay with a range of unconfined compressive strength values were prepared by varying the water content. The samples were tested in the tilting flume to measure soil erosion rates. The measured erosion-rate-versus-shear-

stress curves were used to investigate the relationship between soil erosion rate, critical shear stress, and unconfined compressive strength.

1.4 Thesis Layout

The thesis will begin with a literature review of previous studies on EFA devices and soil erosion testing. Then the experimental equipment and methods will be described including the PIV system, PIV data processing and calibration methods, soil sample preparation and geotechnical laboratory testing, and soil erosion testing in the tilting flume. The experimental results on soil erosion will then be presented, followed by the measurement of the bed shear stress using the side-wall correction method and the logarithmic law method. The results for the fixed gravel bed will be presented, including an alternative log-law method, followed by the results for the clay bed. A discussion of the results will follow to compare the findings in this study with previous studies. Conclusions will be drawn on how the EFA device in this study improves upon previous devices, and how the alternative log-law method developed may improve bed shear stress estimates. Finally, recommendations for future research will be stated for further improving the experimental methods and procedures introduced in this study.

Chapter 2

Background and Literature Review

2.1 Introduction

Scour is a result of fluid stresses from the flow being applied to the sediment bed in a river or stream. When soil erosion occurs, it is because the fluid stresses that are being applied to the bed by the flowing water exceeds the resisting strength of the soil. Scour in cohesive soils is believed to be slower than in cohesionless soils. Cohesive soils have soil properties and erodibility that can differ greatly from a cohesionless soils. The effects of the soil eroding in blocks, chunks, or non-uniformly are just some of the ways cohesive soils may behave. Many studies have been conducted to investigate the erosion processes of cohesive soils, but our understanding is still far from complete. This chapter gives a summary of previous studies that are directly related to the present study.

2.2 Erosion Function Apparatus

Cohesive soils erode differently from cohesionless soils. Cohesive soils generally erode more slowly than cohesionless soils, even when their erosion depths at equilibrium conditions may be similar (HEC-18; Arneson et al. 2012). The scour depth that may take a cohesionless soil to reach in one flood could take several flood events to develop for a cohesive soil.

The bridge scour that may develop in a flowing stream depends on many factors including discharge, soil properties, and site characteristics, such as bridge crossing layout. The HEC-18 document (Arneson et al. 2012) is the procedure commonly used by practicing engineers to evaluate scour at bridges in the United States. Of the different

types of scour, contraction scour is most directly related to the present study. To predict clear-water scour in a long contraction, the effect of local scour around piers, and abutments, and the effect of sediment transport into the contracted section may be ignored. Under these simplifying assumptions, scour depth will increase until the bed shear stress is equal to the critical shear stress of the bed materials. A soil erosion function can then be used with the calculated bed shear stress to compute the contraction scour depth as a function of time by increasing the flow depth in the contraction in a stepwise manner. In this simplified model, the equilibrium scour depth is directly related to the critical shear stress and the time to reach equilibrium scour depth to the soil erosion rate. The latter is typically modelled as a function of the fluid shear stress.

An objective of this study is to develop a working, yet cost-effective, laboratory method to measure the erosion rates of cohesive soils. Reliable measurements of soil erosion rates are imperative for accurate prediction of the scour depth that would be developed at a certain time. Briaud et al. (2001a) developed an erosion function apparatus (EFA) to measure the erosion rates of cohesive and cohesionless soils. The apparatus was designed to test samples taken from a thin-walled Shelby tube, 76.2 mm outside diameter. Briaud et al. (2001b) incorporated the EFA into a new procedure called the Scour Rate in Cohesive Soils (SRICOS) method to predict the time development of scour at bridges using site-specific measurements of soil erosion rates and a measured or constructed hydrograph. Thus, the SRICOS method can predict not only the equilibrium scour depth but also the time history of scour.

The EFA produces a steady flow through a water tunnel with a smooth wall. A thin-walled tube is attached to the floor of the water tunnel and a piston driven by a

stepping motor is used to push the soil sample 1mm into the flow initially. The soil sample is pushed another 1 mm into the water tunnel after the protruded soil is eroded or after 1 hour of flow, whichever comes first. This procedure is repeated with different flow velocities to create a curve of soil erosion rate versus applied bed shear stress.

Briaud et al. (2001a) found no clear relationship between soil erodibility and soil properties including grain size, undrained shear stress and plasticity index. Therefore, the erosion resistance of cohesive soils cannot be determined reliably based on measured soil properties. Soil samples must be collected from bridge sites and tested in an EFA type apparatus to measure the soil's critical shear stress and erosion rate.

The advantages of the EFA are that the erodibility of soils at a given site and from a specific depth can be measured using relatively undisturbed samples, and the results can be used in conjunction with the SRICOS method to predict the time history of scour. A major disadvantage of the EFA set up is to decide when to advance the soil sample and how far the sample should protrude into the flow. Since cohesive soils erode non-uniformly and develop an irregular surface while being eroded, deciding when to advance the soil sample is nontrivial and often subjective, which may produce inconsistent test results. Experimental uncertainty is also introduced by using the Moody Chart or Colebrook equation to estimate the bed shear stress acting on the soil sample

Improvements to the EFA have been made by other researchers to reduce measurement uncertainties. Shan et al. (2012) developed an ex-situ scour testing device (ESTD) which uses a direct force gauge (DFG) to measure the forces that are exerted on a soil sample, thus eliminating the need to estimate the fluid shear stress using the Moody chart originally developed for pipe flows. In addition, a moving belt and pump are used

to generate the log-law velocity profile in open channel flows. The soil specimen is mounted on a sensor disk that is servo-controlled by the DFG, and automatically advanced to maintain a constant shear stress to produce more consistent measurements of soil erosion rate. The design of the ESTD allows for more accurate and consistent measurements of the applied bed shear stress and soil erosion rates under conditions that mimic open channel flows. However, the ESTD has the same drawbacks as other EFA devices in that the fluid stresses acting on the eroding sample can vary significantly during a test period as the sample erodes non-uniformly. These effects are discussed in the next section.

A cohesive soil develops a rough surface as it erodes. This rough surface can experience varying local fluid stresses. Crowley et al. (2012) used a sediment erosion rate flume (SERF) to conduct an experimental investigation on different methods for estimating the shear stress in a flume erosion rate testing device. The SERF was equipped with a shear stress-measuring instrument that can measure shear stress directly. Pressure drops across the soil sample were also measured to estimate the shear stress. Their results showed that direct shear stress measurements closely corresponded to shear stress estimates obtained using the Colebrook equation, but measurements of pressure drop across the soil sample underestimated the applied shear stresses. The pressure differential between the upstream and downstream sides of the test area did not change substantially as the soil sample was eroded. Therefore, the bed stress cannot be calculated reliably from pressure measurements.

Crowley et al. (2014) used a computational fluid dynamics (CFD) model to simulate the bed shear stresses developed on a test samples in the SERF. Different bed

configurations of the samples were simulated in the numerical model to investigate the effects of blocking, chunking, and sample over-advancement during an erosion test. Their results showed that small deviations in sample geometry, such as surface roughness, had large effects on local shear stresses. These large, localized shear stresses increased as the roughness of the soil increased. They concluded that keeping the surface of the eroding sample flush with the bottom of the flume would provide the most conservative measurements of soil erosion rate.

2.3 Soil Properties

Soil properties affect the erosion rate and erosion pattern of a soil specimen. Straub and Over (2010) used the EFA to obtain the erosion-rate-versus-shear stress curves of soil samples collected from bridge sites in Illinois. They also conducted laboratory testing on the soil samples to measure the common geotechnical properties. They computed coefficients of determination of individual soil properties with the soil erosion parameters. The found a strong correlation between soil critical shear stress and unconfined compressive strength. They also used the SRICOS-EFA method to compute the equilibrium scour depth in pier and contraction scour for the 100- and 500-year floods. They found that the HEC-18 method predicted larger scour depths compared to the SRICOS-EFA method.

Straub and Over (2010) studied the relationship between soil erosion rate and excess shear stress given by the following equation:

$$\dot{z} = a(\tau - \tau_c)^b \tag{2.1}$$

In Eq. (2.1), τ_c is the critical shear stress, *a*, and *b* are empirical constants. The equation was fit to measurements of soil erosion rate and bed shear stress for soil samples collected from bridge sites in Illinois to determine values of τ_c and the coefficients *a* and *b*. Their results showed a linear relationship between τ_c and the natural logarithm of the unconfined compressive strength, Q_u, given by:

$$\tau_c = 5.098 \ln(Q_u) + 10.01 \quad (2.2)$$

where τ_c is measured in Pascals and Q_u in tons/ft^2. Eq. (2.2) has a coefficient of determination (R^2) of 0.95. Only weak correlation was found between the coefficient α and the unconfined compressive strength, but the exponent *b* can be related to Q_u by:

$$b = 1.089 Q_u^{-0.353} \quad (2.3)$$

With an $R^2 = 0.61$

Shan et al. (2015) prepared cohesive soil specimens with different percentages of clay, silt, and non-uniform sand and a range of water contents for testing using the ESTD. They found a weaker correlation between the measured critical shear stress and unconfined compressive strength compared to the field samples tested by Straub and Over (2010). They also developed the following relationships for τ_c and α in Eq. (2.1):

$$\tau_c = 0.07 \left(\frac{W}{F}\right)^{-2.0} PI^{1.3} Q_u^{0.4} \quad (2.4)$$

$$\alpha = (Q_u)^{-1.0} PI^{-1.1} \quad (2.5)$$

where W is water content, F is percent particles finer than 0.075mm, PI is plasticity index, and Q_u is unconfined compressive strength of the soil. A constant of 1.8 for *b* was found to provide the best fit to their bed shear stress data. Eq. (2.4) underpredicted the

critical shear stress data from Straub and Over (2010). With *b* equal to 1.8 and τ_c and *a* given by Equations. (2.4) and (2.5). Eq. (2.1) was found to over-predict the erosion rate data from Straub and Over (2010)

Chapter 3

Methods and Procedures

3.1 Introduction

This chapter gives an overview of the materials and procedures that were used in the laboratory experiments. All the experiments were conducted in the Geotechnical Engineering Laboratory and Fluid Mechanics Laboratory. Soil properties were measured in the Geotechnical Engineering Laboratory while the flume tests were conducted in the Fluid Mechanics Laboratory. ASTM standard procedures were followed for measuring the soil properties.

3.2 Erosion Test Soil Specimen Preparation Procedure

Soil specimen preparation was conducted in the Geotechnical Engineering Laboratory before the samples were transported to the Fluid Mechanics Laboratory for erosion testing in the hydraulic channel.

1. About 1.5 Gallons of mostly Dry Soil was taken from the storage bins labeled "Nora Moody Clay" in the Geotechnical Engineering Lab.
2. The soil was placed in a metal container.

Figure 3.1 Dry Soil in metal container before preparation

3. Water was blended evenly into dry soil using a spray bottle while soil clumps were broken apart.
4. The process was continued until there were no clumps big enough to be retained on a No. 4 sieve (4.75mm)

Figure 3.2 Hydrated Soil

5. When the soil was mixed to a consistency that was visually moistened. The container was covered, and sealed, in a plastic bag to ensure that the soil became uniformly hydrated for erosion tests.
6. After at least 24 hours the soil was mixed again to ensure uniform hydration.

7. The well mixed and hydrated soil was scooped and compacted in a 4-inch diameter Proctor Mold following the ASTM D 698 – 91 procedure.

Figure 3.3 Rammer (left) and mold (right) used to compact soil

8. The soil was filled 1/3 of the way then compacted using a man-powered rammer.

Figure 3.4 Layer of soil before being compacted

9. Another layer of soil was added, then compacted using same number of blows with the rammer.

10. The third layer was filled to the brim of the proctor mold then compacted using the same number of blows as the two layers below it.

Figure 3.5 Specimen after full compaction effort

11. The soil specimen was then extracted from the proctor mold using a jack lift.

Figure 3.6 Jack used to extract specimen from Proctor Mold

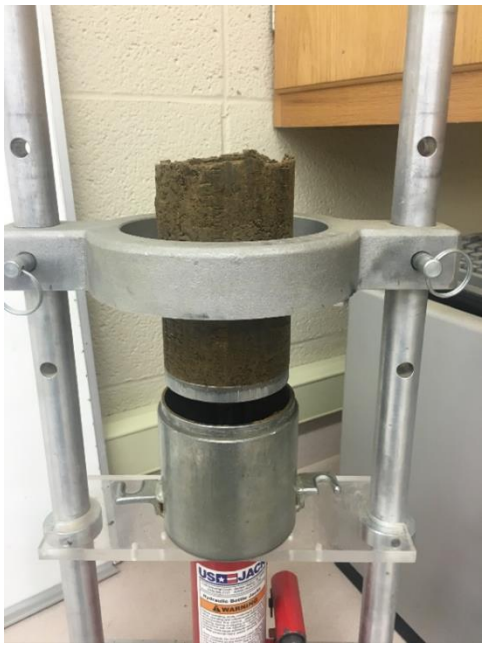

Figure 3.7 Specimen being extracted from Proctor Mold

12. A duplicate soil specimen was prepared from the same batch of soil following the same procedures as described in steps 7-11.
13. Each cylindrical soil specimen was trimmed to a diameter 2.75 inches while keeping the same height.

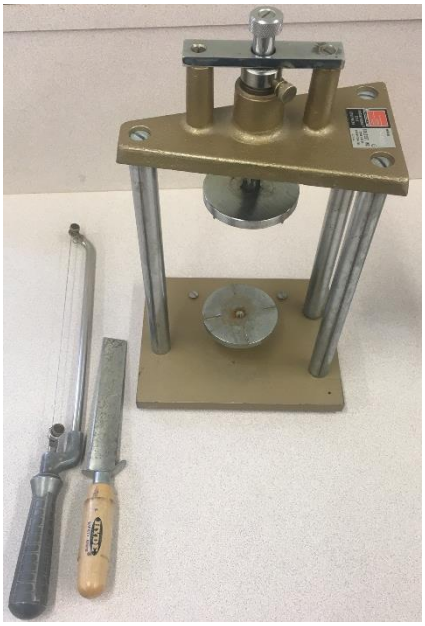

Figure 3.8 Device and tools used to trim soil specimen

14. Representative trimmings from each sample were weighed in a tin container and placed in an oven to measure the moisture content.

$$w(\%) = \frac{M_{cws} - M_{cs}}{M_{cs} - M_c} \quad (3.1)$$

where M_c is the Mass of container, g; M_{cs} is the mass of the container plus dry soil, g; M_{cws} = Mass of the container plus wet soil, g; and w is the moisture content of the trimmings, %.

A1: Unconfined Compressive Test Trimmings		A2: Flume Test Trimmings		Unconfined Compressive Test Specimen after being tested	
M_c (g)	3.63	M_c (g)	3.6	M_c (g)	4.33
M_{cs} (g)	122.27	M_{cs} (g)	123.48	M_{cs} (g)	998.24
M_{cws} (g)	141.23	M_{cws} (g)	143.23	M_{cws} (g)	1156.42
w	15.98%	w	16.47%	w	15.91%

Table 3.1 Sample results of moisture content of soil specimen's trimmings used for unconfined compressive strength test (A1) and flume test (A2), and for the specimen tested for unconfined compressive strength

15. One soil sample was stored in a cylindrical metal container and sealed in a zip lock bag for transport to the Fluid Mechanics Laboratory.

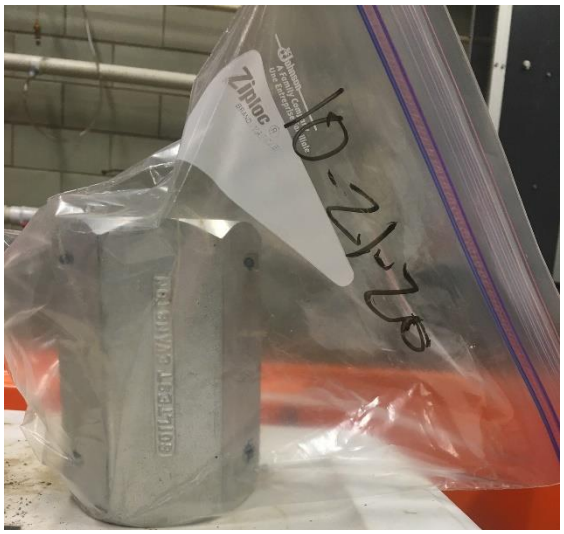

Figure 3.9 Soil specimen in sealed container ready for transport

16. The other specimen had its initial height (h_0) and diameter (D) measured. If the h/D ratio was > 2 then an Unconfined Compressive Strength test was conducted.

Figure 3.10 Specimen tested for Unconfined Compressive Strength

17. The Unconfined Compressive Strength machine measures the deflection (ΔL) and resistance (lbf) of the soil specimen. (ASTM D 2166-91)
18. A video was taken of the display of the soil testing machine and the video-recorded data is manually entered into a spreadsheet to calculate the unconfined compressive strength of the soil.

Raw Data						
Vertical Dial Reading (in)	Load Dial (lbs)	Sample Deformation, ΔL (in)	Unit Strain (ΔL/Lo)	Area Correction Factor (1-ε)	Corrected Area, A' (in^2)	Sample Stress (lb/in^2)
0	0	0	0.000%	1.0000	5.940	0.000
0.006	0	0.006	0.101%	0.9990	5.946	0.000
0.017	0	0.017	0.286%	0.9971	5.957	0.000
0.025	2	0.025	0.421%	0.9958	5.965	0.335
0.034	5	0.034	0.573%	0.9943	5.974	0.837
0.041	12	0.041	0.691%	0.9931	5.981	2.006
0.048	20	0.048	0.808%	0.9919	5.988	3.340
0.056	29	0.056	0.943%	0.9906	5.996	4.836
0.064	40	0.064	1.078%	0.9892	6.004	6.662
0.072	56	0.072	1.213%	0.9879	6.012	9.314
0.08	73	0.08	1.347%	0.9865	6.021	12.125
0.086	89	0.086	1.448%	0.9855	6.027	14.767
0.091	101	0.091	1.533%	0.9847	6.032	16.744
0.097	116	0.097	1.634%	0.9837	6.038	19.211
0.103	132	0.103	1.735%	0.9827	6.044	21.838
0.108	149	0.108	1.819%	0.9818	6.050	24.630
0.115	168	0.115	1.937%	0.9806	6.057	27.737
0.121	182	0.121	2.038%	0.9796	6.063	30.017
0.127	193	0.127	2.139%	0.9786	6.069	31.799
0.133	204	0.133	2.240%	0.9776	6.076	33.577
0.139	213	0.139	2.341%	0.9766	6.082	35.022
0.146	221	0.146	2.459%	0.9754	6.089	36.293
0.162	234	0.162	2.728%	0.9727	6.106	38.322
0.176	241	0.176	2.964%	0.9704	6.121	39.373
0.185	242	0.185	3.116%	0.9688	6.131	39.474
0.192	241	0.192	3.234%	0.9677	6.138	39.263

Table 3.2 Unconfined Compressive Strength Test sample results

where,

Sample Deformation, $\Delta L = L_0 - L_i$ (3.2)

$\varepsilon(\%) = \frac{\Delta L}{L_0} * 100$ (3.3)

Area Correction Factor = 1-ε (3.4)

Corrected Area = Initial Area / Area Correction Factor (3.5)

Sample Stress (psi) = Load Dial Reading / Corrected Area (3.6)

ΔL= Difference from the initial length
(Using Vertical Dial on unconfined compressive test device)

L_0= Initial Length
(Using tape measure)

L_i= Length at load reading

$$L_i = L_0 - \Delta L$$

ε = Unit Strain (%)

$$\varepsilon = \Delta L / L_0$$

Sample calculations for highlighted row in Table 3.2:

L_0 = 5.9375 in

Initial Area = 5.9 in^2

$$\varepsilon = \frac{\Delta L}{L_0} * 100 == \frac{0.185}{5.9375} * 100\ \% = 3.116\%$$

Area Correction Factor = 1 – ε = 1- 0.03116 = 0.9688

$$\text{Corrected Area} = \frac{Initial\ Area}{Area\ Correction\ Factor} = \frac{5.9\ in^2}{0.9688} = 6.131\ in^2$$

$$Sample\ Stress = \frac{Load\ Dial\ Reading}{Corrected\ Area} = \frac{242\ lb}{6.131\ in^2} = 10.687\ psi$$

A plot was made using the Axial Stress vs Unit Strain to show the specimen's point of failure.

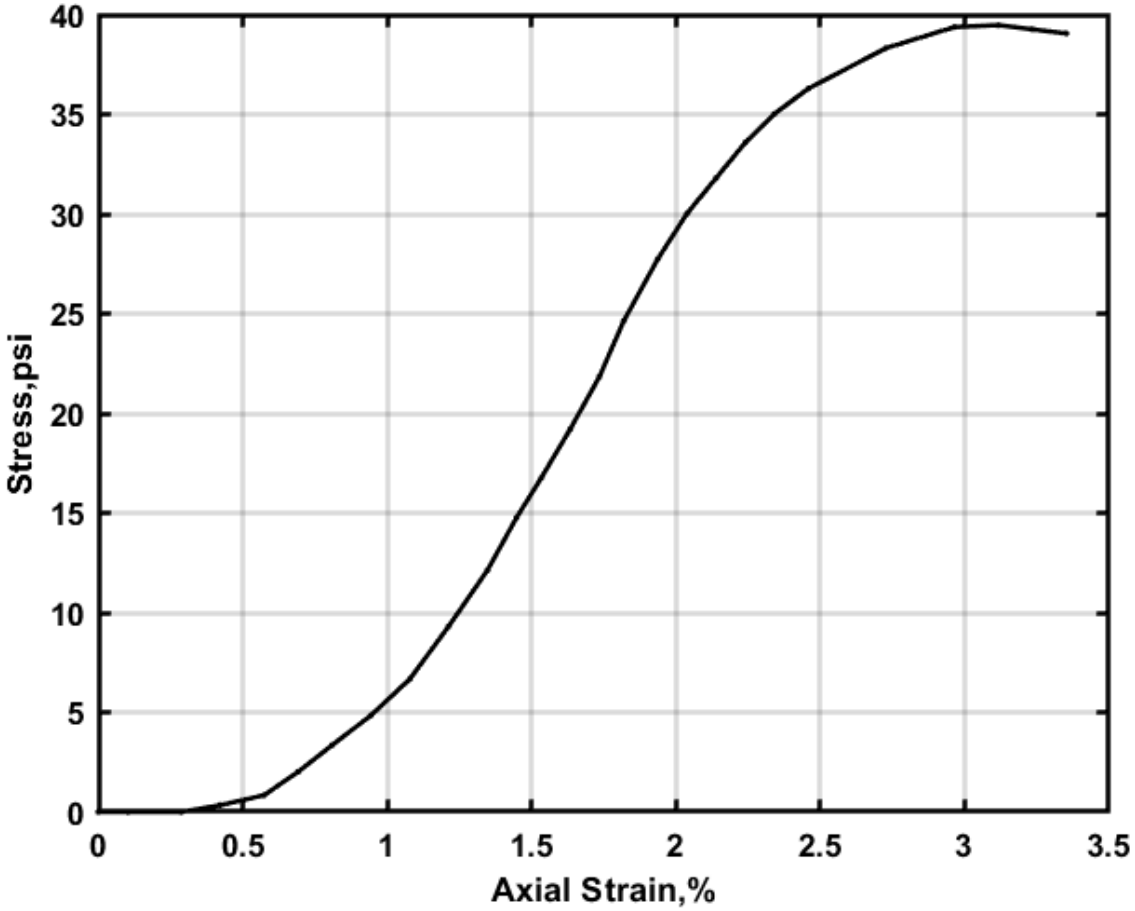

Figure 3.11 Stress vs Axial Strain for Specimen

The maximum measured axial stress was taken to be the Unconfined Compressive strength of the soil.

The undrained shear strength of the soil specimen was estimated as ½ the Unconfined Compressive Strength of the soil specimen. Therefore, if Q_u is 39.474 psi then C_u results

is 19.74 psi; where Q_u is the Unconfined Compressive Strength, psi; and C_u is the Estimated Undrained Shear Strength, psi.

19. After the soil specimen failed in the unconfined compressive strength machine, it was weighed and placed in the oven to measure the moisture content. Moisture content was measured to verify the moisture content on the soil trimmings.

Figure 3.12 Soil Specimen after failure

20. The specimen that was put aside in the sealed container was taken to the Fluid Mechanics Laboratory for soil erosion testing in the hydraulic channel.

The unconfined compressive strength data was summarized and plotted in Figure 3.13. This plot shows that there is a clear trend that the unconfined compressive strength of an artificial soil specimen can be predicted by the measured water content.

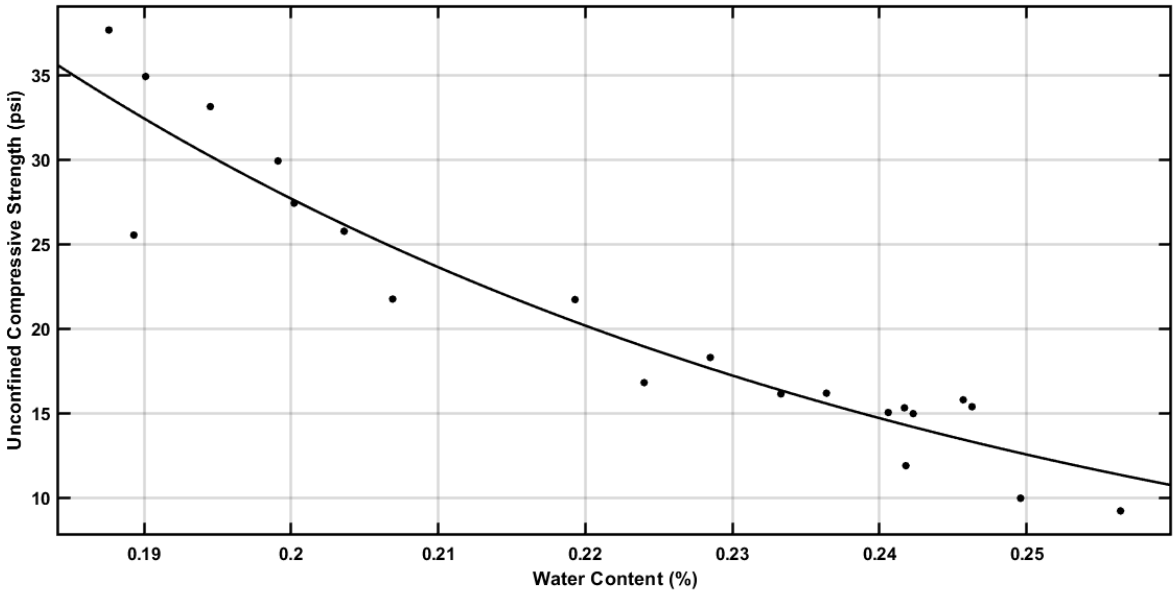

Figure 3.13 Unconfined Compressive Strength vs. Water Content of soil specimens

The best fit line to predict the unconfined compressive strength of soil samples was an Exponential model with an R^2 value = 0.9028 and an RMSE of 2.636.

$$Q_u = 708.5e^{-16.18w}$$

3.3 Soil Particle Size Distribution Procedure

A laboratory experiment was conducted in the Geotechnical Engineering Laboratory to determine the particle size distribution of Nora Moody Clay used in the soil erosion tests conducted in the A-8 Hydraulic Channel. The procedure followed ASTM D422 – 63: Standard Test method for Particle-Size Analysis of Soils.

1. 50 grams of soil was taken from storage bins labeled “Nora Moody Clay” in the Geotechnical Engineering Laboratory. The soil was dried in an oven and the dry mass measured.
2. Dry Soil was dispersed on the No. 10 Sieve (2.00 mm) to determine percent of soil coarser than 2.0 mm.

   (100% of the soil sample was finer than the No. 10 Sieve, which has 2.0 mm openings)
3. The portion of soil sample passing the No. 10 Sieve was transported into a 250 mL beaker.
4. A solution of 125 mL of sodium hexametaphosphate with a concentration of 40 g of sodium hexametaphosphate/liter of distilled or demineralized water (40 g/L) was poured into a 250 mL beaker, covering the soil sample. Soil slurry was stirred until the soil was thoroughly wetted. The mixture was soaked for at least 16 hours.

5. After the soaking period, the slurry was transferred to a dispersion cup (A). The soil residue in the beaker was washed into the dispersion cup using distilled water from a spray bottle filling the cup until it was more than half full.

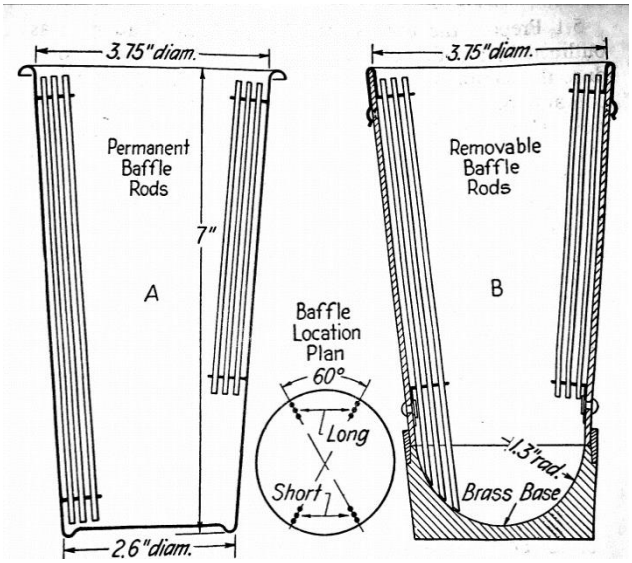

Figure 3.14 Dispersion cup used to entirely mix soil slurry (A)

6. Soil Slurry was then vigorously dispersed further using a Hamilton Beach stirring apparatus with a round stirring paddle (a). Soil was stirred for a period of 1 minute.

Figure 3.15 Hamilton Beach Dispersion device used to thoroughly mix soil slurry

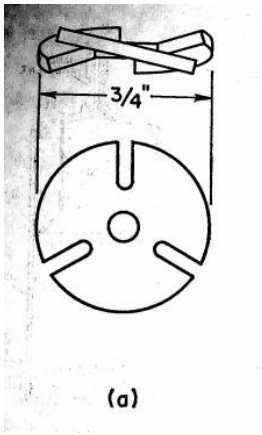

Figure 3.16 Detail of Stirring Paddle used (a)

7. Immediately after the soil slurry was dispersed in the mixing apparatus, it was transferred to a 1000 mL glass sedimentation cylinder. The mixing cup was rinsed using a spray bottle filled with distilled water. The glass cylinder was filled to the 1000 mL mark with distilled water.

8. Using a rubber stopper at the open end, the glass cylinder was turned upside down and back for a period of 1 minute at a rate of 1 turn per second.
9. The glass cylinder was set in a convenient location.
10. A 151H hydrometer was used to take hydrometer readings at 0.5, 2, 5, 15, 30, 60, 120, 250, 500, and 1440 minutes from the start of sedimentation. The temperature of soil-water slurry in the cylinder was also taken at each time interval.

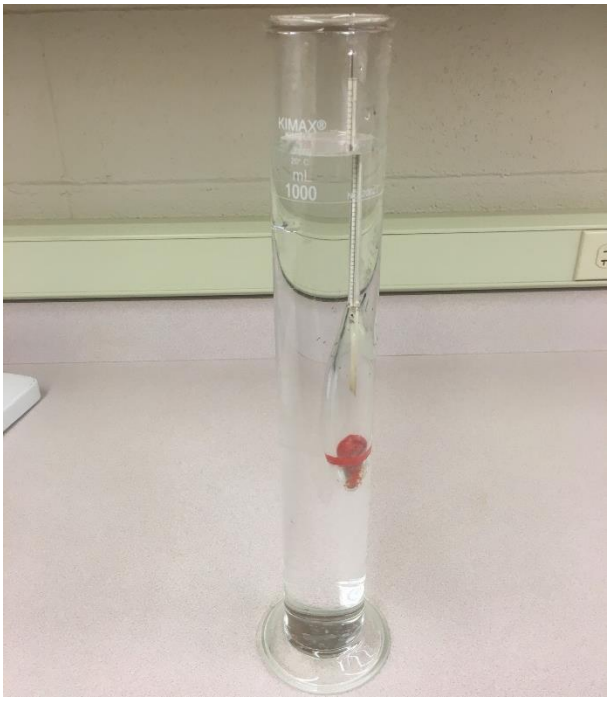

Figure 3.17 Glass sedimentation cylinder with 151H hydrometer

11. When a reading was taken, the 151H Hydrometer was carefully inserted into the glass cylinder for about 20-25 seconds before the reading time at the approximate depth it would settle at. For accuracy, readings were taken at the top of the meniscus formed by the suspension around the stem of the hydrometer.
12. After the reading, R, was taken the hydrometer was removed and placed in a graduated cylinder of clean distilled water until the next reading.

13. After taking the final hydrometer reading, the soil suspension was transferred to a No. 200 sieve (75-µm) and washed with tap water until the wash water was clear.
14. The material retained on the No. 200 sieve was transferred to a suitable container and dried in the oven at 230°F ± 9°F (110°C ± 5°C).
15. The results were recorded in a table, and the percentage of soil remaining in suspension (percent finer than) and diameter of particles, in mm, corresponding to that percentage indicated by the hydrometer reading were calculated according to Stoke's Law.

Hydrometer 151H						
Hydrometer Readings				Mass of Dry Soil, W (g)		56.95
Time(min)	Temp (°C)	G_1	R	*L* (cm) *Table 2*	P (%)	D (mm)
0.5	21	0.997992	1.033	7.6	95.53	0.05033
2	21	0.997992	1.026	9.4	76.43	0.02799
5	21	0.997992	1.022	10.5	65.51	0.01871
15	21	0.997992	1.019	11.3	57.33	0.01121
30	21.5	0.997882	1.017	11.8	52.17	0.00805
60	21.5	0.997882	1.016	12.1	49.44	0.00576
120	22	0.99777	1.015	12.3	47.01	0.00409
250	23	0.997538	1.0135	12.75	43.55	0.00285
500	23	0.997538	1.013	12.9	42.18	0.00203
1440	22.5	0.997655	1.012	13.4	39.14	0.00122

Table 3.3 Hydrometer 151H sample results table

16. The Hydrometer readings were taken recording the Time from start (minutes), Temperature of soil-water suspension (°C), and the Hydrometer reading (R).
17. The percentage of soil remaining in suspension (P) at the level where the hydrometer is measuring (R) the density of the soil-water suspension at the specific time was calculated as:

$$P = \left[\left(\frac{100{,}000}{W}\right) * \frac{G}{(G-G_1)}\right](R - G_1) \quad (3.7)$$

where W is the oven-dry mass of soil sample recorded before test, g; G is the Specific Gravity of soil particles, 2.7992; G_1 is the Specific Gravity of liquid in which soil particles are suspended.

18. The effective depth, *L* (cm), was taken from Table 2, in ASTM D 422, pertaining to the actual hydrometer reading that was recorded.
19. The diameter of the soil particle corresponding to the percentage indicted by a hydrometer reading was calculated according to Stoke's Law. This assumes that if a particle of the calculated diameter was at the surface of the suspension at the beginning of sedimentation it would have settled to the level that the hydrometer density measurement was read. The diameter of the soil particle in suspension at the time of the reading was calculated by.

$$D = K\sqrt{L/t} \tag{3.8}$$

Where D is the Diameter of Particle, mm; K is the constant depending on the temperature of the suspension and specific gravity of the soil sample. (K values were taken from Table 3 in ASTM D 422); *L* is the Effective Depth, cm (found from Table 2); *t* is the time from the beginning of sedimentation to the recorded reading, min.

20. After the percent finer than, P, and Diameter of particles, D, were calculated for each time interval and No. 200 Sieve, the results were plotted on a percent finer than vs. particle diameter chart.

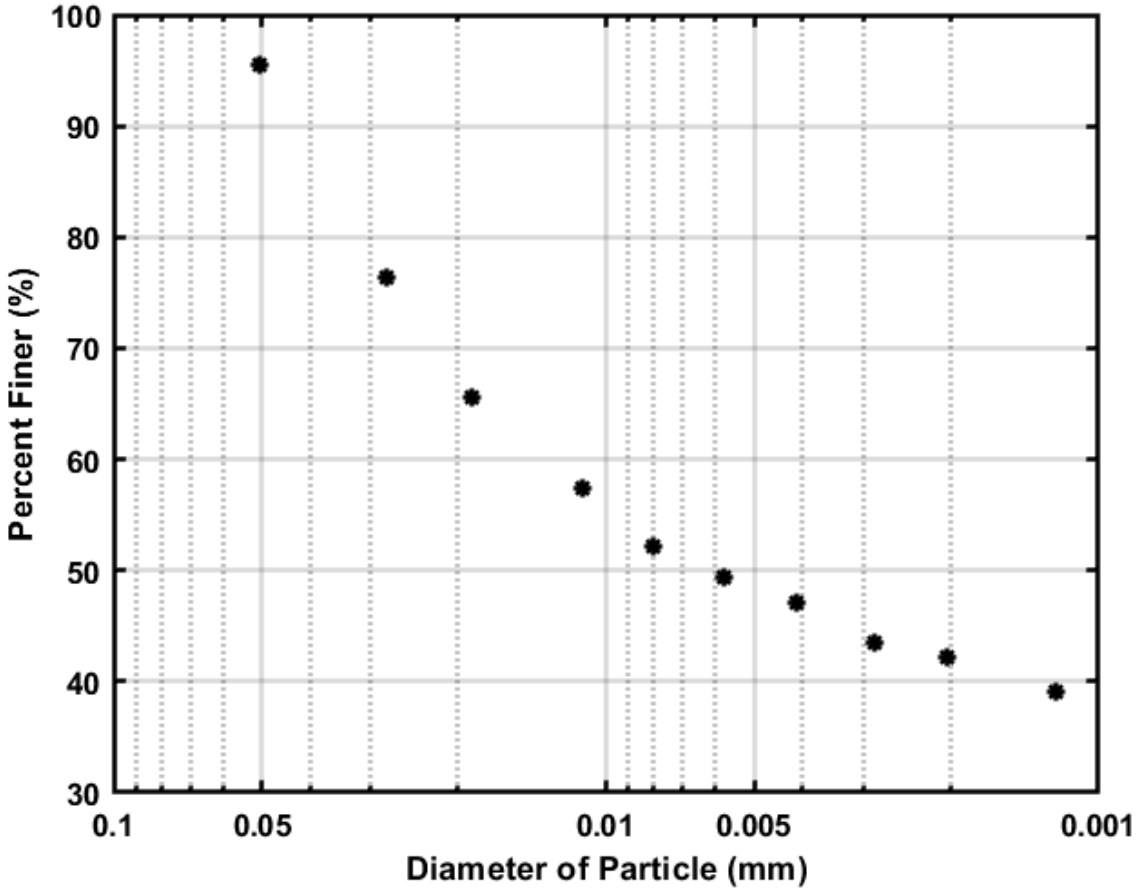

Figure 3.18 Example plot of particle size analysis results

Table 3.4 displays the geotechnical soil properties that were held constant in the present study while the water content, unconfined compressive strength, and estimated undrained shear strength were varied.

Soil Property	
Liquid Limit (LL)	37%
Plastic Limit (PL)	24%
Plasticity Index (PI)	13%
Percent Finer than 0.075 mm	> 95%
d_{50} (mm)	0.006

Table 3.4 Measured soil properties

3.4 Sieve Analysis on Fixed Gravel Bed in A-8 Hydraulic Channel

A sieve analysis was conducted on the gravel used to construct the rough bed in the hydraulic channel used for the soil erosion tests. The ASTM D 422 – 63: Standard Test Method for Particle-Size Analysis was followed for measuring the gravel size distribution.

The following sieve sizes were used: 3/8" (9.5 mm), 0.265" (6.7 mm), ¼" (6.3 mm), No. 3 ½ (5.6 mm), No. 4 (4.76 mm), No. 5 (4 mm), No.6 (3.36 mm), No. 7 (2.8 mm), and No. 8 (2.36 mm).

1. The mass of each sieve was recorded, in grams, using a digital scale with a precision of 0.01-grams.
2. The total mass of the gravel, not being greater than about 1500 grams, used in each trial was recorded.
3. The sieves were stacked in order, with the largest sieve opening at the top, and the smallest at the bottom. A pan was placed under all sieves to collect the fine materials.
4. The gravel sample was dispersed on the top of the sieve stack.
5. The stack of sieves was placed in a mechanical shaker and shook for ten minutes.
6. After the 10-minute shaking period, the sieves were removed from the shaker.
7. Each sieve's mass with the gravel that was retained on it was recorded.
8. The mass of the gravel retained on each sieve was found by subtracting the sieve mass from the sieve plus gravel mass.
9. Each mass was recorded on a data sheet and the percent retained and percent passing was calculated.

$$Percent\ Retained(\%) = \frac{Mass\ of\ gravel\ retained\ on\ sieve}{Total\ gravel\ mass} * 100 \quad (3.9)$$

$$Percent\ Passing(\%) = 100\% - Cummulative\ Percent\ Retained \quad (3.10)$$

Sieve No.	Sieve Size (mm)	Mass of sieve only (g)	Mass of sieve with soil (g)	Soil mass (g)	Percent Retained	Cumulative Percent Retained	Percent Passing
3/8"	9.5	483.66	483.66	0	0.00	0.00	100.00
5/16"	8	505.41	509.41	46.52	0.57	0.57	99.43
0.265"	6.7	491.25	681.76	1689.65	20.67	21.24	78.76
1/4"	6.3	495.67	584.87	722.07	8.83	30.07	69.93
3 1/2	5.6	493.28	741.78	1731.58	21.18	51.25	48.75
4	4.75	466.34	664.72	1142.48	13.97	65.22	34.78
5	4	478.05	771.26	1382.84	16.91	82.13	17.87
6	3.35	474.68	673.42	766.61	9.38	91.51	8.49
7	2.8	460.3	608.65	463.57	5.67	97.18	2.82
8	2.36	459.14	516.86	145.03	1.77	98.95	1.05
Pan	0	490.4	545.52	85.47	1.05	100.00	0.00

Table 3.5 Average results for sieve analysis with a total soil mass of 8175.82 grams

10. A total of five trials were completed. The results of the different trials were then averaged and plotted to estimate the d_{50} of the gravel.

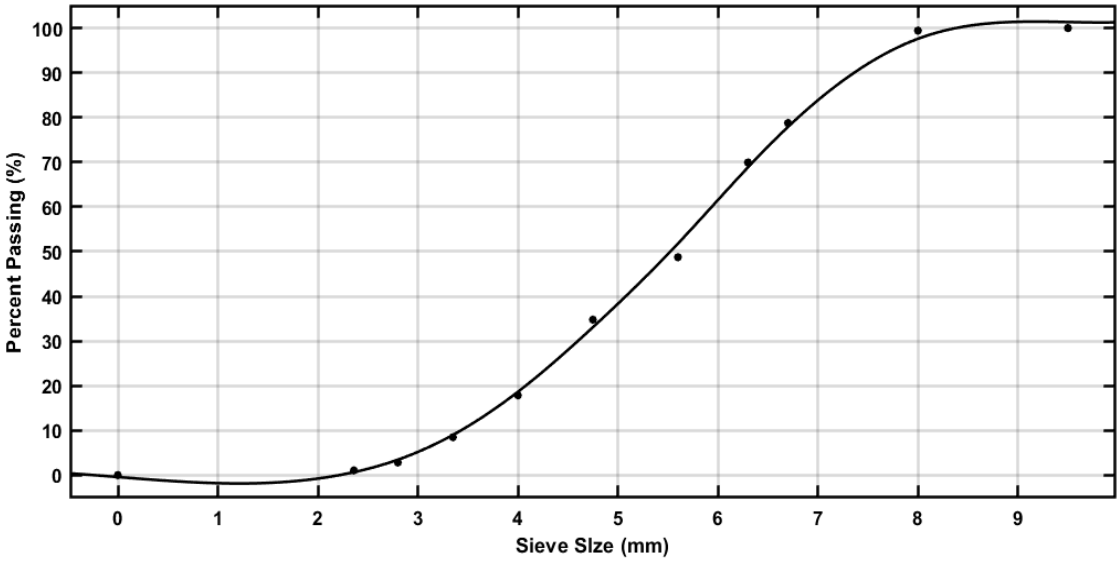

Figure 3.19 Grain size distribution of gravel

r % of particles finer	d_r (mm)
10	3.5
20	4.1
30	4.6
40	5.1
50	5.6
60	6.0
65	6.1
70	6.3
80	6.8
84	7.0
90	7.4

Table 3.6 Grain size distribution of gravel

3.5 Soil Erosion Test Procedure in A-8 Hydraulic Channel

The soil erosion tests were conducted in an A-8 hydraulic channel in the Fluid Mechanics laboratory. The objective was to erode the soil specimen that was prepared in the Geotechnical Engineering Lab, and then relate the erosion rate of the specimen to the measured soil and flow properties.

Figure 3.20 A-8 Hydraulic Channel

1. Soil specimen prepared in the Geotechnical Laboratory was trimmed to a height of about 1.5 inches to match the height of the sediment bed recess.

Figure 3.21 Soil Specimen before being placed in hydraulic channel

2. The mass of the trimmed soil specimen was taken, in grams, on a digital scale with 0.01-gram precision prior to the flume test.

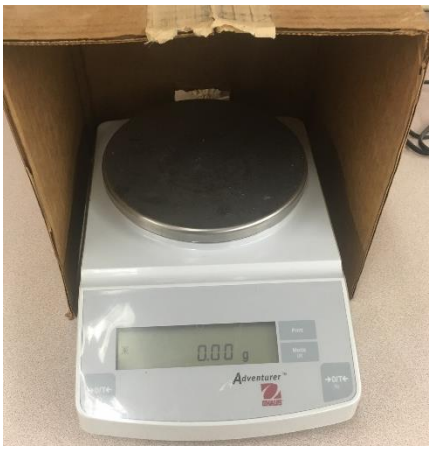

Figure 3.22 Electronic scale used to measure soil mass

3. The soil sample was placed in an insert in the false bottom installed in the flume. The top of soil sample was set at or slightly above the top of the rock bed.

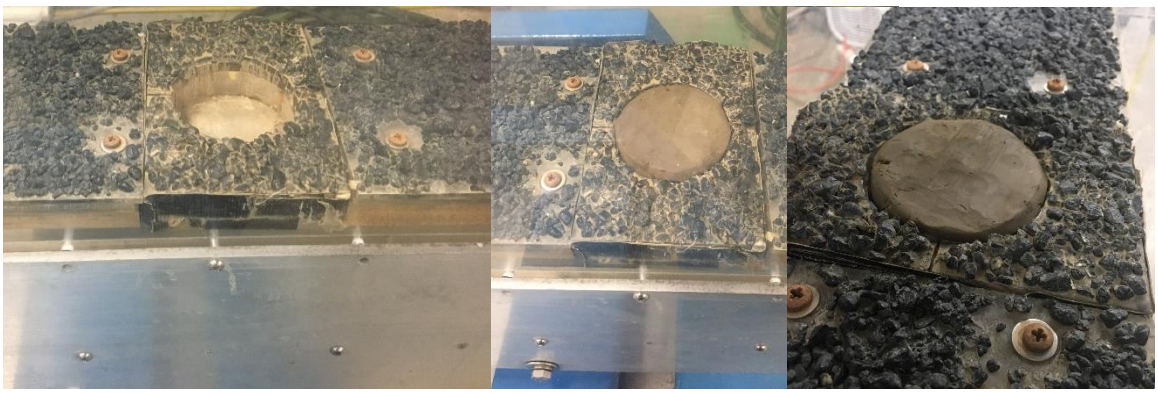

Figure 3.23 Soil recess in rock bed in A-8 hydraulic channel

4. The flume was set to the maximum flow rate of 0.158 ft^3/s and the desired slope was set using the Smart Tool digital inclinometer with a precision of ± 0.1%. The Slope was chosen according to the desired bed shear stress to induce erosion.

Figure 3.24 Slope measuring device

5. A point gage with a precision of ± 0.1 mm was used to record the height of the acrylic sheet where the gravels were adhered. Measurements were taken at a specific location upstream, at, and downstream of the sediment recess.
6. The hydraulic channel flow and a timer were started.

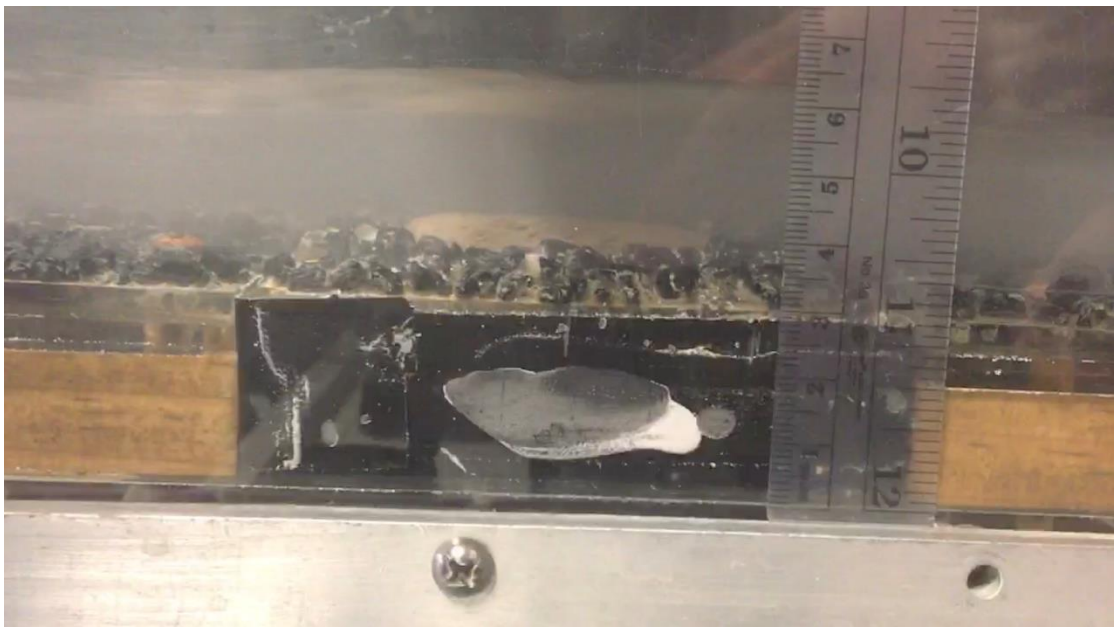

Figure 3.25 Profile view of test area after steady flow was established

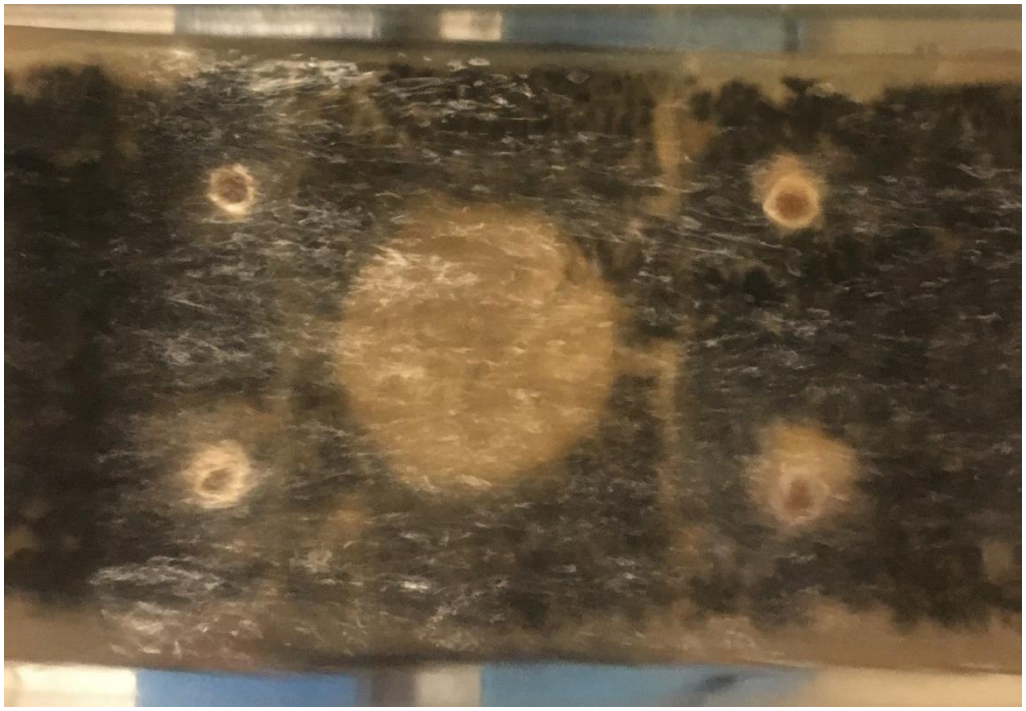

Figure 3.26 Plan view of test area after steady flow was established

7. The top of water upstream, at the sediment recess, and downstream was measured using a point gage. The water depth was calculated, relative to the bottom of the acrylic sheet, using the water height and bed height measured in step 6 and the results were averaged.

$$Y_{Avg} = \frac{Y_{Upstream} + Y_{Downstream} + Y_{Test\ Area}}{3} \quad (3.11)$$

8. Flow through the hydraulic channel was stopped before the soil had visually been eroded below the gravel bed. The soil sample was to be eroded enough to accurately measure a difference in soil mass, but small enough to not significantly change the flow configuration or bed shear stress around the test area; this will be demonstrated in Section 4.1.

Figure 3.27 Example of soil specimen after being eroded

9. The mass of a tin container was measured in grams.
10. The sediment recess was removed from the hydraulic channel. The insert was set aside so the soil specimen could be extracted.
11. Soil was extracted from insert by dumping it into the pre-weighed tin container.
12. The mass of soil plus container was measured using a digital scale with a precision of 0.01-gram.
13. Soil sample and dish were placed in an oven and dried for at least 24 hours.
14. After 24 hours the eroded soil specimen was removed from the oven and cooled for at least 15 minutes.
15. The mass of dry soil plus dish was measured using an electronic scale.
16. The moisture content of the soil specimen after being eroded was calculated for comparison with the water content before the test.

$$w(\%) = \frac{M_{cws} - M_{cs}}{M_{cs} - M_c} \quad (3.12)$$

17. The difference between the dry mass of the soil before and after the test was considered the amount eroded in hydraulic channel.

The wet mass of the soil specimen before($M_{0,\,Wet}$) and after ($M_{f,\,Wet}$) erosion, as well as the dry mass before ($M_{0,\,Dry}$) and after ($M_{f,\,Dry}$) erosion, were recorded. The dry mass of the soil specimen before being eroded ($M_{0,\,Dry}$) was estimated using the initial moisture content from the specimen's trimmings, which was found in **Section 3.2, Step 14**.

$$M_{0,Dry} = \frac{M_{0,wet}}{w+1} \tag{3.13}$$

18. The average erosion rate was calculated as:

$$\dot{z} = \frac{l}{t} \tag{3.14}$$

where $\dot{z}$ is the erosion rate (mm/hr); l is the length of the soil sample eroded (mm); and t is the time elapsed (hours).

The length is calculated using the percent difference by mass from before and after erosion test.

$$\dot{z} = \frac{H_0 * \%\ of\ soil\ eroded}{t} \tag{3.15}$$

where % of soil eroded is calculated as:

$$\%\ of\ soil\ eroded = \frac{M_{0,Dry} - M_{f,Dry}}{M_{0,Dry}} \tag{3.16}$$

3.6 Procedure to Determine Bed Shear Stress from Water Depth in the A-8 Hydraulic Channel

The procedure used to find the bed shear stress from the measured flow depth in the A-8 Hydraulic Channel is explained in this section. The flow discharge rate was measured using the procedure described in Appendix A, and the result was used with the average flow depth measured during each erosion test to calculate of the bed shear stress. The flow depth and channel slope were varied in the erosion tests, but the flow rate was kept constant. The measured bed shear stress accounts for side wall correction using the method in Cheng (2011), as well as the estimated porosity of the fixed gravel bed.

The average discharge rate used in the bed shear stress calculations was 0.158 ft^3/s. In this method an effective water depth, h_e, is estimated using the d_{50} and the porosity of the gravel bed. Loosely packed gravel typically has a porosity of 0.4 (Frings et al., 2011). The void fraction of a single layer of gravel will have a larger porosity. An estimated porosity of n = 0.5 was used as the calculated bed shear stress is insensitive to the porosity of the gravel bed being used. As stated earlier, the d_{50} of the gravel bed was 5.6 mm.

The inputs included the measured discharge, channel slope, and flow depth from the base of the gravel.

1. The effective flow depth and velocity was calculated as:

$$h_e = h - (1 - n) * \varepsilon \tag{3.17}$$

where h_e is the effective flow depth (m); n is the porosity of the fixed gravel bed (%); and ε is the effective thickness of the gravel layer taken to be d_{50} = 5.6 mm.

$$V = \frac{Q}{b*h_e} \quad (3.18)$$

where b is the width of the channel; V is the flow velocity; and Q is the discharge rate.

2. The bulk hydraulic radius, Reynolds number, and friction factor were calculated as:

$$R_h = \frac{b*h_e}{(b+2h_e)} \quad (3.19)$$

$$Re = \frac{V*4R_h}{\nu} \quad (3.20)$$

$$f = \frac{8gR_hS}{V^2} \quad (3.21)$$

where ν is the kinematic viscosity at a defined temperature (m^2/s); Re is the Reynold's Number; and f is the bulk friction factor.

3. The friction factor for the Plexiglas side wall (f_w) was calculated as:

$$f_w = 31 * \left[\left(ln\left(\frac{1.3*Re}{f}\right)\right)^{-2.7}\right] \quad (3.22)$$

4. The bed-related friction factor, hydraulic radius, and bed shear stress were calculated.

$$f_b = f + \frac{2h_e}{b}(f - f_w) \quad (3.23)$$

$$r_b = \frac{f_b}{f} * R_h \quad (3.24)$$

$$\tau_b = \rho g r_b S \quad (3.25)$$

where f_b is the bed related friction factor; r_b is the bed-related hydraulic radius (m); S is the channel slope (m/m); and τ_b is the bed-related shear stress (N/m^2). The sidewall related hydraulic radius and shear stress were also calculated in this step.

$$r_w = \frac{f_w}{f} * R_h \tag{3.26}$$

$$\tau_w = \rho g r_w S \tag{3.27}$$

where r_w is the sidewall-related hydraulic radius (m); and τ_w is the sidewall-related shear stress (N/m^2).

3.7 Procedure for PIV measurements in A-8 Hydraulic Channel

Particle Image Velocimetry (PIV) measurements were taken over the gravel bed and soil sample in the A-8 Hydraulic Channel. The velocity profile measurements were used to determine the bed shear stress using the logarithmic law. PIV measurements over the soil sample were conducted to investigate the effects of erosion depth on the bed shear stress.

The PIV system used is manufactured by TSI incorporated. The seeding consisted of latex particles with a mean diameter of 55 μm and a SG of 1.016. The seeding was illuminated using a Model IL-105X high -power-LED illuminator manufactured by HARDsoft microprocessor system. The light sheet created by the LED illuminator was directed downward from its mounting position above the test area as seen in Figure 3.29. Since the LED light sheet was about 10 mm wide, the measured velocities were averaged to find the time-averaged velocities. Images of the illuminated light sheet were captured using a PowerView Plus 4MP camera (2048 x 2048 pixels, 12-bit intensity dynamic range). It was equipped with a 105 mm/F 2.8 NIKKOR focal lens. The camera was mounted on the side of the flume, aligned parallel with the channel slope, with the lens about 20.5 cm away from the side wall. The LED and image capture were synchronized to capture images of the seeding particles as the LED light was shooting. The time interval between straddle frames was 100 μs and the repetition rate was 7.25 Hz. The maximum field of view (FOV) was about 34 mm x 34 mm with a spatial resolution of 16 μm/pixel.

The procedure for PIV measurements were similar for the fixed bed and soil sample, with exception of the installation of the soil insert. The procedure for the setup of these experiments are as follows:

The PIV camera was mounted facing the hydraulic channel at the location of the test area. The camera was set at the same slope as the hydraulic channel.

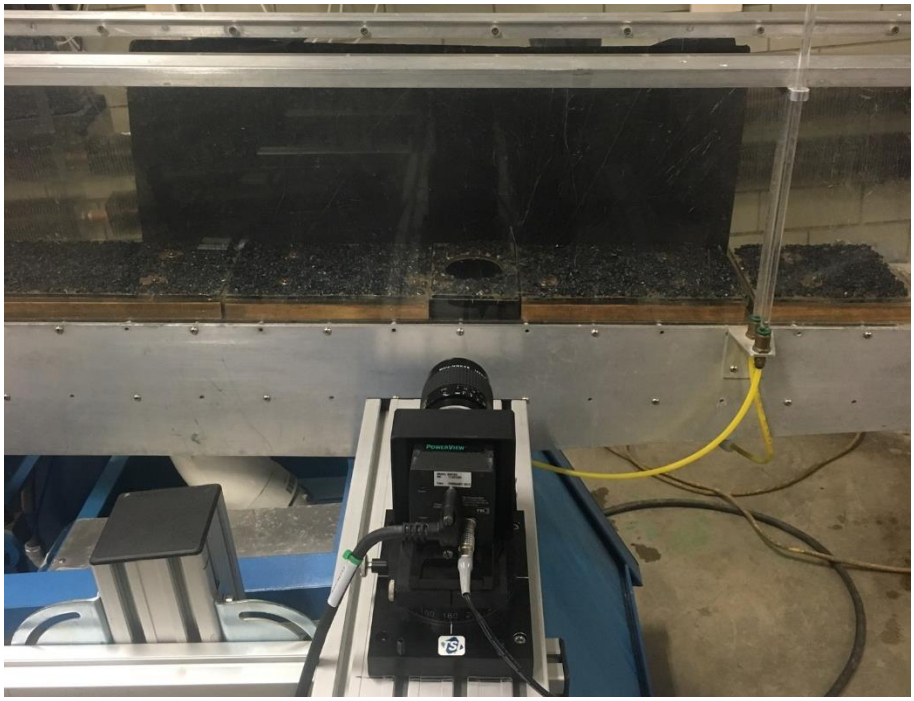

Figure 3.28 PIV Camera set up with gravel bed and sediment recess installed in the hydraulic channel

1. The camera field-of-view was checked to ensure that the image captured the channel bed and most of the flow depth.
2. The distance from the sidewall to the camera lens was measured.
3. The gravel bed and sediment recess were removed, and a calibration target was placed at the centerline of the channel.

4. The LED Illuminator was set on top of the hydraulic channel. A light sheet was generated and projected downward to align with the calibration target.

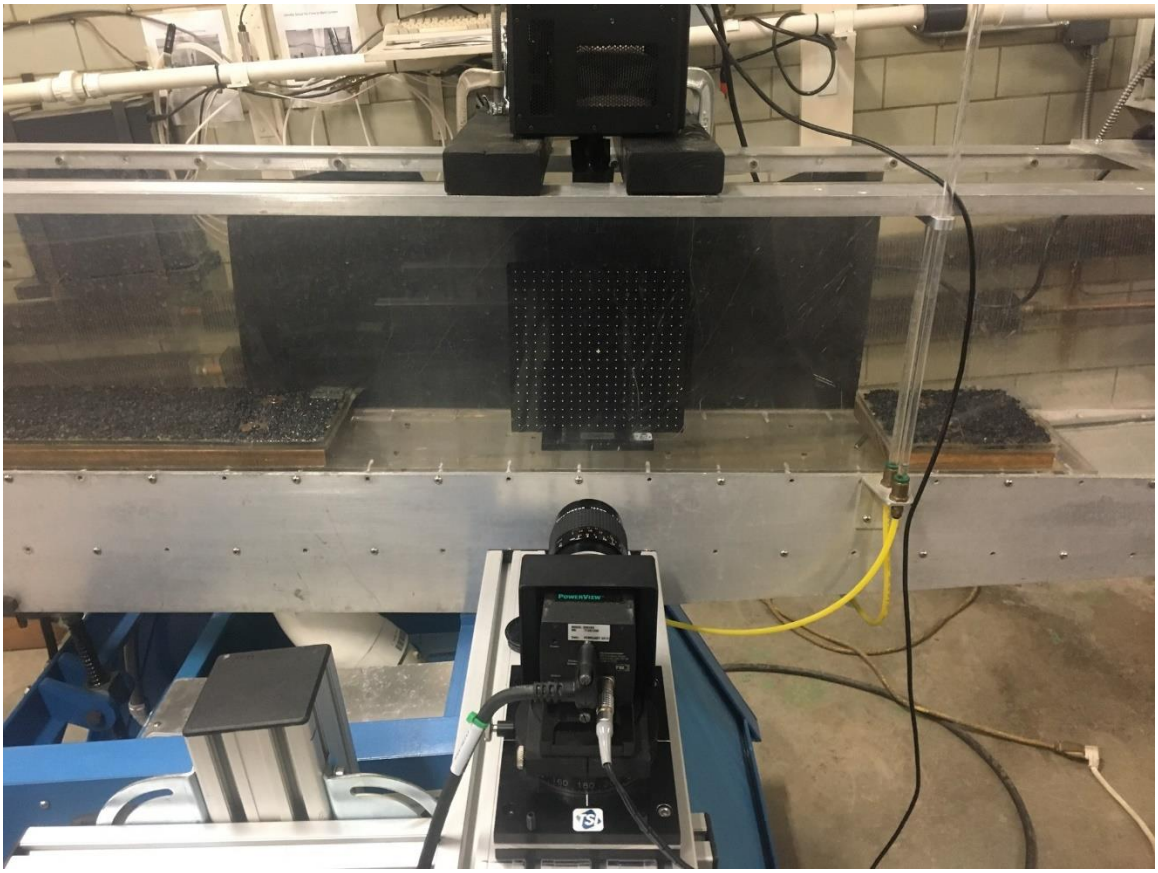

Figure 3.29 LED Illuminator, PIV Camera, and calibration target set up

5. The water pump was started to fill the hydraulic channel for calibration with the target submerged.
6. The PIV camera was focused on the target using Aperture F 2.8.
7. The slope difference between the camera and hydraulic channel was checked using the calibration target and minimized by adjusting the camera mount.
8. A calibration Image was captured and calibrated using the ‘Measure’ function in the PIV Insight program.

9. The distance between adjacent dots on the calibration target was measured 8 times and averaged (twice along the Top, Bottom, Left, and Right side of the image of the calibration target) to determine the calibration factor in mm/pixel.
10. The gravel bed and sediment recess were re-installed in the channel for the PIV measurements.

Chapter 4
Results

4.1 Soil Erosion Tests

Soil erosion rate testing was conducted in an A-8 Hydraulic Channel in the Fluid Mechanics Laboratory at South Dakota State University. A gravel bed was constructed by gluing a single layer of fine gravels with a d_{50} of 5.6 mm to acrylic sheets and secured them to the flume floor using metal screws and floor inserts. The fixed gravel bed had a 2.75-inch (69.85mm) diameter recess for housing a soil sample. The objective of the tests was to determine if there is a correlation between the sediment erosion rate and unconfined compressive strength. The open channel flow created a logarithmic velocity profile over the bed, and the gravel increased the bed roughness, which in turn would increase the fluctuating bed shear stress acting on the soil specimen. A rough bed would also reduce the effect of the soil sample on the flow and maintained a more consistent fluctuating bed shear stress on the soil surface as the sample eroded. A summary of the test results is presented in Appendix B.

Figure 4.1 A-8 Hydraulic Channel

Figure 4.2 Soil sample at start of erosion test

The soil sample was trimmed to approximately the same level as the top of the fixed gravel bed in the hydraulic channel. The height of the trimmed sample was about 1.5 inches (38.1mm), and its diameter was about 2.75 inches (69.85mm). After its mass was measured, the sample was placed in the sediment recess in the fixed gravel bed. The slope of the channel was set using a digital inclinometer. The flow and a timer were started, and the test was stopped before the soil sample was eroded to the same level as the base of the surrounding gravel bed.

Figure 4.3 Soil sample after erosion test is complete

The eroded soil sample was then extracted from the sediment recess and its mass was measured. The soil was dried to determine the dry mass of the sample. The dry mass of the sample before the test was determined during the soil preparation and unconfined compressive strength test. The dry mass before erosion test and after, and the difference between the two, was used to calculate the average erosion rate.

$$\dot{z} = \frac{l}{t} \tag{4.1}$$

where $\dot{z}$ is the average erosion rate (mm/hr.); l is the estimated length of the soil sample eroded (mm); and t is the time elapsed (hours).

The estimated length of the eroded soil was found by taking the difference between the dry mass before erosion ($M_{0,\,Dry}$) and the dry mass after erosion ($M_{f,\,Dry}$) and calculating the percentage of the soil specimen that had been eroded. The percentage change was used to find the erosion rate:

$$\dot{z} = \frac{H_0 * \%\ of\ soil\ eroded}{t} \tag{4.2}$$

where H_0 is the initial height of the soil specimen (inches); and t is the time elapsed (minutes). The result was then converted into the units of mm/hr.

The results from the erosion tests are summarized in Appendix B. Figures 4.4 to 4.6 present the results for the average measured erosion-rate-versus-unconfined compressive strength for three different ranges of bed shear stress values, and Figures 4.7 to 4.9 present results for the same tests, but for average measured erosion-rate-versus-water-content. Each data point is the result of one soil erosion test conducted under one flow condition in the hydraulic channel.

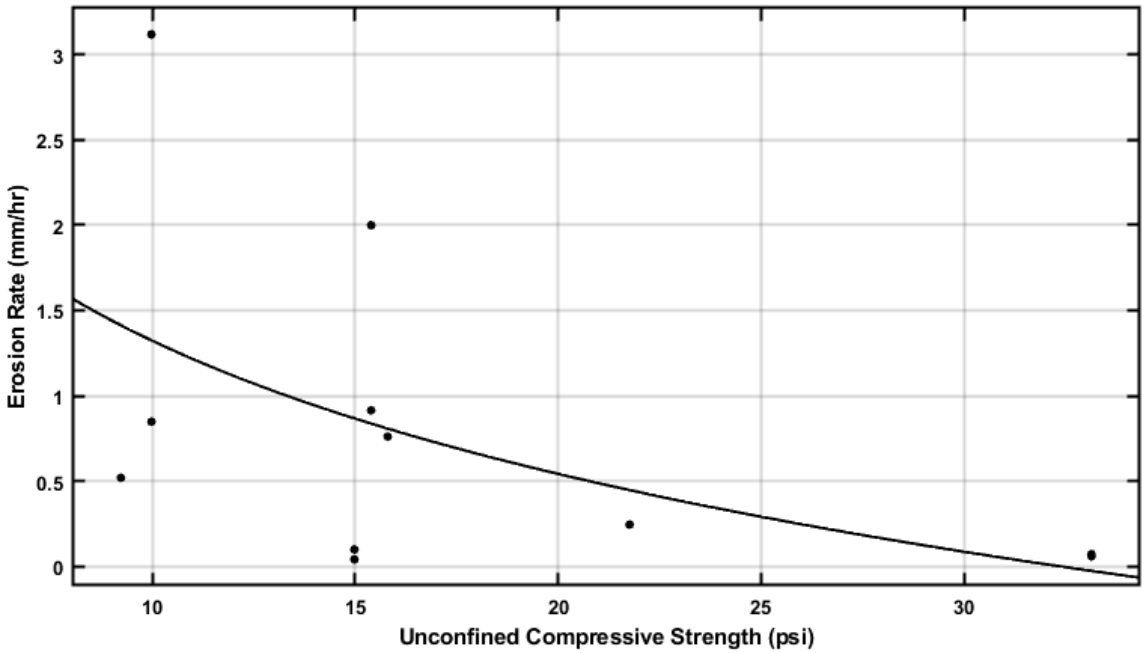

Figure 4.4 Erosion Rate vs Unconfined compressive strength for $\tau_b < 16$ N/m^2

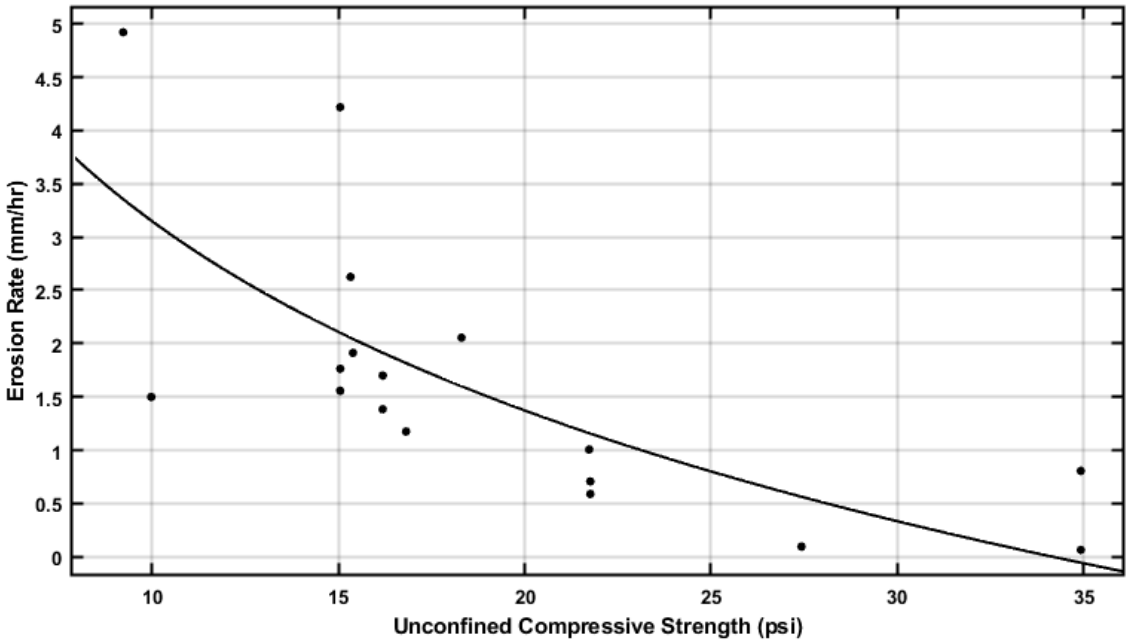

Figure 4.5 Erosion rate vs unconfined compressive strength for $16 < \tau_b < 19.5$ N/m^2

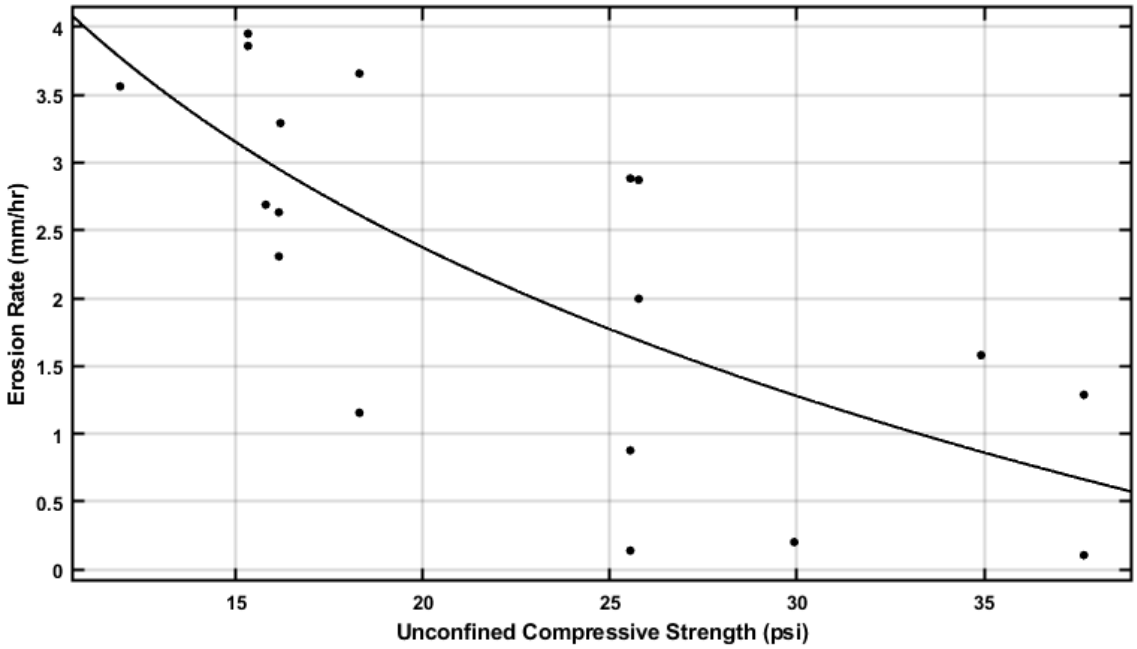

Figure 4.6 Erosion rate vs unconfined compressive strength for $\tau_b > 19.5$ N/m^2

The results were separated into three bed shear stress ranges. The lowest bed shear stress range, $\tau_b < 16$ N/m^2, produced results with the weakest correlation due to the critical shear stress of some of the soil specimens being greater than the applied bed shear stress resulting in little or no soil erosion.

The results were more consistent for the bed shear stress greater than 19.5 N/m^2. This is the range in which the soil specimens consistently had a critical shear stress that was much less than the applied bed shear stress. The soil specimens that were tested with a bed shear stress between 16 and 19.5 N/m^2 showed a similar trendline and slope to the data with a bed shear stress greater than 19.5 N/m^2.

Soil samples with similar unconfined compressive strength measurements were found to sometimes produce a wide range of erosion rates. This could be due to the variation in surface roughness and erosion pattern, as these were the two parameters that

could not be controlled during the tests. This is especially true when the bed shear stress is greater than 19.5 N/m^2 (See Figure 4.6). These soil samples had estimated bed shear stress results that were as high as 24 N/m^2. The wide range of bed shear stress values could result in large variations in the average erosion rates.

The strongest correlation between measured bed shear stress and unconfined compressive strength was found in the bed shear stress range greater than 19.5 N/m^2, with an R^2 = 0.527 and RMSE = 0.9265, producing a relationship of:

$$\dot{z} = -2.7 \ln(Q_u) + 10.5$$

Similarly good correlation was also found in the bed shear stress range between 16 and 19.5 N/m^2, with R^2 = 0.5207 and RMSE = 0.9273, producing a relationship of:

$$\dot{z} = -2.56 \ln(Q_u) + 9.05$$

The weakest correlation, with an R^2 = 0.2594 and RMSE = 0.8774, was found when the bed shear stress was less than 16 N/m^2, and the relationship is given by:

$$\dot{z} = -1.125 \ln(Q_u) + 3.9$$

The unconfined compressive strength was changed during the preparation of each sample by varying the moisture content of the soil. The moisture content results for the average erosion-rate-versus-water-content for three different ranges of bed shear stress experiments are presented in a similar way as the unconfined compressive strength results as follows:

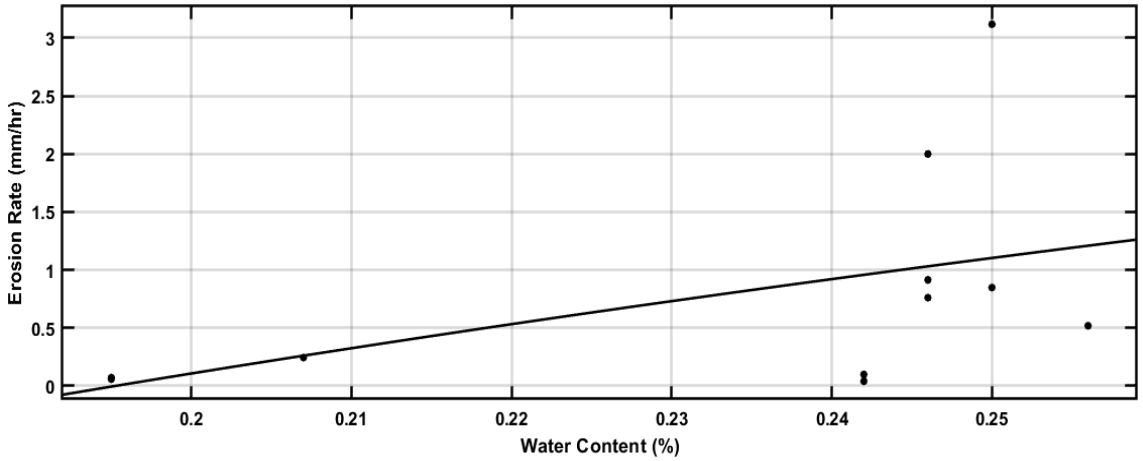

Figure 4.7 Erosion Rate vs. water content for $\tau_b < 16$ N/m^2

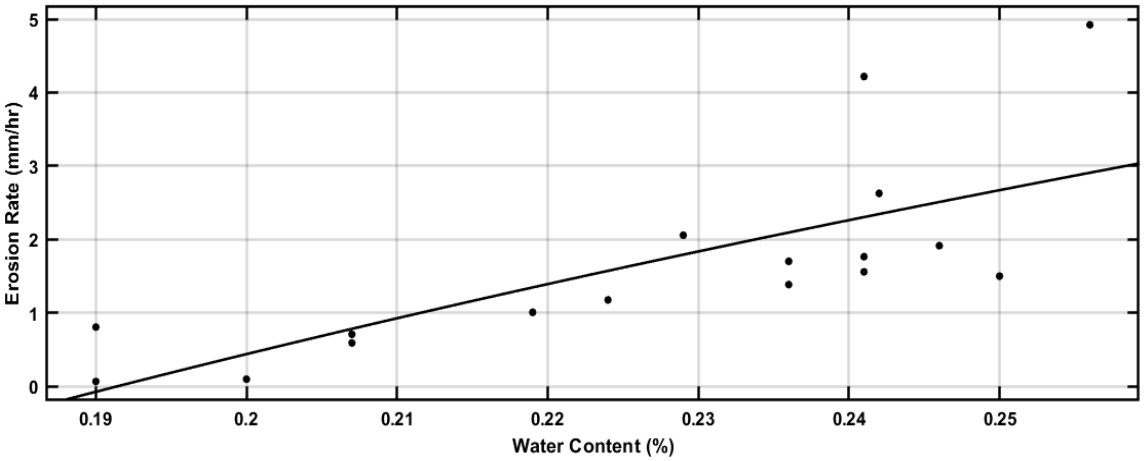

Figure 4.8 Erosion rate vs. water content for $16 < \tau_b < 19.5$ N/m^2

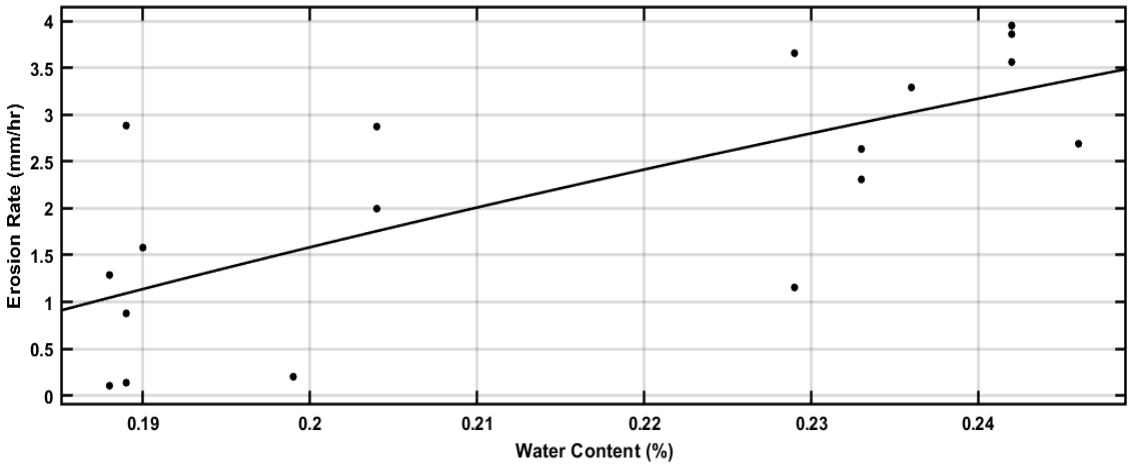

Figure 4.9 Erosion rate vs. water content for $\tau_b > 19.5$ N/m^2

The erosion-rate-versus-water-content results produced similar correlations as the erosion-rate-versus-unconfined-compressive-strength results as shown in the following:

The strongest correlation between measured bed shear stress and water content was found in the bed shear stress range greater than 19.5 N/m^2, with an $R^2 = 0.5263$ and RMSE = 0.9272, producing a relationship of:

$$\dot{z} = 8.7 \ln(w) + 15.6$$

The bed shear stress between 16 and 19.5 N/m^2 also resulted in good correlation, with and $R^2 = 0.542$ and RMSE = 0.907, producing a relationship of:

$$\dot{z} = 10 \ln(w) + 16.54$$

The weakest correlation, with an $R^2 = 0.23$ and RMSE = 0.895, were the results from when the bed shear stress was less than 16 N/m^2 which had a relationship of:

$$\dot{z} = 4.46 \ln(w) + 7.3$$

These results suggest the soil erosion rate may be related to either the unconfined compressive strength or water content.

The applied bed shear stress in each erosion test was also related to the measured erosion rate for different ranges of unconfined compressive strength.

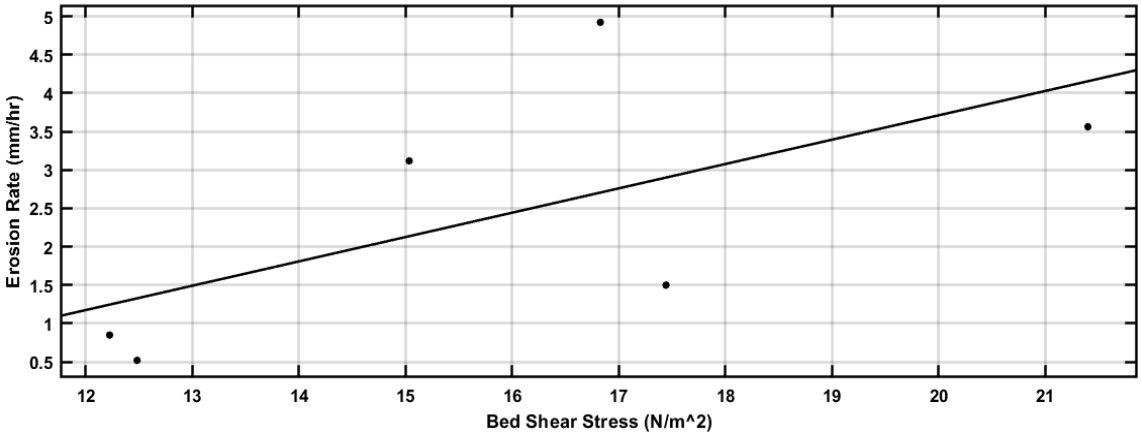

Figure 4.10 Erosion Rate vs. Bed Shear Stress for Q_u < 12psi

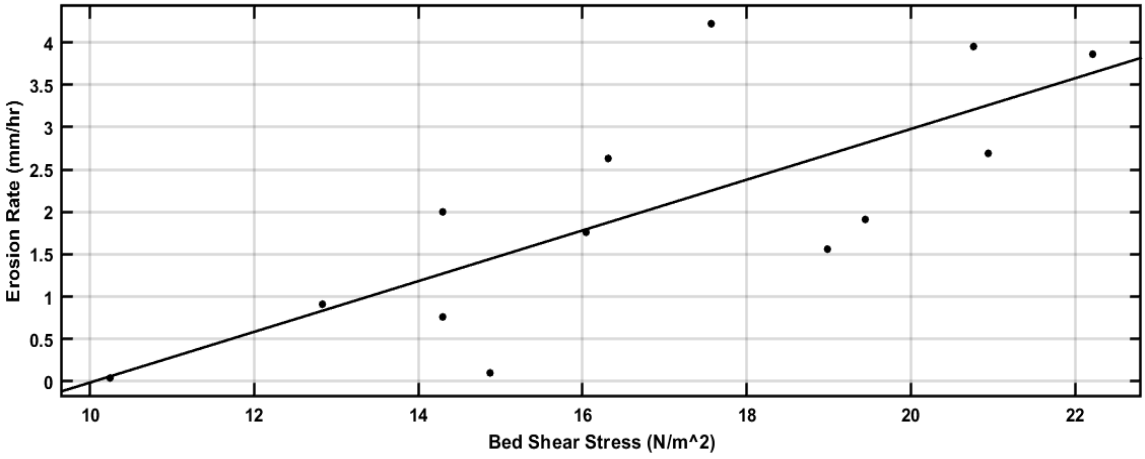

Figure 4.11 Erosion Rate vs Bed Shear Stress for 12 psi < Q_u < 16psi

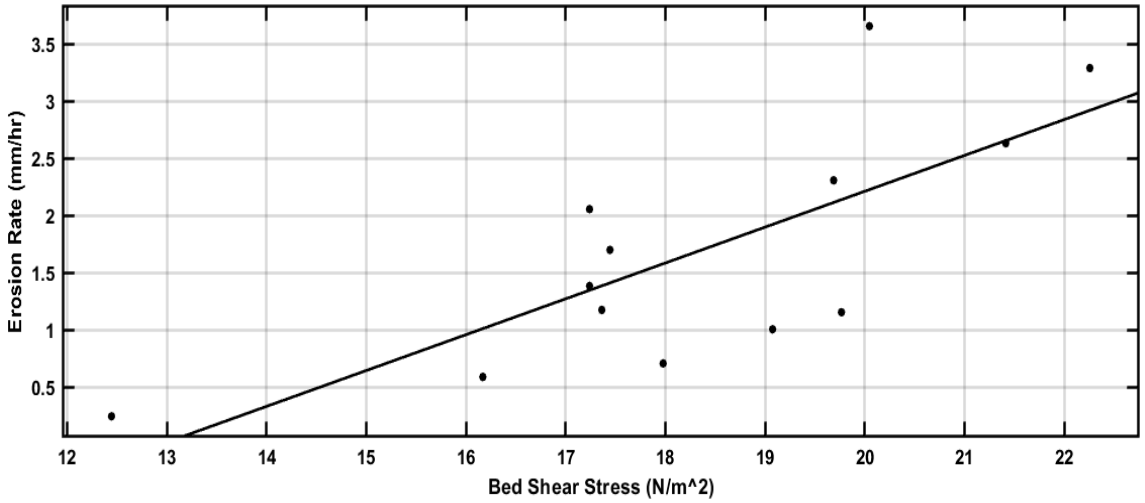

Figure 4.12 Erosion Rate vs Bed Shear Stress for 16psi < Q_u < 22psi

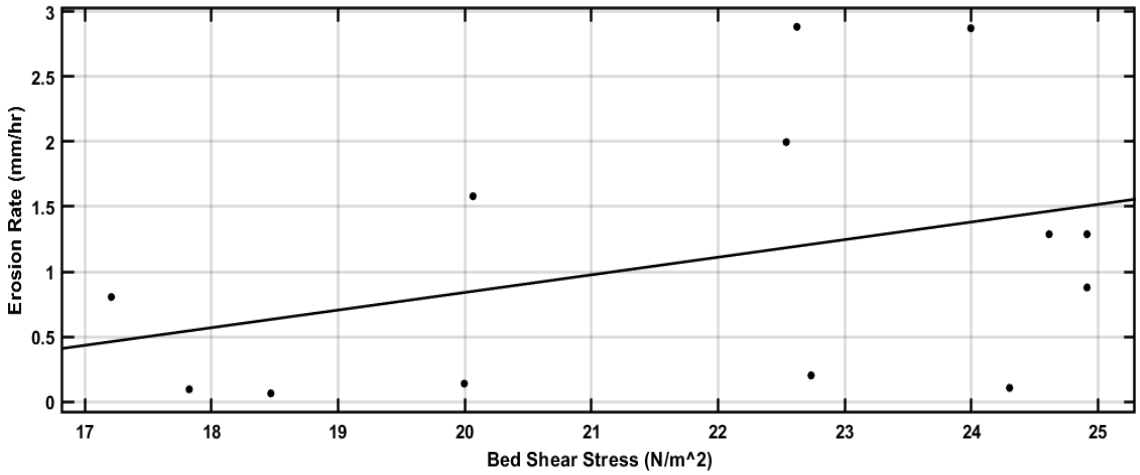

Figure 4.13 Erosion Rate vs Bed Shear Stress for Q_u > 22psi

The results are separated into four different unconfined compressive strength ranges. The strongest correlations were found for soils samples with an unconfined compressive strength between 12 and 16 psi, and between 16 and 22 psi. Soil specimens that had an unconfined compressive strength less than 12 psi and greater than 22 psi had the least consistent results. As discussed, this could be due to the critical shear stress being greater than the shear stress exerted by the flow or variations in unconfined compressive strength and configuration of the eroding surface. Different forms of equations were fit to each data set. A straight-line fit was found to produce the most consistent results for the critical shear stress.

The soil specimens with an unconfined compressive strength less than 12 psi had an estimated critical shear stress of 8.3 N/m^2, and a best straight-line-fit with an R^2 value = 0.3989 and RMSE = 1.5.

$$\dot{z} = 0.317\tau_b - 2.632$$

The soil specimens with an unconfined compressive strength between 12 and 16 psi had an estimated critical shear stress of 10.05 N/m^2, and a best straight-line-fit with an R^2 value = 0.5727 and RMSE = 0.9552.

$$\dot{z} = 0.3\tau_b - 3.01$$

The soil specimens with an unconfined compressive strength between 16 and 22 psi had an estimated critical shear stress equal to 12.95 N/m^2, and a best straight-line fit with an R^2 value = 0.5643 and RMSE = 0.7234.

$$\dot{z} = 0.3134\tau_b - 4.06$$

The soil specimens with an unconfined compressive strength greater than 22 psi had an estimated critical shear stress equal to 13.8 N/m^2, and a best straight-line fit with an R^2 value of 0.1406 and RMSE = 0.9827.

$$\dot{z} = 0.1355\tau_b - 1.87$$

The critical shear stress was found by extrapolating the best-fit line to where ż was equal to zero. The estimated critical shear stress increases as the unconfined compressive strength of the soil increases.

The erosion of the clay sample was not smooth or uniform. The specimens eroded in chunks and irregular patterns. Below are a few examples of how the soil samples had eroded. Some of the clay specimens eroded in blocks or chunks creating a deep hole in the soil surface. The holes then created a change in bed configuration, which would produce non-uniform bed shear stresses. The average shear stress on the soil surface was investigated using the Particle Image Velocimetry in the next section.

Figures 4.14 to 4.19 show an erosion pattern developing from downstream to upstream in one test. The soil sample had an unconfined compressive strength of 10 psi, and the estimated bed shear stress was 12.23 N/m^2.

Figure 4.14 Beginning of erosion test

Figure 4.15 About 1-hour after start of erosion test

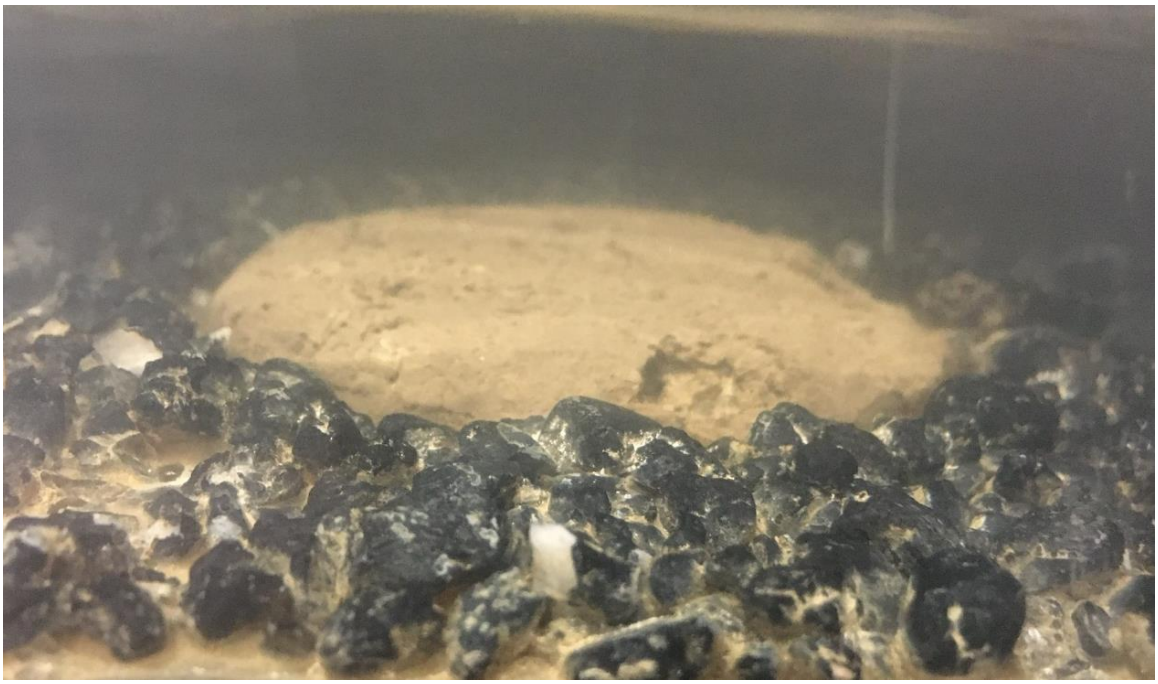

Figure 4.16 About 2-hours after start of erosion test

Figure 4.17 About 3-hours after start of erosion test

Figure 4.18 About 4-hours after start of erosion test

Figure 4.19 Final erosion depth after about 5-hours

The following images show some examples of other erosion patterns observed in the erosion tests.

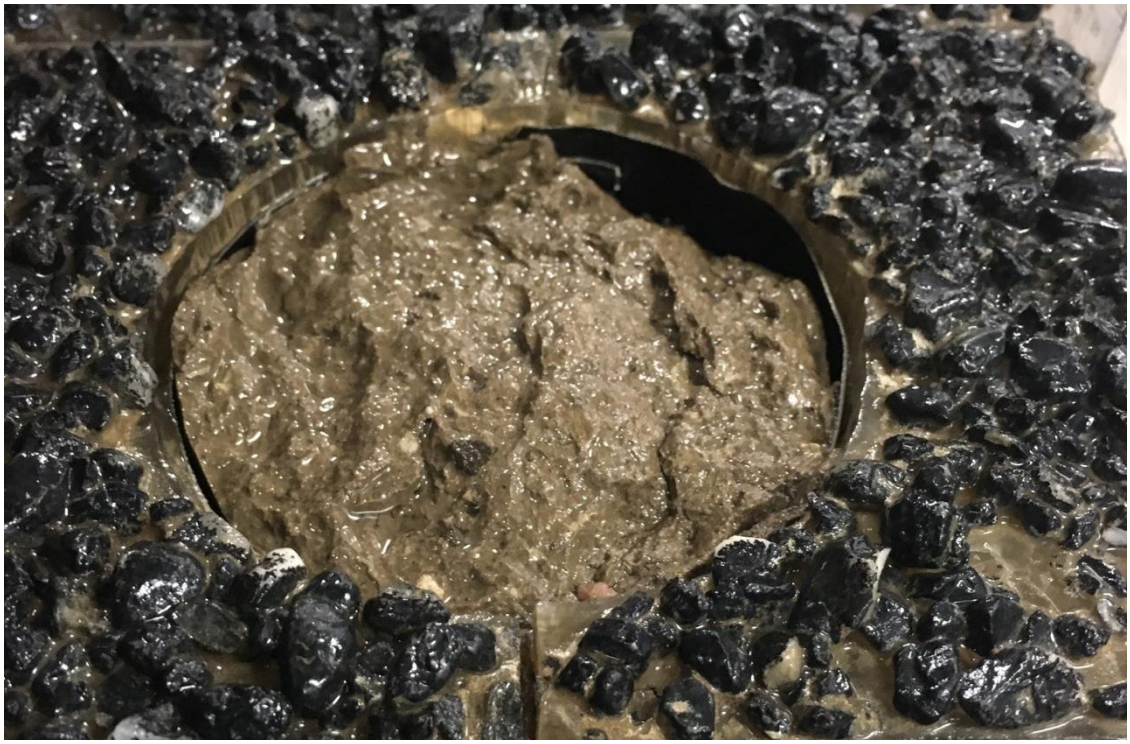

Figure 4.20 Example of a wavy erosion pattern from front to back

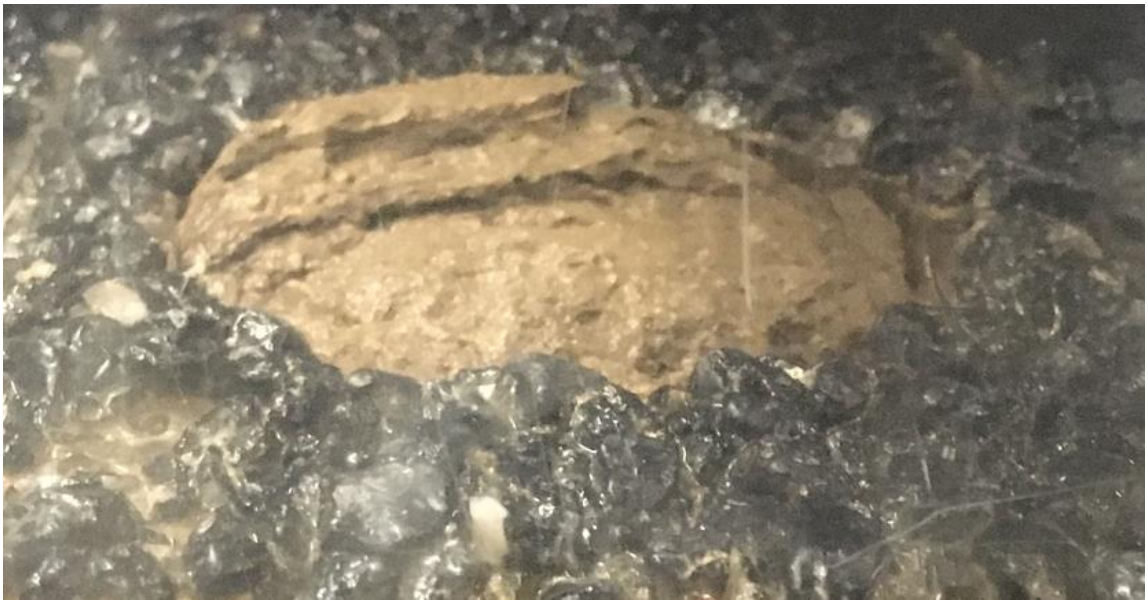

Figure 4.21 Example of block erosion pattern from side-to-side

Figure 4.22 Example of Cone shaped erosion pattern

Figure 4.23 Example of a non-uniform erosion pattern in the downstream portion of soil sample

Figure 4.24 Example of little-to-no Erosion

4.2 Particle Image Velocimetry Measurements on a Fixed Gravel Bed

Particle Image Velocimetry (PIV) measurements were conducted on a fixed bed made of a single layer of gravel with a d_{50} of 5.6 mm in the A-8 Hydraulic Channel. The objective of the PIV measurements was to measure the time-averaged velocity profile over the gravel bed and use the measured data to estimate the bed shear stress using the logarithmic law. The results showed that the bed shear stress estimates are in good agreement with the values obtained from the measured flow depth and channel slope when the equivalent grain diameter is approximated by d_{84} or smaller.

The procedure for operating the camera and LED Illuminator as well as channel bed set up is described in Section 3.7. The plane of PIV measurements was located 7.5 cm from the side wall closest to the camera. Figure 4.25 shows the experimental set up for the PIV camera and LED illuminator with the fixed gravel bed installed in the hydraulic channel.

After uniform flow was established, the flow depth was measured using a point gauge approximately 42 cm upstream from the center of the test area. In each run, two hundred (200) straddled frames (frames A and B) were captured at a sampling rate of 7.25 Hz. Ensemble correlation processing was performed on all 200 images to obtain the mean velocity field. Spatial averaging was then conducted on the mean velocity field to obtain a time- and space-averaged velocity profile for finding the bed shear stress.

The false bottom with the gravel bed was secured to the smooth acrylic channel using metal screws and in-floor inserts. The false bottom had a height of about 1.5-inches (38.1mm) from the top of the rock to the bottom of the wood base. The channel width

was 6-inches (152.4mm) and the average discharge rate for the water flowing over the gravel bed was 0.1580 $ft.^3/s$ (4.5 L/s).

PIV measurements were taken at six different slopes in 11 tests to cover a wide range of bed shear stress values. Each test contained 3 or 4 consecutive runs. The PIV measurements were typically taken with the fixed gravel bed in the lower part of the PIV camera's FOV and the free surface just above the top of the captured images. Five of the six flow conditions were repeated as shown in Table 4.2. Two hundred (200) velocity vector fields were captured in each run except for Test 5 where 100 images were captured.

After the PIV images were taken for each test, the data was processed using the *INSIGHT 4G™* software by TSI. An ensemble correlation velocity field was created with the dimensions of the interrogation regions being 64 pixels x 32 pixels with a 50% overlap. The spatial resolution was approximately 0.53 mm in the streamwise direction and 0.27 mm in the vertical direction. A plot of the measured velocity filed using Tecplot is shown in Figure 4.27. The ensemble correlation velocity field has 56 vector columns but only every three columns are displayed in Figure 4.27 for clarity. The dashed line marks the very top of the gravel bed within the FOV. There is flow within the gravel bed below the dashed line. Missing vectors were interpolated from the neighboring vectors. The free surface in Figure 4.27 is located above but close to y = 30 mm.

The different runs in each test performed during the experiment were averaged to obtain an ensemble- and space-averaged (average) velocity profile. Typically, the runs that were averaged had good repeatability and plotted similarly to one another.

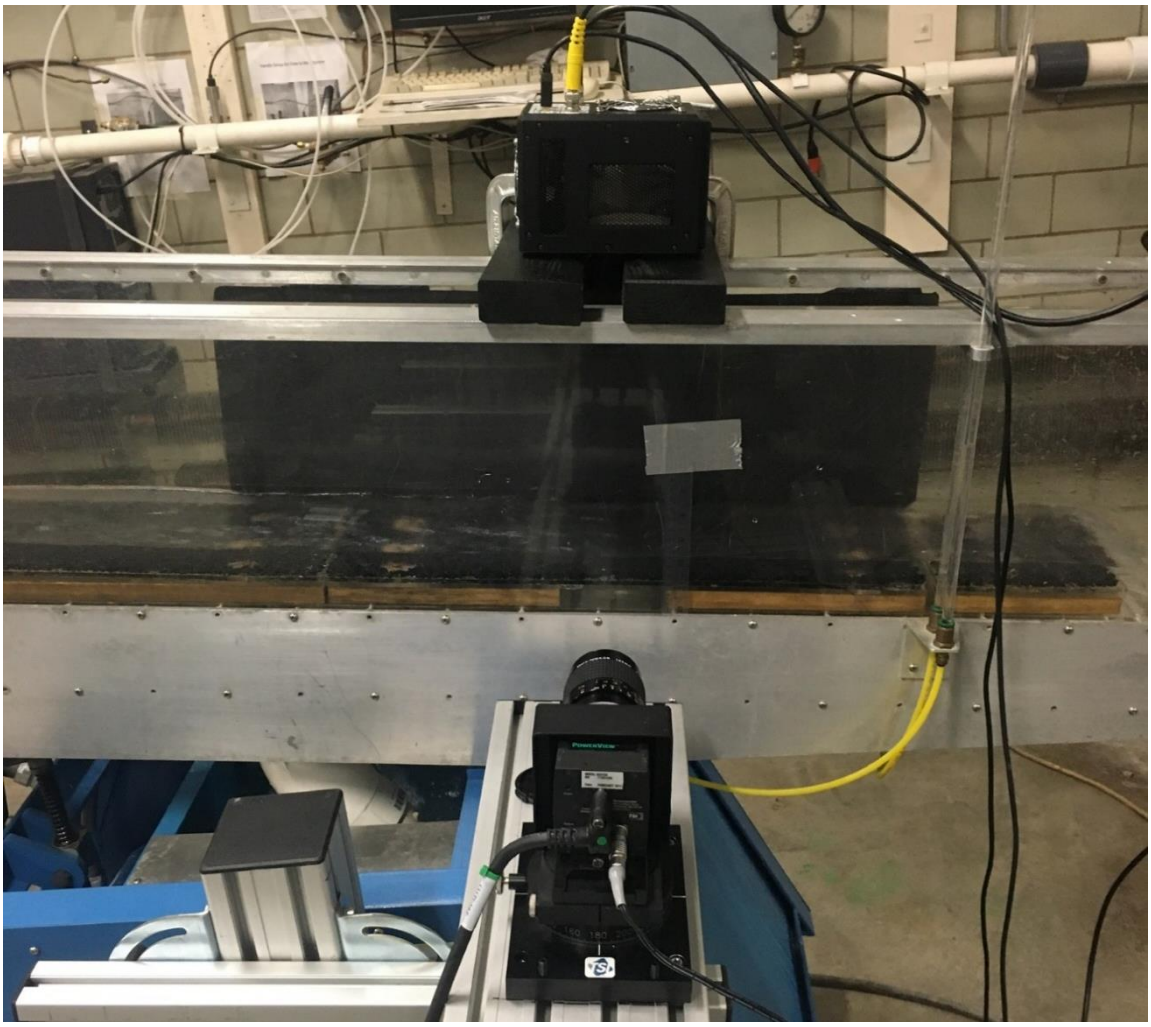

Figure 4.25 Fixed gravel bed PIV measurement set up

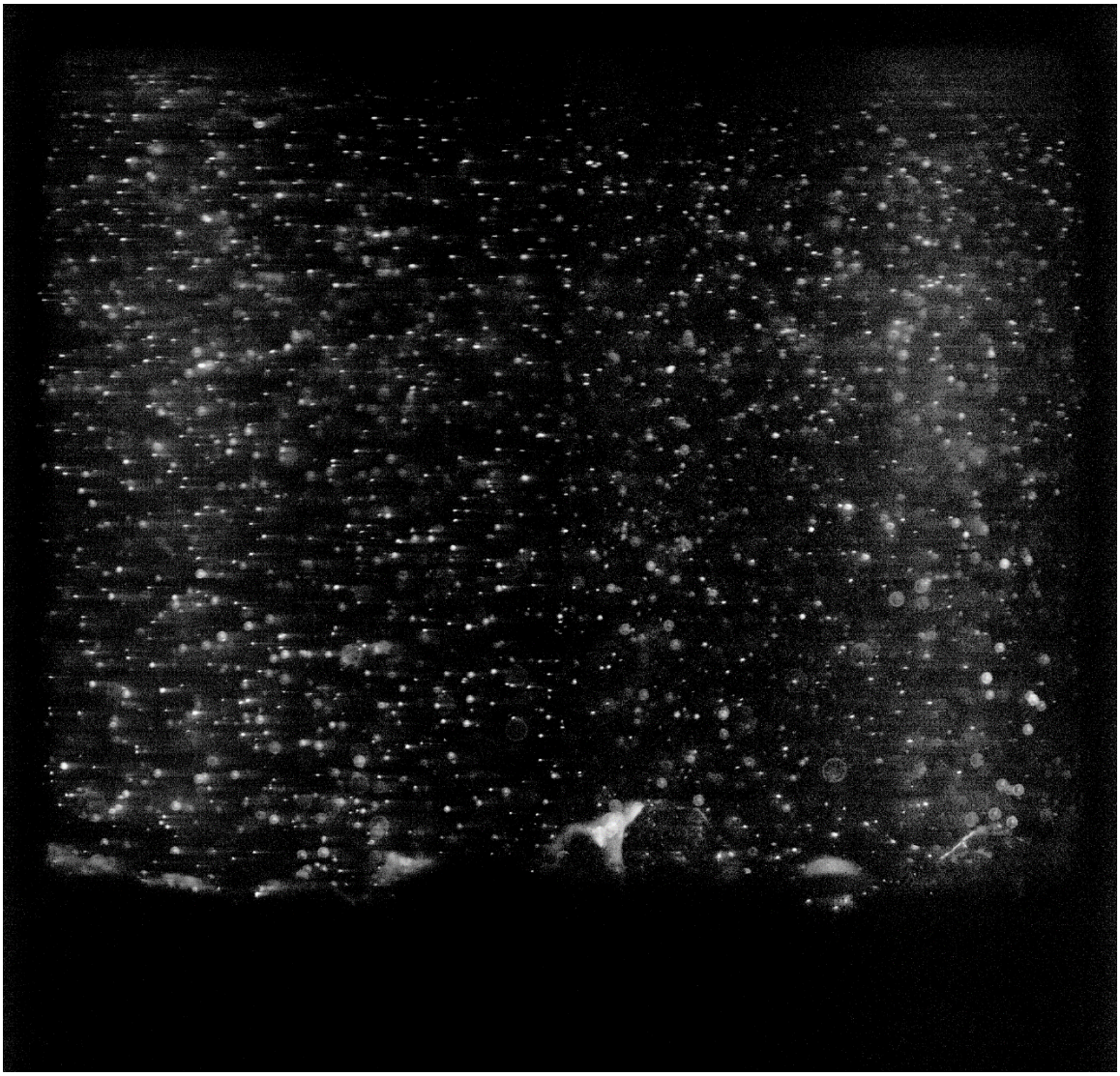

Figure 4.26 Example PIV image from fixed gravel bed

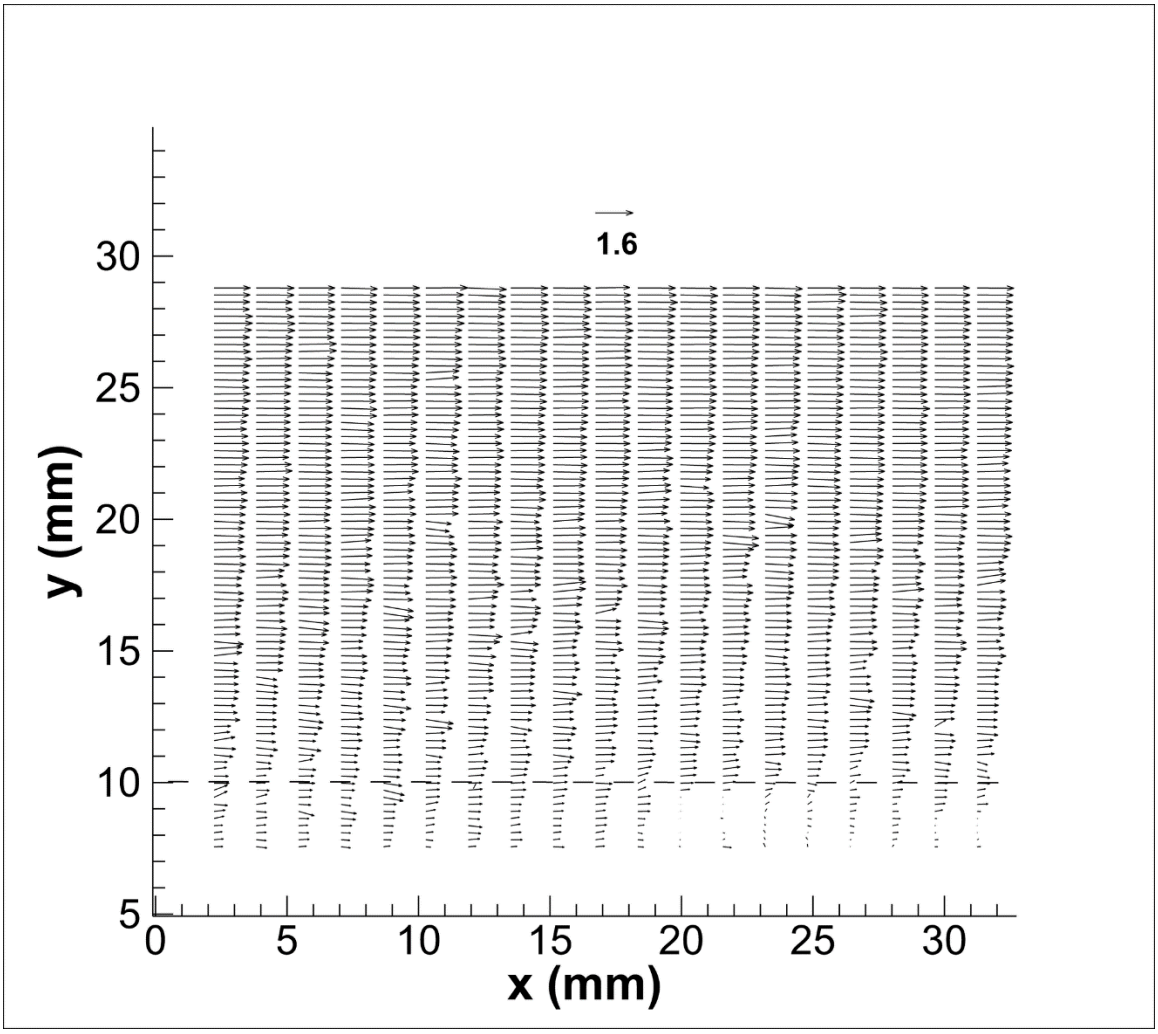

Figure 4.27 Measured velocity profile from Test 8, Run 1

The side-wall correction method, described in Section 3.6, and log-law method described below were employed to find the bed shear stress in each test.

Test	Q (L/s)	S	T (°C)	h (mm)	h_e (mm)	V (m/s)	V_1 (m/s)	f_b	R_b (mm)	τ_{b1} (N/m^2)
1 (4)	4.5	0.02	26	39.1	36.3	0.808	0.782	0.0764	31.8	6.22
2 (4)	4.5	0.02	27	39.4	36.6	0.803	0.795	0.0782	32.1	6.28
3 (4)	4.5	0.04	27	32.5	29.7	0.988	0.988	0.0866	26.9	10.53
4 (4)	4.5	0.04	27	32.5	29.7	0.988	0.995	0.0866	26.9	10.53
5 (3)	4.5	0.05	23.5	30.5	27.7	1.061	NA	0.0881	25.3	12.35
6 (4)	4.5	0.06	27	29.6	26.8	1.096	1.098	0.0969	24.7	14.49
7 (4)	4.5	0.06	27	29.6	26.8	1.096	1.103	0.0969	24.7	14.49
8 (4)	4.5	0.08	24	26.8	24.00	1.223	1.139	0.0933	22.2	17.40
9 (4)	4.5	0.08	28	26.9	24.1	1.22	1.18	0.0941	22.3	17.44
10 (4)	4.5	0.10	27	25.4	22.6	1.299	1.309	0.0982	21.1	20.64
11 (4)	4.5	0.10	27	24.4	22.6	1.299	1.304	0.0982	21.1	20.64

Table 4.1 Summary of flow parameters for each test

In Table 4.1, the velocity, V, is the cross-sectional average velocity computed from the measured discharge and flow depth, while the velocity, V_1, was obtained from the PIV measured velocity profile and is the depth-averaged velocity. In parenthesis in the first column of Table 4.1 is the number of runs that were ensemble-averaged in each test. The bed shear stress, τ_{b1}, was found by using:

$$\tau_{b1} = \rho g R_b S \tag{4.3}$$

where ρ is the fluid density (kg/m^3); g is the acceleration due to gravity (m/s^2); R_b is the bed-related hydraulic radius (m); and S is the channel slope (m/m). Equation 4.3 is used for steady, uniform flows. The sidewall correction method was used to estimate the bed related friction factor, f_b, and hydraulic radius, R_b as described in Section 3.6.

The method described in Ting and Kern (2021) is used to obtain the bed shear stress from the average velocity profile. The method assumes that the von Kármán constant is a universal constant with a value equal to 0.4 and the equivalent grain

roughness, k_s, is known. The procedure for finding τ_b is briefly described using Figures 4.28 through 4.30, and Table 4.2. For more details about the procedure and the results the interested reader is referred to Ting and Kern (2021).

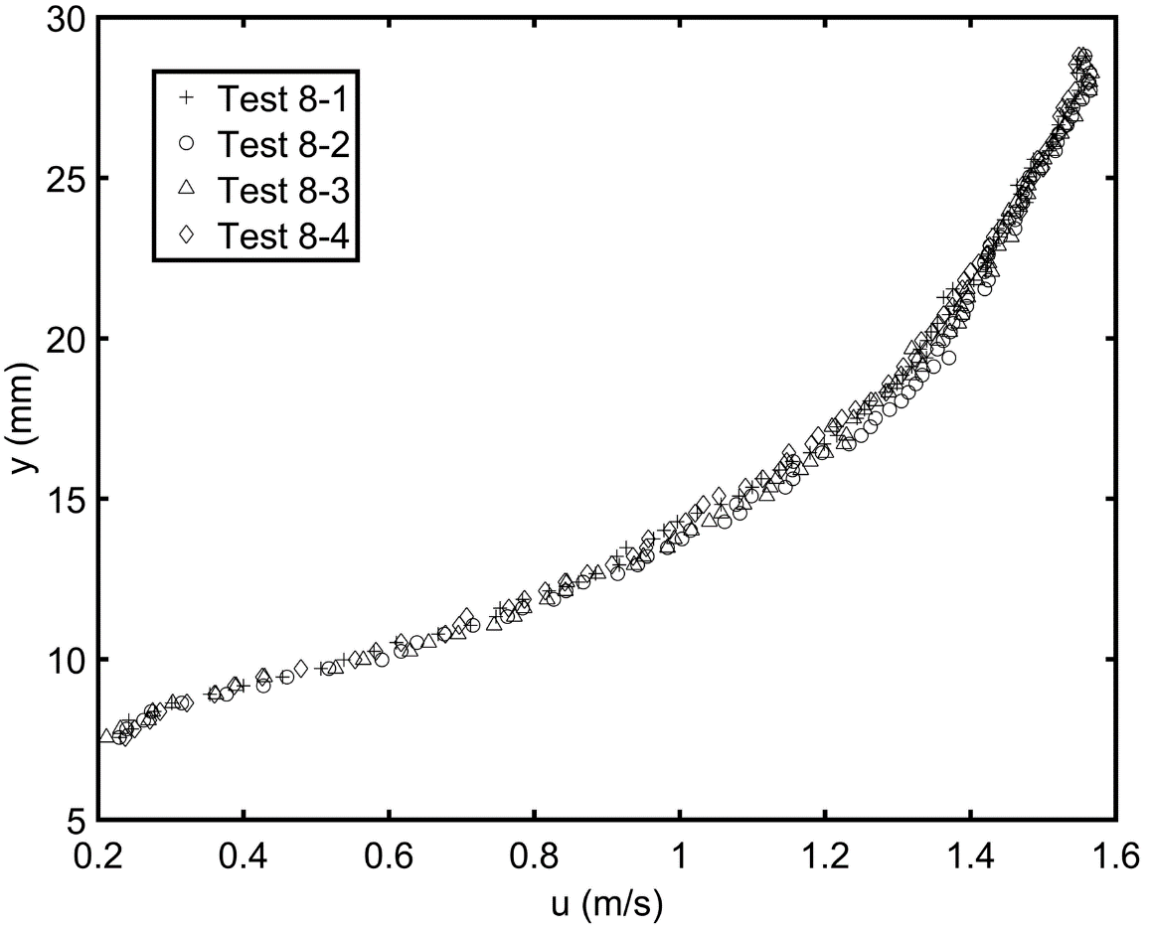

Figure 4.28 Time- and space-averaged velocity profiles from Test 8, Runs 1 to 4

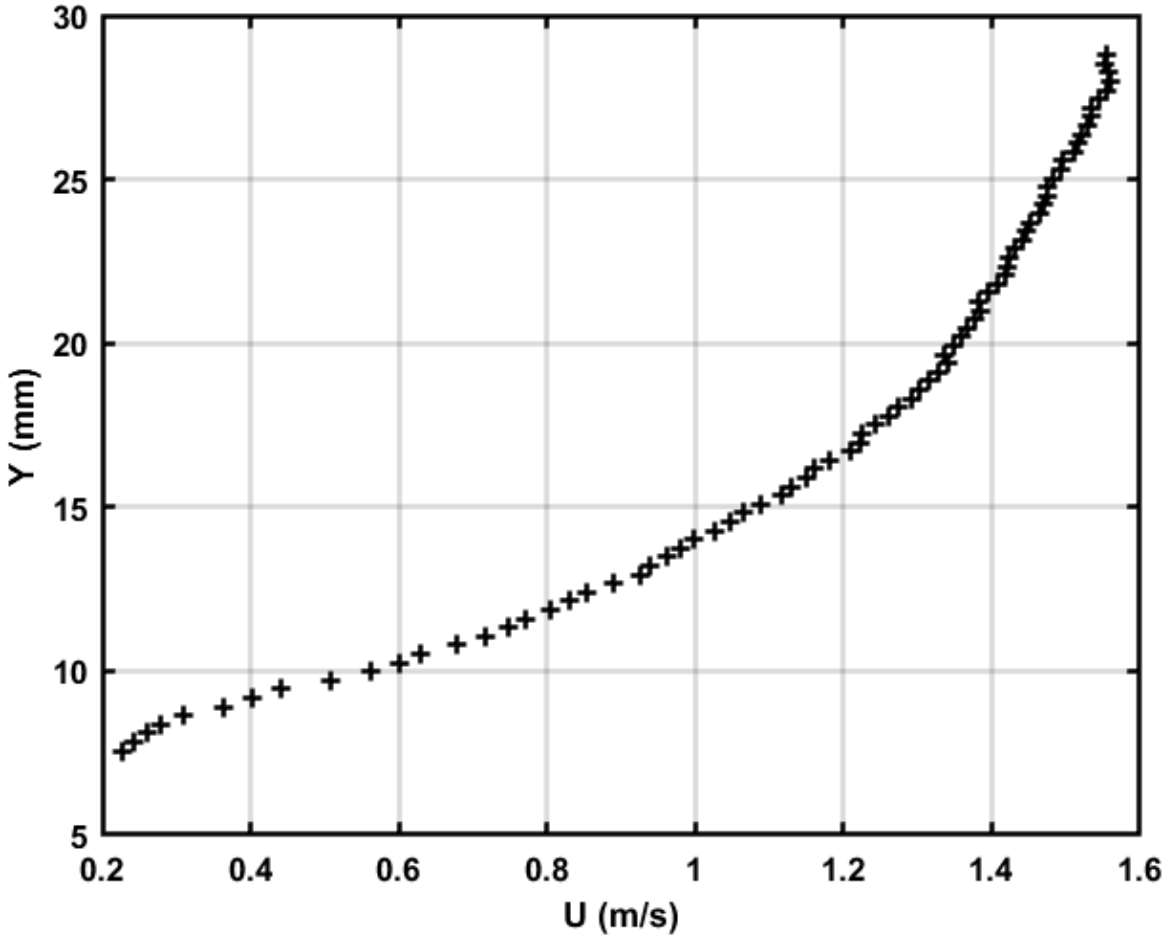

Figure 4.29 Average profile from Runs 1 to 4 in Test 8

Figure 4.28 displays the time- and space-averaged velocity profiles from four runs conducted consecutively in Test 8. The measured velocity profiles show good repeatability and were averaged to produce a single average velocity profile for finding the bed shear stress, as shown in Figure 4.29.

The average velocity profiles are then graphed on a $\ln(y-y_0)$ versus u plot, as shown in Figure 4.30, and the displacement height (which denotes the virtual bottom), y_0, is varied until the von Kármán constant obtained from the y-intercept of the best straight-line fit to Equation 4.4, is equal to 0.4.

$$\ln(y - y_0) = \frac{k}{u^*}u + (ln(k_s) - kB) \tag{4.4}$$

In Eq. (4.4), k/u* is the slope of the fitted straight line; $\ln(k_s)$-kB is the y-intercept; and B has a value of 8.5 for a fully developed turbulent flow over a bed of uniform grains (e.g., Middleton and Southard, 1984).

Table 4.2 shows how the virtual bottom is varied to find the correct bed shear stress using the average velocity profile shown in Figure 4.29. This test had a measured water temperature of 24 °C and an average water depth of 1.055 inches (26.8 mm). Typically, the points used for the log-law curve fitting method are taken to be no higher than 20 to 30% of the flow depth above the channel bed. The lower bound is set away from any direct influence of the roughness of the bed. In Test 8, point number 30 was used as the conservative upper bound of the lower 30% of the log-law curve fitting. Test 8 also has part of its velocity profile plotted below the top of the gravel indicated by the dashed line at y =10 mm in Figure 4.27. This eliminates the lower 10 data points for use in curve fitting. Therefore, the log-law region was assumed to lie somewhere between points 10 and 30.

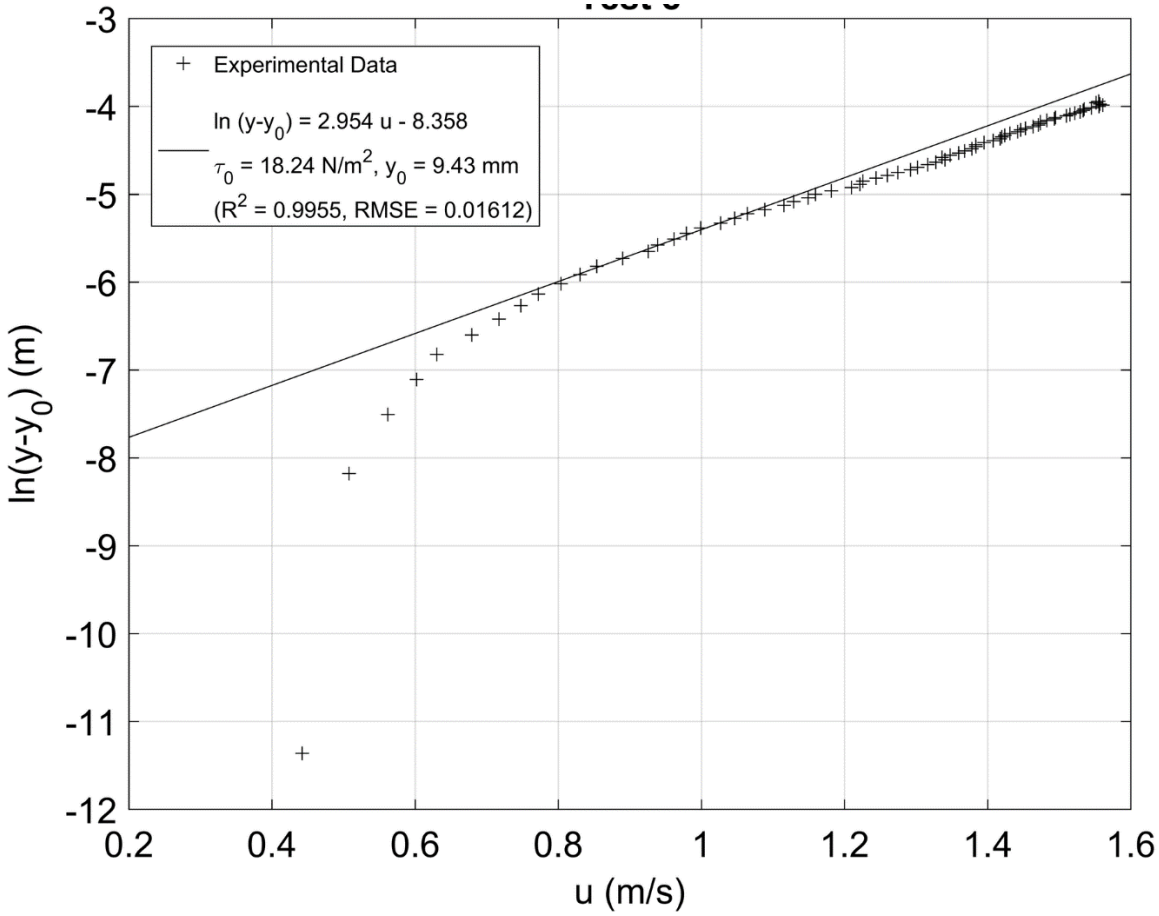

Figure 4.30 Semi-log plot for Test 8

(1) y_0 (mm)	(2) $\boldsymbol{a}$ =k/u*	(3) $\boldsymbol{b} = \ln(k_s) - 8.5k$	(4) u* = k/a (m/s)	(5) $k_s = e^{(8.5k+b)}$ (mm)	**(6) τ_{b2} = $\rho(u^*)^2$ (N/m²)**	(7) R^2	(8) RMSE	(9) k_s (mm)	(10) $k = \frac{(ln(k_s) - b)}{8.5}$	(11) u* = k/a (m/s)	**(12) τ_{b2} = $\rho(u^*)^2$ (N/m²)**
9.1	2.718	-8.051	0.1472	9.55	**21.60**	0.9957	0.01453	7	0.36	0.1337	**17.83**
9.2	2.786	-8.139	0.1436	8.75	**20.56**	0.9956	0.01496	7	0.37	0.1342	**17.95**
9.3	2.856	-8.232	0.1401	7.97	**19.56**	0.9956	0.01543	7	0.38	0.1347	**18.10**
9.4	2.931	-8.328	0.1365	7.24	**18.57**	0.9955	0.01595	7	0.40	0.1351	**18.21**
9.43	**2.954**	**-8.358**	**0.1354**	**7.03**	**18.29**	**0.9955**	**0.01612**	**7**	**0.40**	**0.1353**	**18.24**
9.5	3.01	-8.43	0.1329	6.54	**17.61**	0.9954	0.01652	7	0.41	0.1356	**18.33**
9.6	3.093	-8.536	0.1293	5.88	**16.68**	0.9953	0.01717	7	0.42	0.1359	**18.43**
9.65	3.136	-8.591	0.1276	5.57	**16.23**	0.9953	0.01752	7	0.43	0.1361	**18.49**
9.7	3.181	-8.648	0.1257	5.26	**15.77**	0.9952	0.01788	7	0.43	0.1363	**18.54**
9.8	3.275	-8.766	0.1221	4.67	**14.88**	0.9951	0.01869	7	0.45	0.1367	**18.62**
9.9	3.374	-8.89	0.1186	4.13	**14.02**	0.9949	0.0196	7	0.46	0.1370	**18.71**

Table 4.2 Test 8 Log-law iteration results

Table 4.2 summarizes the results of the iterative process for finding the bed shear stress using the traditional method and an alternative method adopted in this study. The value of y_0 is given in Column (1). For each y_0 value, a plot of $\ln(y-y_0)$ versus u was constructed and a straight line was fitted to the velocity data. The slope, *a*, and y-intercept, *b*, of the best-best fit line are shown in Column (2) and Column (3), respectively. From Eq. (4.4), the friction velocity u* in Column (4) is obtained from the slope of the best-fit line assuming a value of 0.4 for k, and the equivalent roughness, k_s, in Column (5) is obtained from the y-intercept of the best-fit line. The R^2 value of the best-fit line is given in Column (7) and the RMSE in Column (8).

Figure 4.30 presents the semi-log plot of $\ln(y-y_0)$ versus u with the best-fit lines drawn to points 18 to 28 with $y_0 = 9.43$. Columns (5) and (6) in Table 4.2 show how the traditional method of varying y_0 to find the best-fit line would produce a wide range of possible values for τ_b and k_s that are difficult to assess. Table 4.2 shows that τ_b decreases from 21.6 to 14.02 N/m^2 and k_s from 9.55 to 4.13 mm, when y_0 is increased from 9.1 to 9.9 mm. The correct value of τ_b and k_s cannot be determined based on the R^2 values because they are all equal to about 0.995.

A different method is used in this study to select the value of y_0. The procedure is illustrated in columns 9, 10, 11, and 12 in Table 4.3. The method assumes a value of k_s ($d_{84} = 7$ mm in this example) and varies y_0 systematically until the value of k found from the y-intercept of the best-fit line is equal to 0.4. The friction velocity u* is then found from the slope of the best-fit line. For $y_0 = 9.43$ mm, we have:

$$k = \frac{\ln\left(\frac{D_{84}}{1000}\right) - \ln(k_s) - 8.5k}{8.5} \tag{4.5}$$

$$=> \frac{\ln\left(\frac{7}{1000}\right) - (-8.358)}{8.5} = 0.4$$

$$u^* = \frac{k}{\left(\frac{k}{u^*}\right)} \tag{4.6}$$

$$=> \frac{0.4}{2.954} = 0.1353$$

$$\tau_b = \rho(u^*)^2 \tag{4.7}$$

$$=> 996.2 * (0.1353)^2 = \mathbf{18.24\ N/m^2}$$

This method produces a narrow range of τ_b values as y_0 is varied as seen in Table 4.2, column (12). The value of τ_b increases from 17.69 to 18.78 N/m^2, when y_0 is increased from 9.1 to 9.9 mm.

The method used for finding τ_b from the measured velocity profile assumed that the equivalent roughness height was known. Table 4.3 shows the results of a sensitivity analysis where the k_s values was set equal to the d_{50}, d_{65}, and d_{84} of the gravel bed. The sensitivity analysis was conducted for six different channel slopes. Table 4.3 shows that the bed shear stress calculated using the d_{84} value matches the value obtained from the measured flow depth and channel slope, given by τ_{b1}, well, up to a channel slope of about 8%. These results are plotted against each other with a line of perfect fit corresponding to $\tau_{b1} = \tau_{b2}$. The bed shear stress values obtained using the log-law with k_s equal to d_{84} (τ_{b2}) are within 10% of τ_{b1}. The results obtained using d_{65} also show good agreement when the slope of the channel is steeper, which results in a smaller flow-depth-to-grain-diameter ratio. In Table 4.3, y_0 is the location of the virtual bottom, y_1 is the top of the gravel bed, and y_2 is the approximate location of the free surface.

Test	Slope	y_0, y_1, y_2	τ_{b1} $=\rho g R_b S$	τ_{b2}, log-law (N/m^2)				Percent difference		
	S	(mm)	(N/m^2)	d_{50}	d_{65}	d_{84}	95% CI	d_{50}	d_{65}	d_{84}
1	0.02	1.1, 4, 36.1	6.22	5.24	5.39	5.77	± 0.1	15.8%	13.3%	7.2%
2	0.02	1.7, 4, 36.4	6.28	5.62	5.82	6.2	± 0.4	10.5%	7.3%	1.3%
3	0.04	4.6, 7, 32.5	10.53	9.36	9.76	10.34	± 0.7	11.1%	7.3%	1.8%
4	0.04	4.8, 7, 32.5	10.53	6.59	10.02	10.63	± 1.0	37.4%	4.8%	-0.9%
5	0.05	12.3, 13.4, 36.5	12.35	11.38	11.87	12.79	± 1.0	7.9%	3.9%	-3.6%
6	0.06	4.3, 7, 29.6	14.49	12.45	12.98	13.72	± 0.6	14.1%	10.4%	5.3%
7	0.06	4.2, 7, 29.6	14.49	12.42	12.94	13.91	± 0.7	14.3%	10.7%	4.0%
8	0.08	9.4, 10, 29.8	17.4	16.26	16.98	18.27	± 1.9	6.6%	2.4%	-5.0%
9	0.08	5.3, 6, 25.9	17.44	15.2	15.99	17.1	± 4.4	12.8%	8.3%	1.9%
10	0.10	10.6, 13.6, 31.9	20.64	21.19	22.1	23.67	± 1.8	-2.7%	-7.1%	-14.7%
11	0.10	10.6, 13.6, 31.9	20.64	21.87	21.75	23.29	± 1.7	-6.0%	-5.4%	-12.8%

Table 4.3 Summary table for each slope comparing two methods to calculate bed shear stress

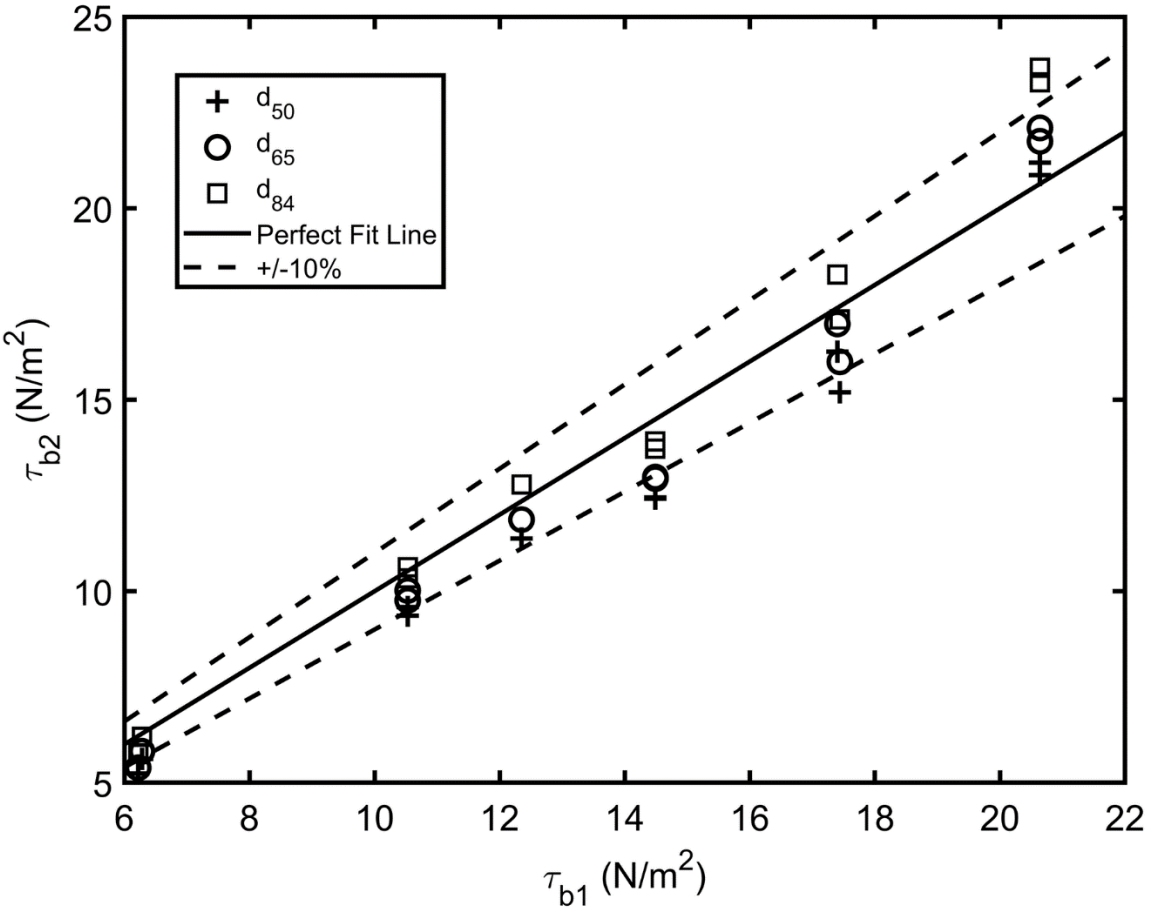

Figure 4.31 Bed shear stress results plotted with a line of perfect agreement

4.3 Particle Image Velocimetry Measurements Over Cohesive Soil Sample

Using a similar procedure, Particle Image Velocimetry (PIV) measurements were taken with a clay sample placed in the sediment recess in the fixed gravel bed. The measured data was used to estimate the average bed shear stress acting on the surface of the clay sample at different soil erosion depths.

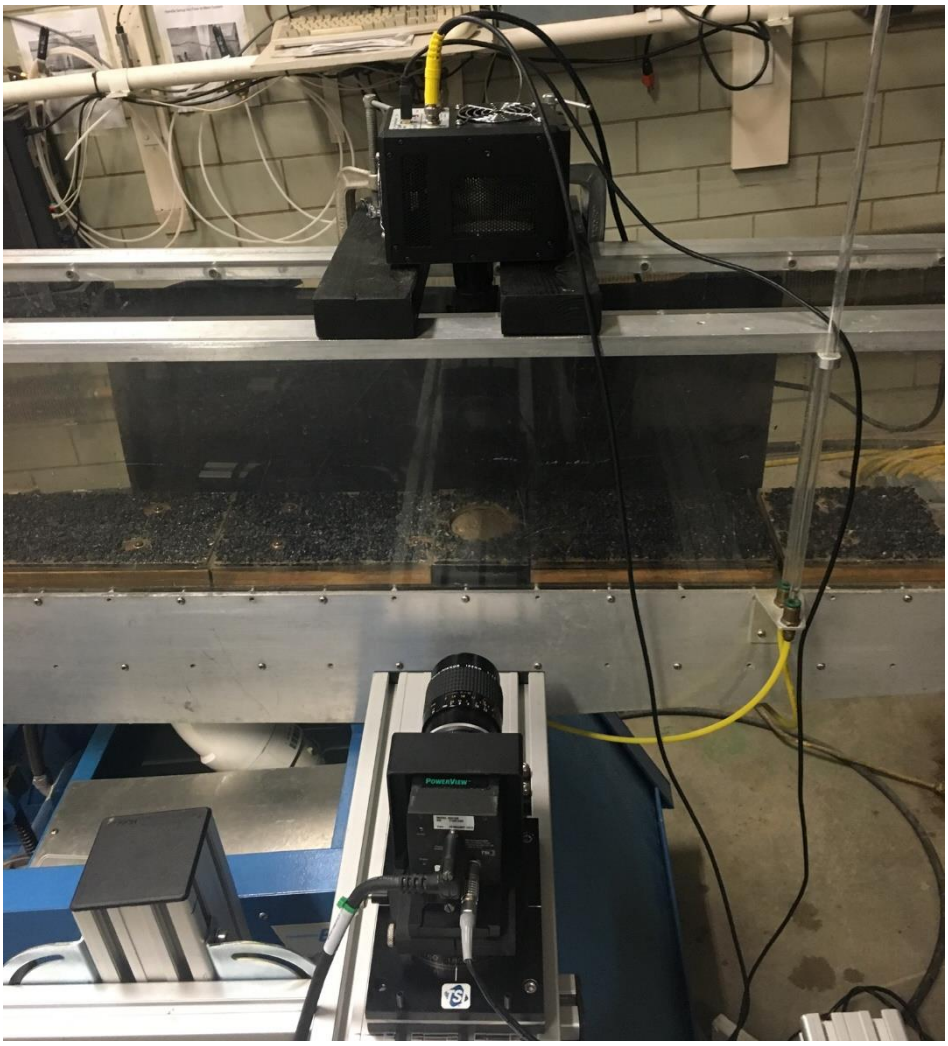

Figure 4.32 Typical set up for PIV tests with a clay sample

4.3.1 No Erosion

The objective of these tests was to measure the bed shear stress on a cohesive soil sample that was surrounded by a rough bed. The top surface of the clay sample was smooth and at about the same elevation as the top of the surrounding gravel at the start of the test. Three tests were conducted for a constant discharge rate of 0.1580 ft^3/sec (4.5 L/s) at a channel slop of 8% for comparison with the measurements obtained on the fixed gravel bed in the previous section

The procedure for operating the camera, LED Illuminator, and channel bed set up can be found in Section 3.7. The measurement plane was set at 7.5 cm from the side wall closest to the camera, along the center line of the test area. The water depth was measured at approximately 42 cm upstream from the soil sample. The water depth was used to estimate the bed shear stress (τ_{b1}) using the method described in Cheng (2011). PIV images were taken after uniform flow was established.

Figure 4.33 shows an example of the PIV image over the clay bed from Test 1. The ensemble correlation velocity field is shown in Figure 4.34, and the ensemble- and space-averaged velocity profile is shown in Figure 4.35.

The average velocity profile was then graphed on a $\ln(y-y_0)$ versus u plot. The virtual height, y_0, was found using the procedure described in Section 4.2. Figures 4.36, 4.37, and 4.38 show the semi-log plots for Tests 1, 2, and 3, respectively. These tests were conducted under the same flow conditions, and four runs were completed in each test to compute the average velocity profile. The test results are summarized in Table 4.4.

Bed shear stress over the clay sample was found from the average velocity profile using the log-law assuming an equivalent bed roughness k_s of 6.1 mm. All PIV erosion test experiments were performed at an 8% slope. As discussed in Section 4.2, when the slope of the hydraulic channel increases above 8%, the equivalent roughness height may be taken as the d_{65} of the fixed gravel bed. It is assumed that the same k_s value may be applied to the clay bed. Because the time it took for the flowing water to pass over the clay sample was very short (< 0.1 second), the structure of turbulence over the soil sample was dominated by the advection of boundary-layer turbulence generated on the gravel bed upstream, instead of locally generated turbulence. However, the presence of a free surface allows the entire velocity profile to adjust quickly to the roughness transition. An argument like that of the law of the wall for flow over a rough bed can then be used to obtain a logarithmic velocity profile over the sediment recess, with an equivalent roughness close to the bed roughness before the transition. More discussion on flow over the soil sample and the sudden change in bed roughness is given in Chapter 5.

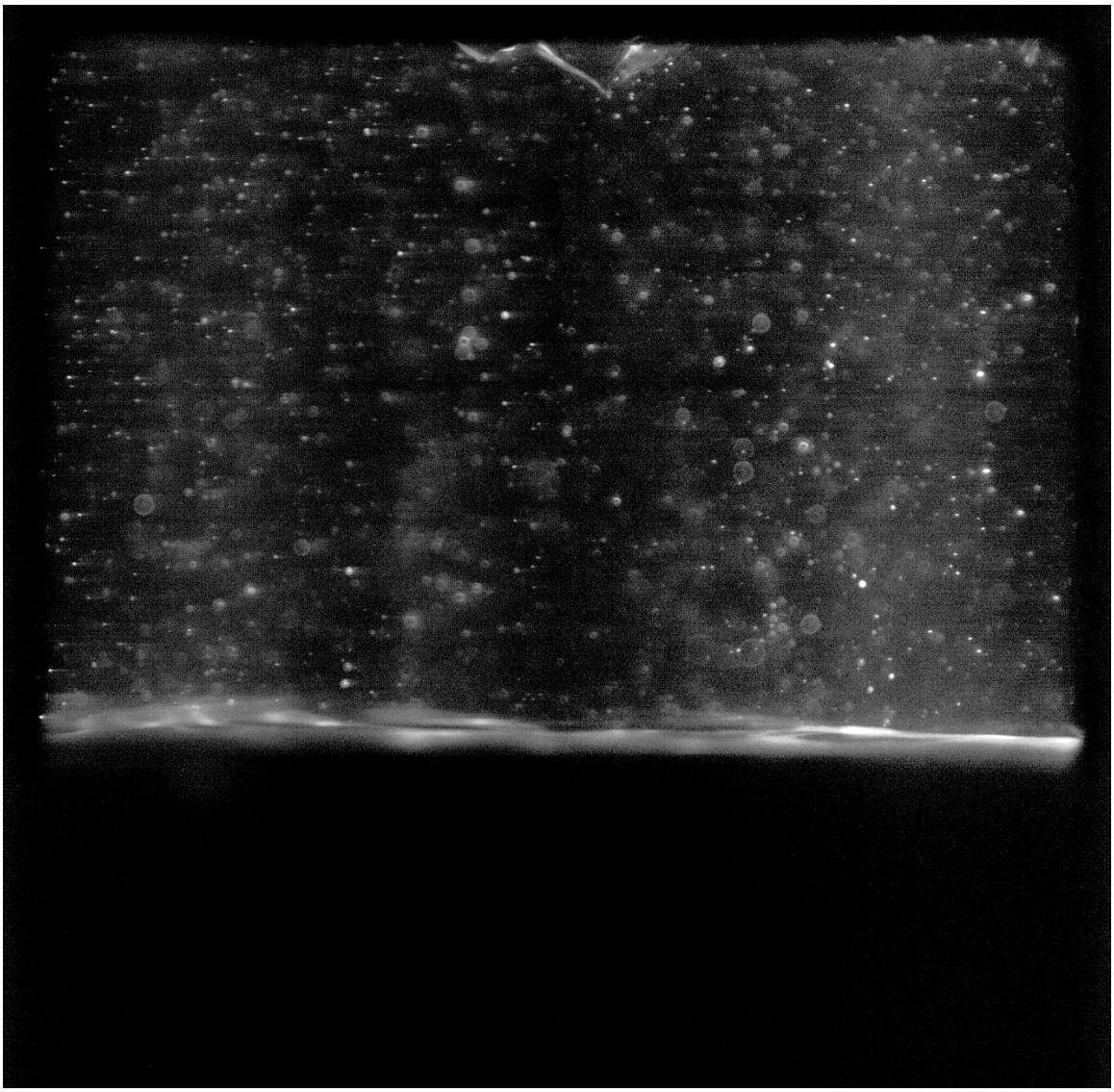

Figure 4.33 Example image from Test 1, Run 1

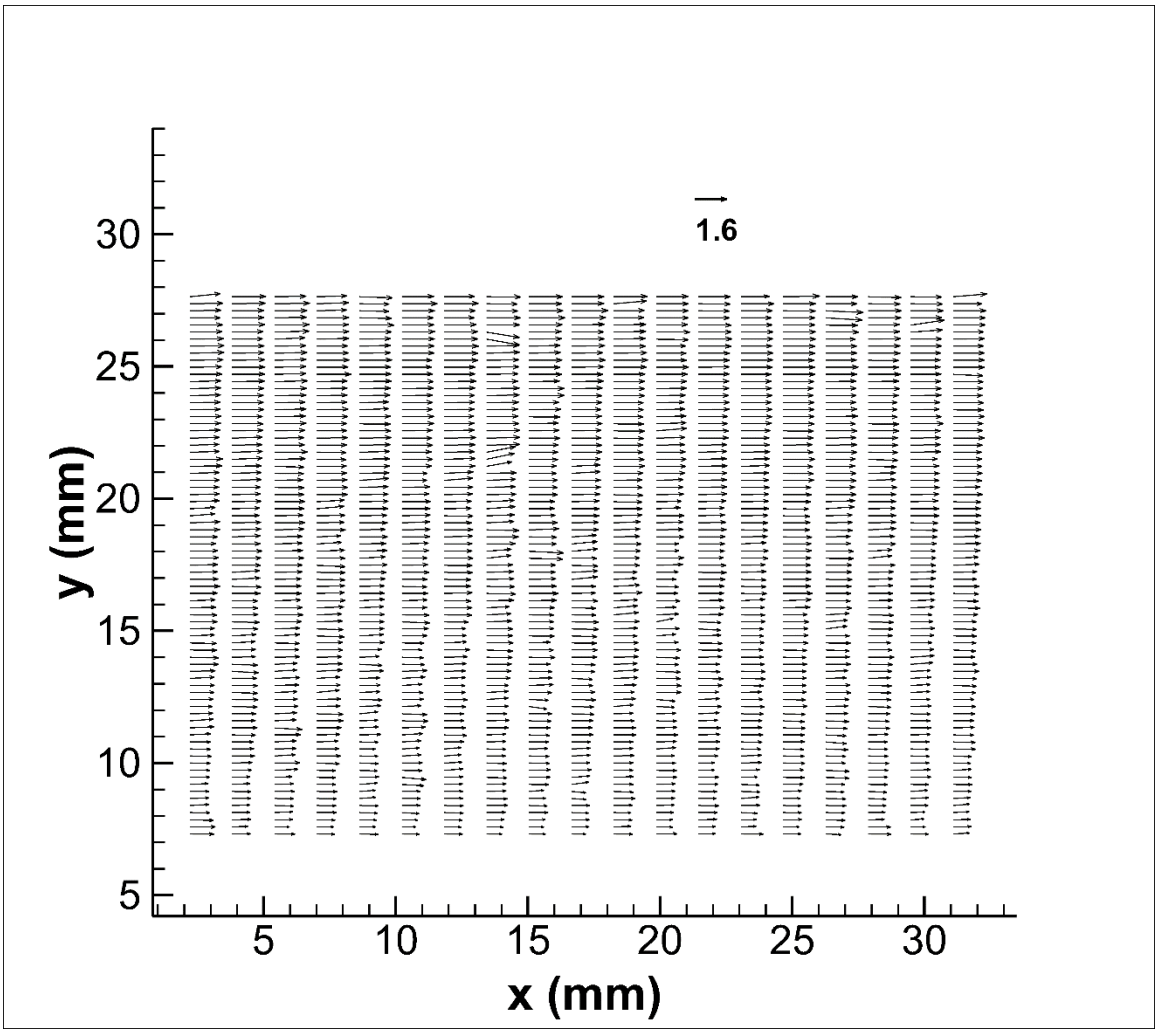

Figure 4.34 Velocity profile vectors of processed data from Test 1

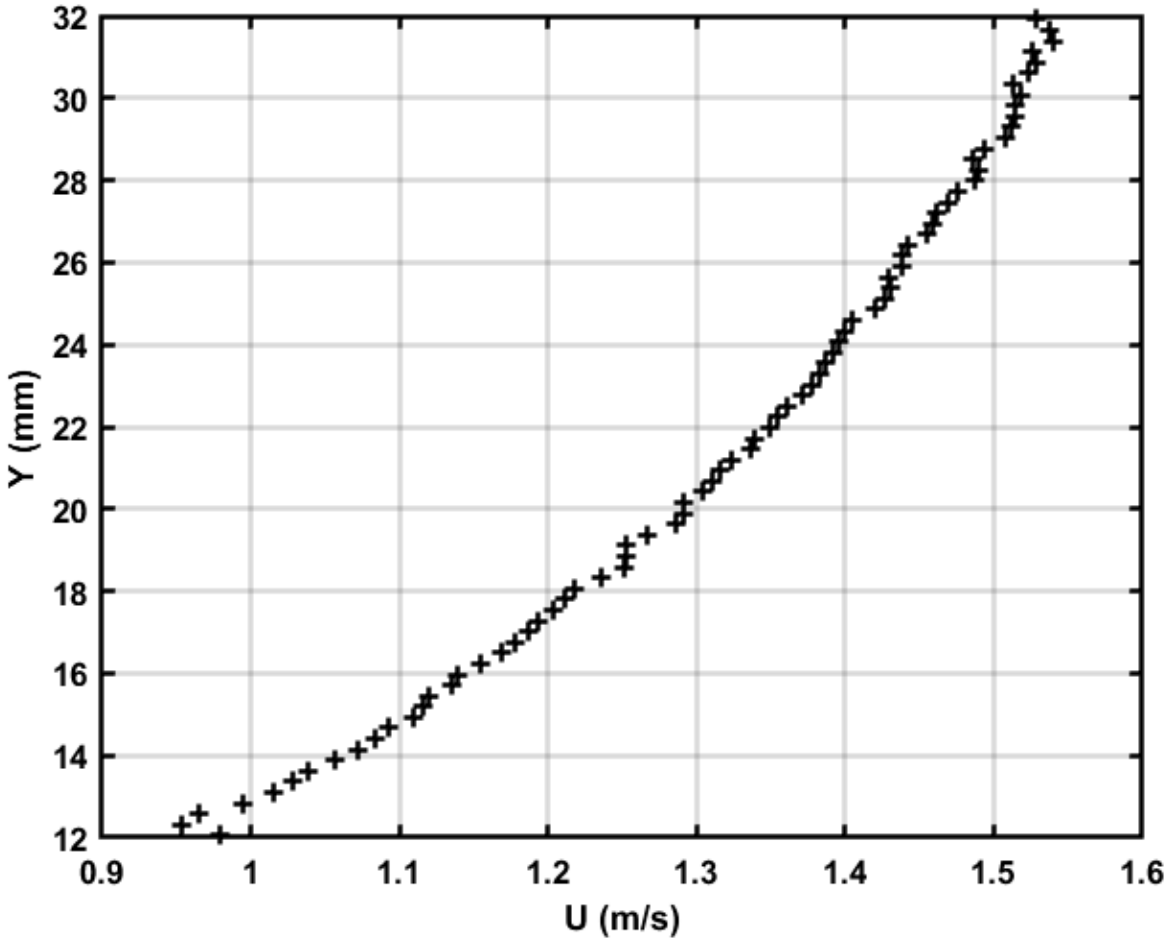

Figure 4.35 Average velocity profile in Test 1

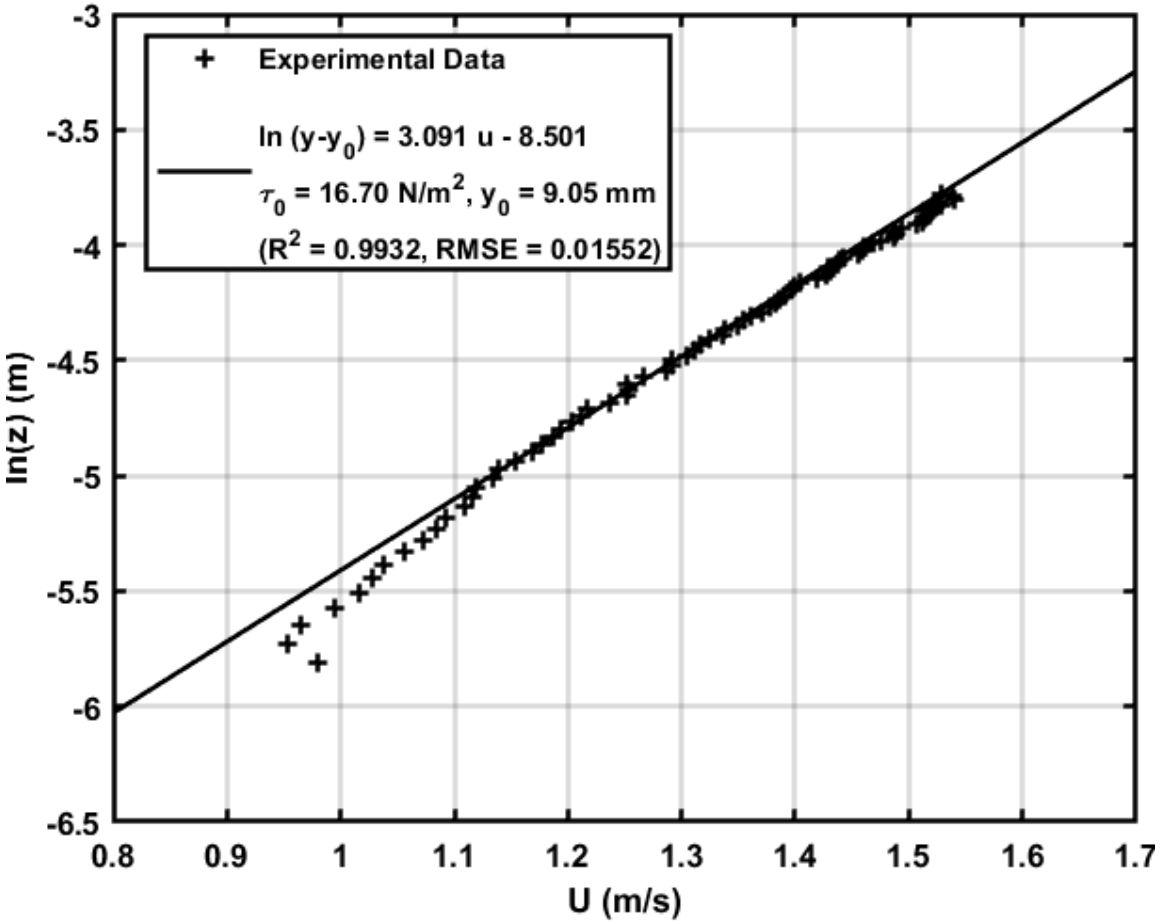

Figure 4.36 Test 1 result clay surface at top of rock

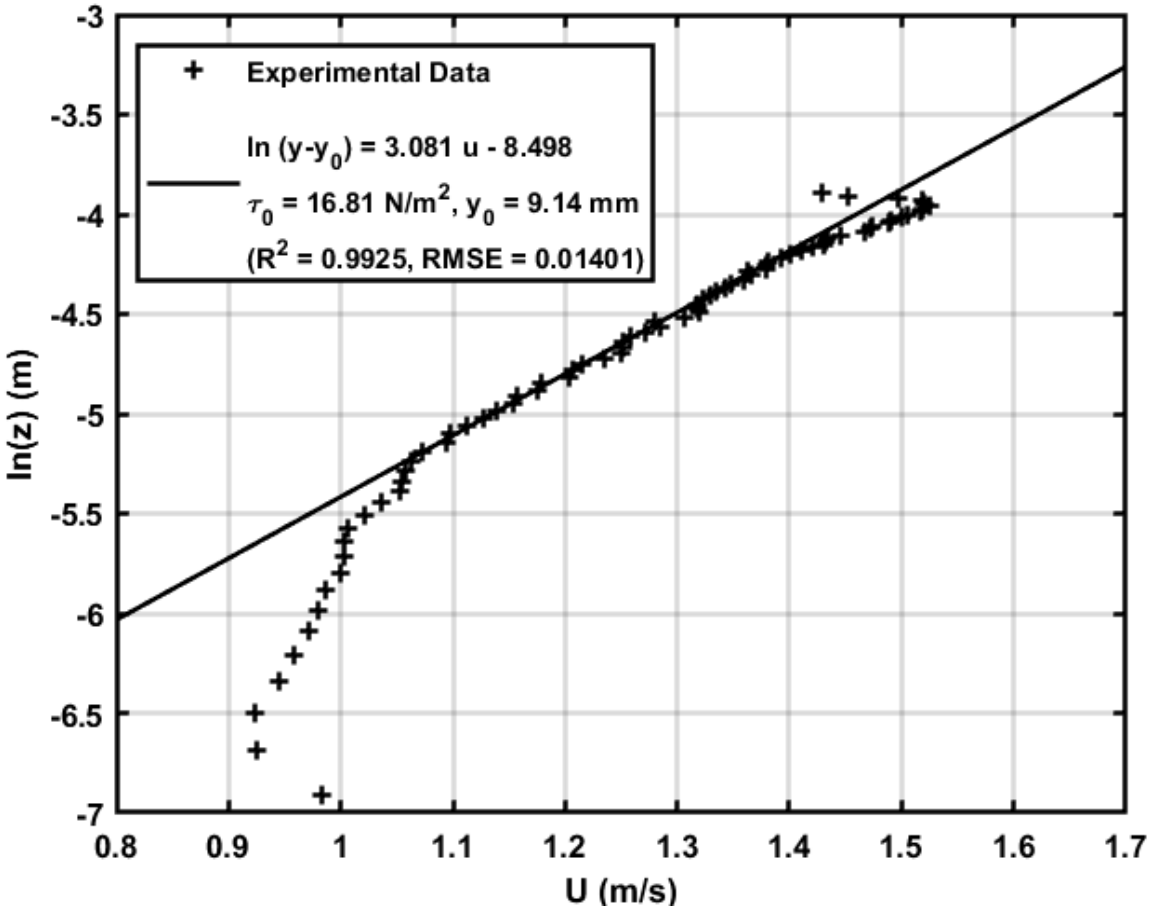

Figure 4.37 Test 2 result clay surface at top of rock

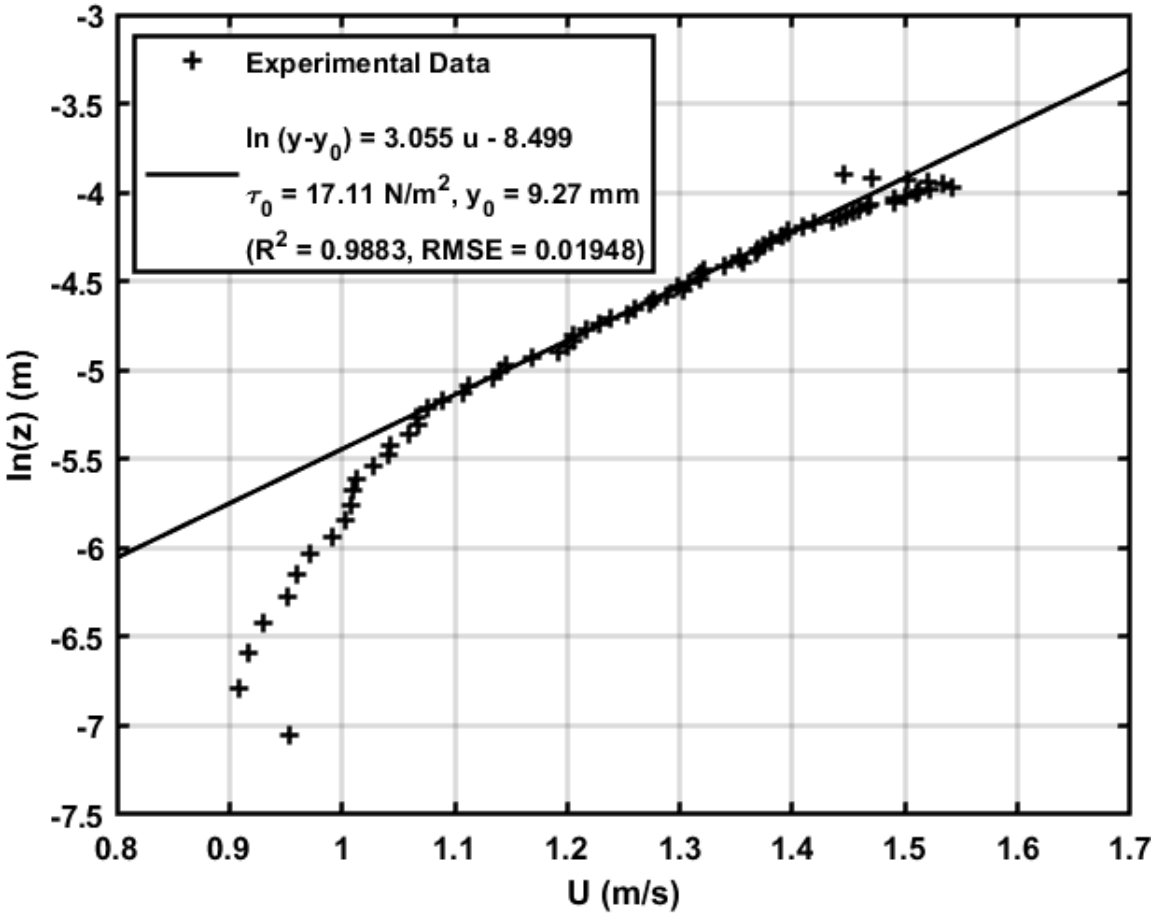

Figure 4.38 Test 3 results clay surface at top of rock

Test	h (mm)	h_e (mm)	y_0, y_1, y_2 (mm)	V (m/s)	V_1 (m/s)	**τ_{b1} (N/m^2)**	**τ_{b2} log-law (N/m^2)**	τ_{b2} [95% CI]	Percent Difference
1 (4)	26.80	24.00	9.05, 11.4, 26.8	1.22	1.22	**17.40**	**16.70**	14.22 - 19.73	4.0%
2 (4)	26.80	24.00	9.14, 9.5, 26.8	1.22	1.22	**17.395**	**16.81**	13.44 - 21.02	3.4%
3 (4)	26.80	24.00	9.27, 9.5, 26.8	1.22	1.23	**17.395**	**17.11**	13.26 - 22.07	1.6%

Table 4.4 Summary results of smooth surface flush with top of rocks

Table 4.4 shows a summary of the bed shear stress measurements obtained in this set of experiments. The top of the cohesive sediment sample was level with the top of the rock that was fixed to the bed surrounding the sediment recess. The results show that the bed shear stress on the gravel bed obtained using the log-law, τ_{b2}, is slightly smaller than, but close to, the bed shear stress obtained from the measured flow depth and channel slope, τ_{b1}. Hence, the bed shear stress did not change significantly during the short period of time when the flow passed over the clay sample.

4.3.2 Bed Shear Stress at Different Soil Erosion Depths

The soil specimen was trimmed to various depths below the general top of the surrounding fixed gravel bed in the hydraulic channel. The soil specimen was trimmed, rather than naturally eroded, because the water would otherwise become too cloudy for good PIV measurements. The results indicate that as the erosion depth gets larger, the bed shear stress in the test area would eventually start to decrease.

An example of the captured PIV images from Test 4 can be seen in Figure 4.39, and the corresponding ensemble correlation velocity field is shown in Figure 4.40. PIV images from other tests can be found in Appendix C.

Multiple runs were conducted in each test and the measured velocity profiles were averaged to obtain an average velocity profile to find the bed shear stress. Figure 4.41 shows an example of the average velocity profile from Test 4. The average velocity profiles from other tests can be found in Appendix D.

Plots of $\ln(y-y_0)$ versus u for the different tests are shown in Figures 4.42 through Figure 4.53 with the summary of bed shear stress results in Table 4.5. As in Section 4.3.1, the value of y_0 for the best-fit line in each plot was found assuming that the equivalent bed roughness height, k_s, is equal to 6.1 mm, or d_{65}, of the fixed gravel bed.

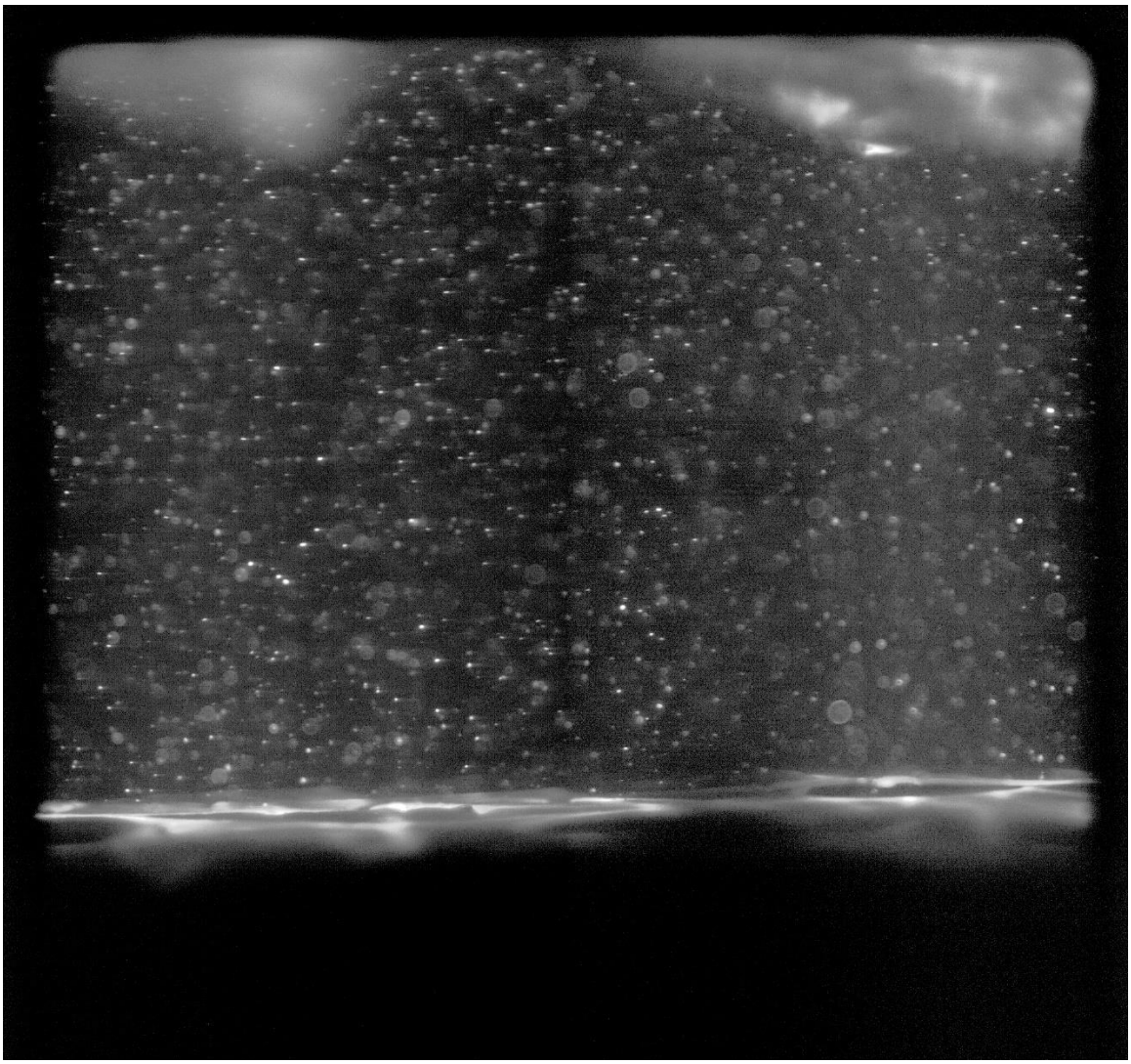

Figure 4.39 Example raw image from Test 4

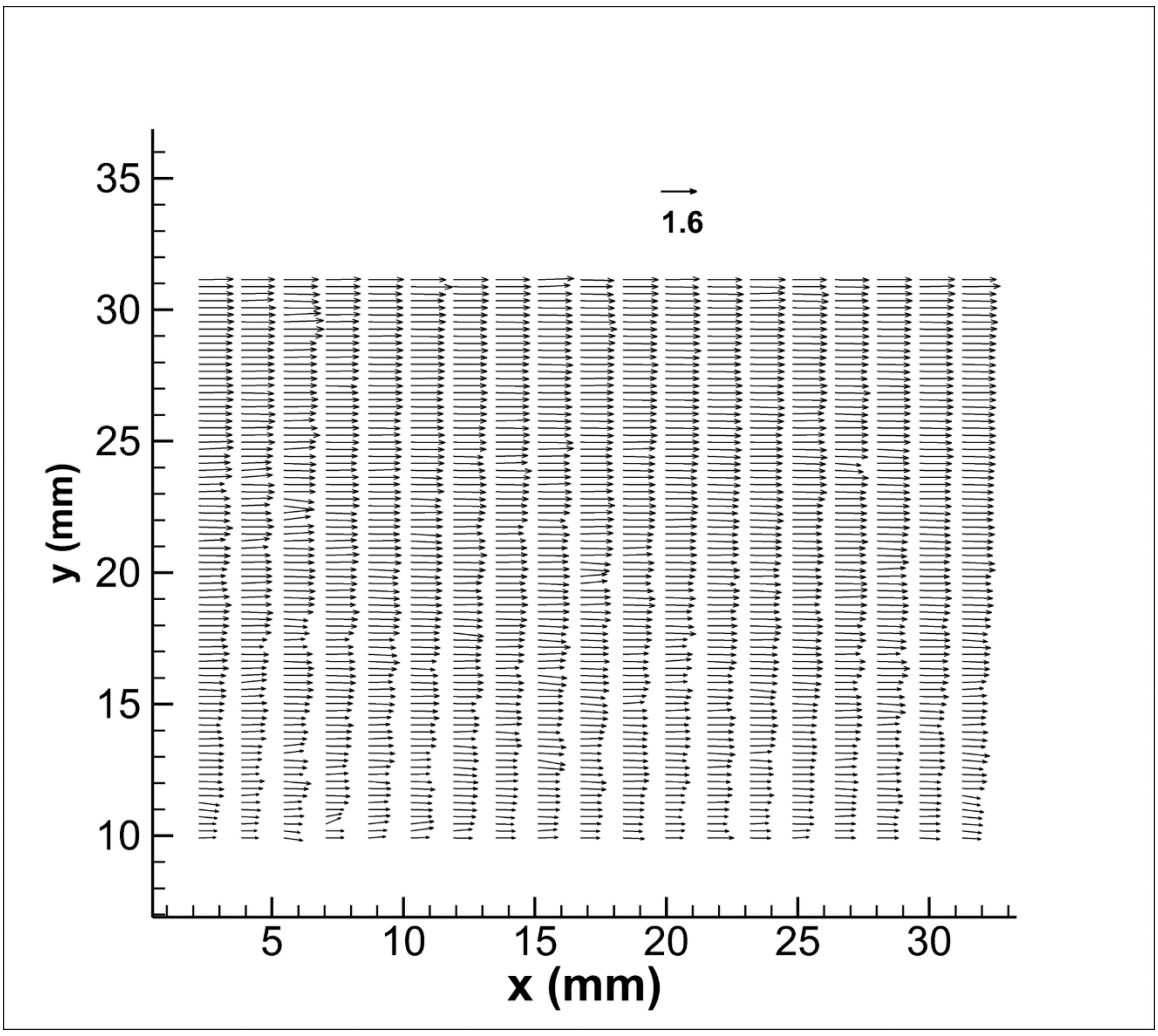

Figure 4.40 Velocity profile vectors of processed data from Test 4

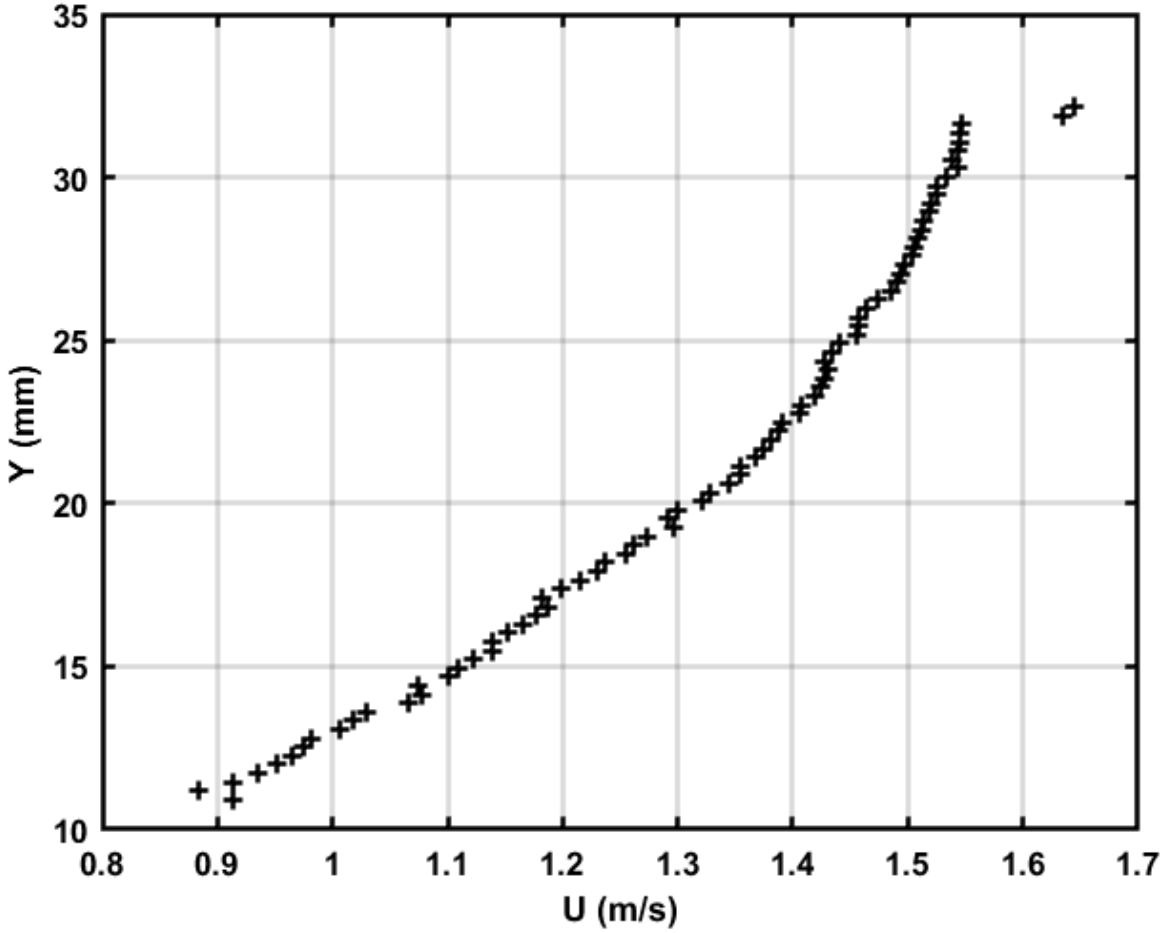

Figure 4.41 Average Velocity Profile Test 4

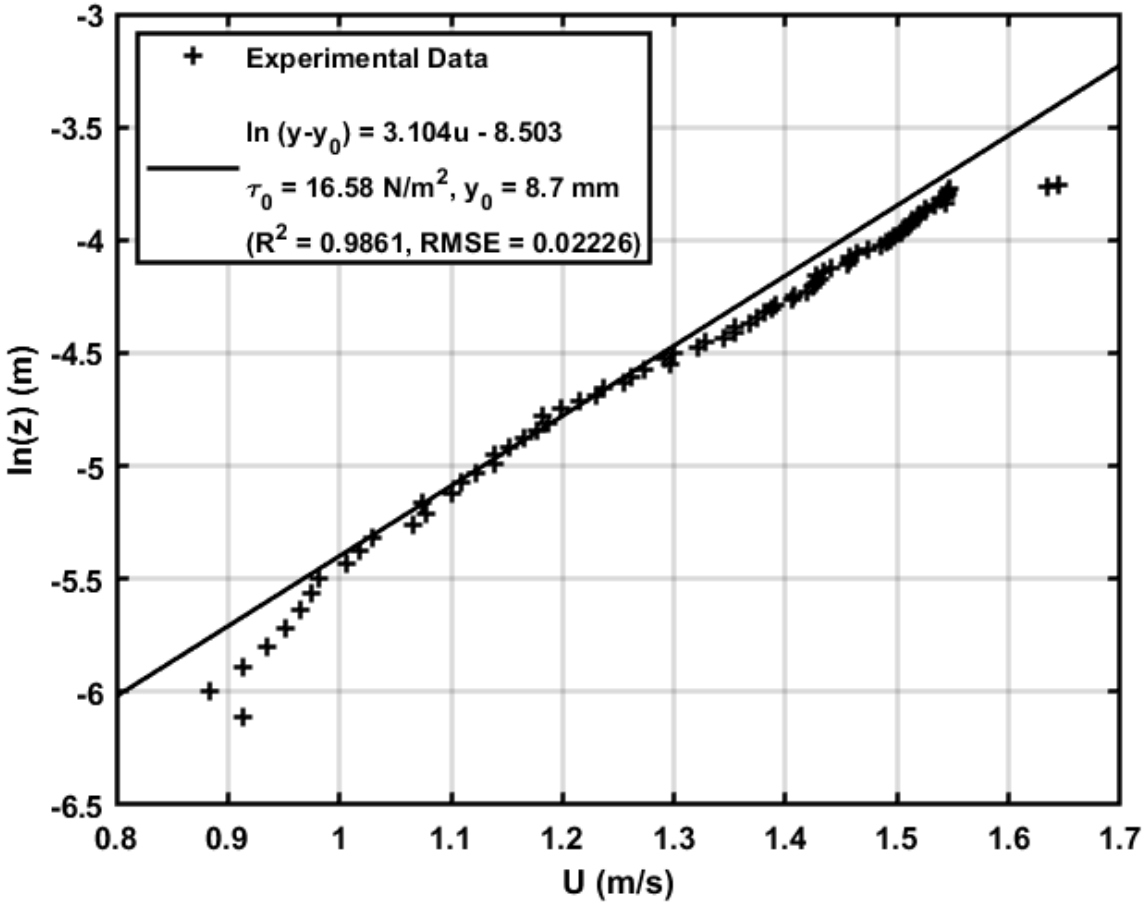

Figure 4.42 Test 4 results for 1.5 mm erosion depth

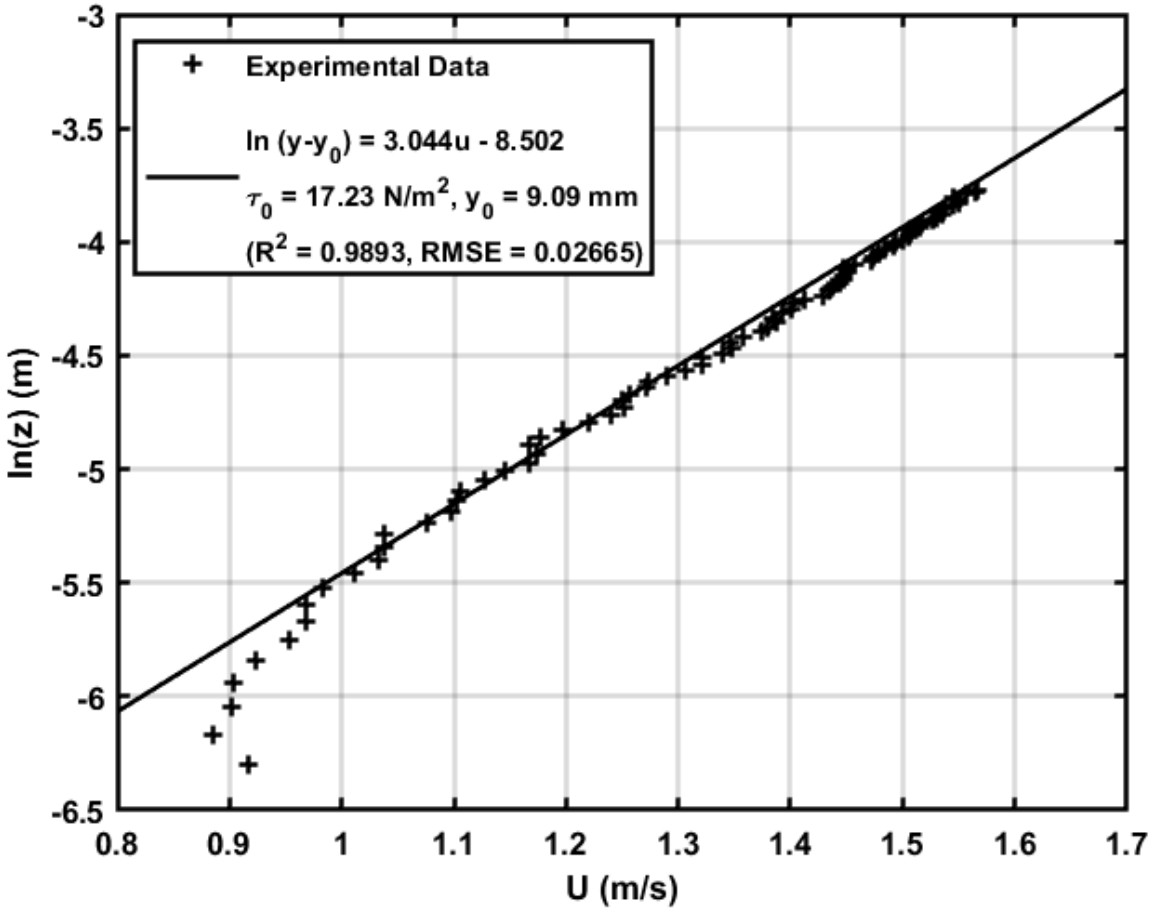

Figure 4.43 Test 5 results for 1.5 mm erosion depth

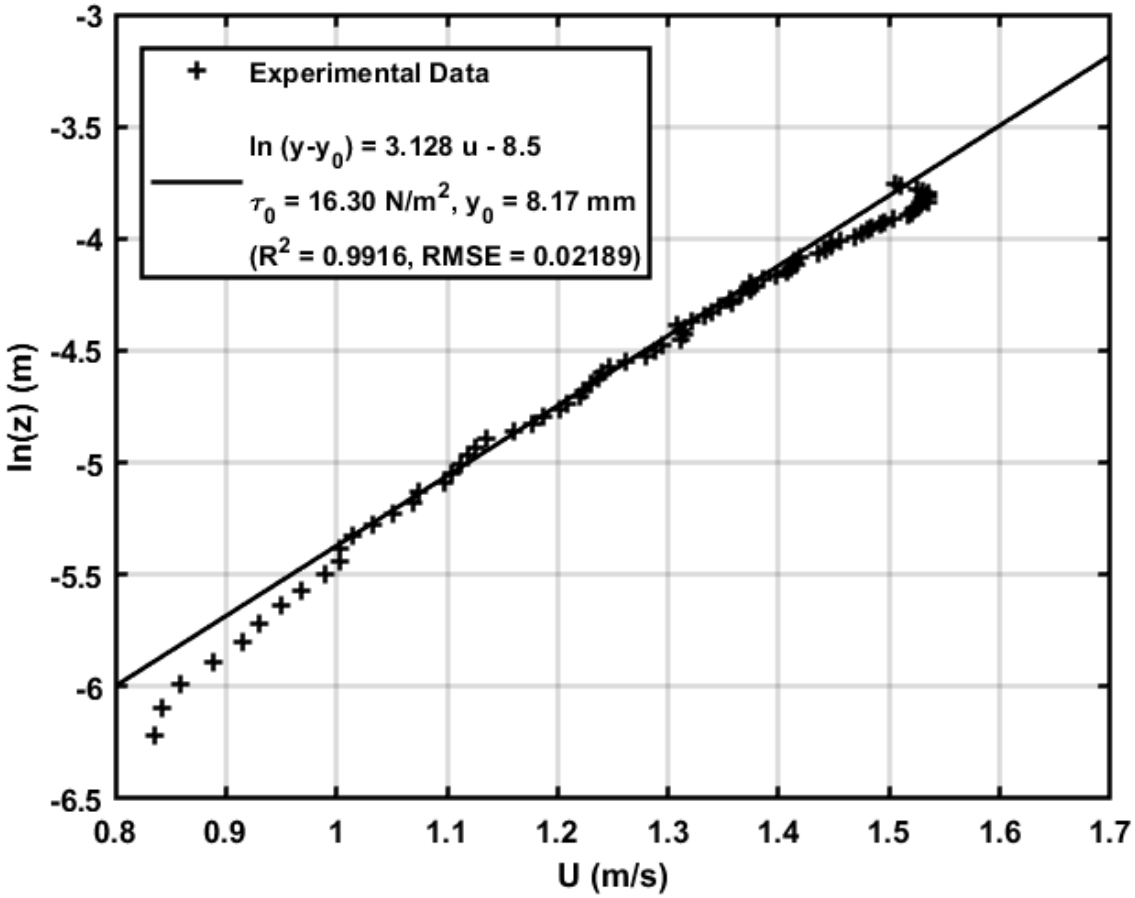

Figure 4.44 Test 6 result 1.6 mm erosion depth

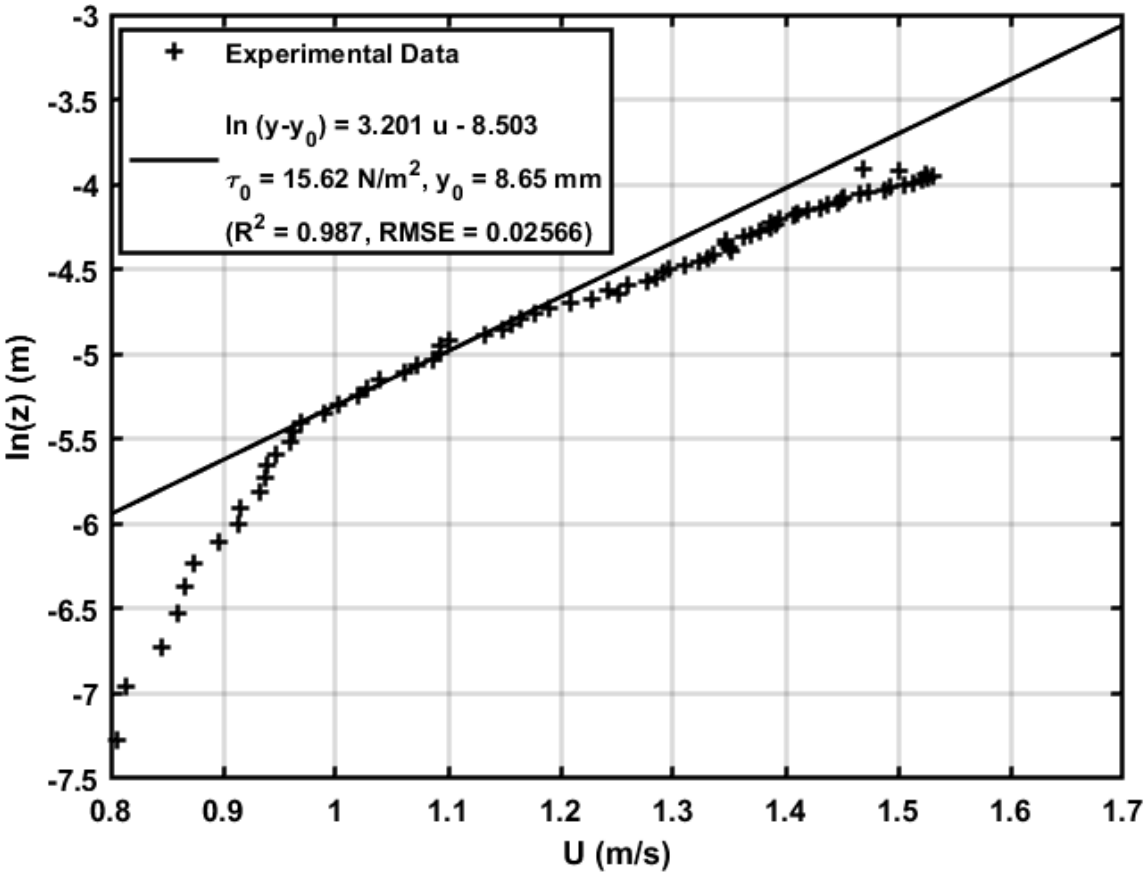

Figure 4.45 Test 7 result 1.6 mm erosion depth

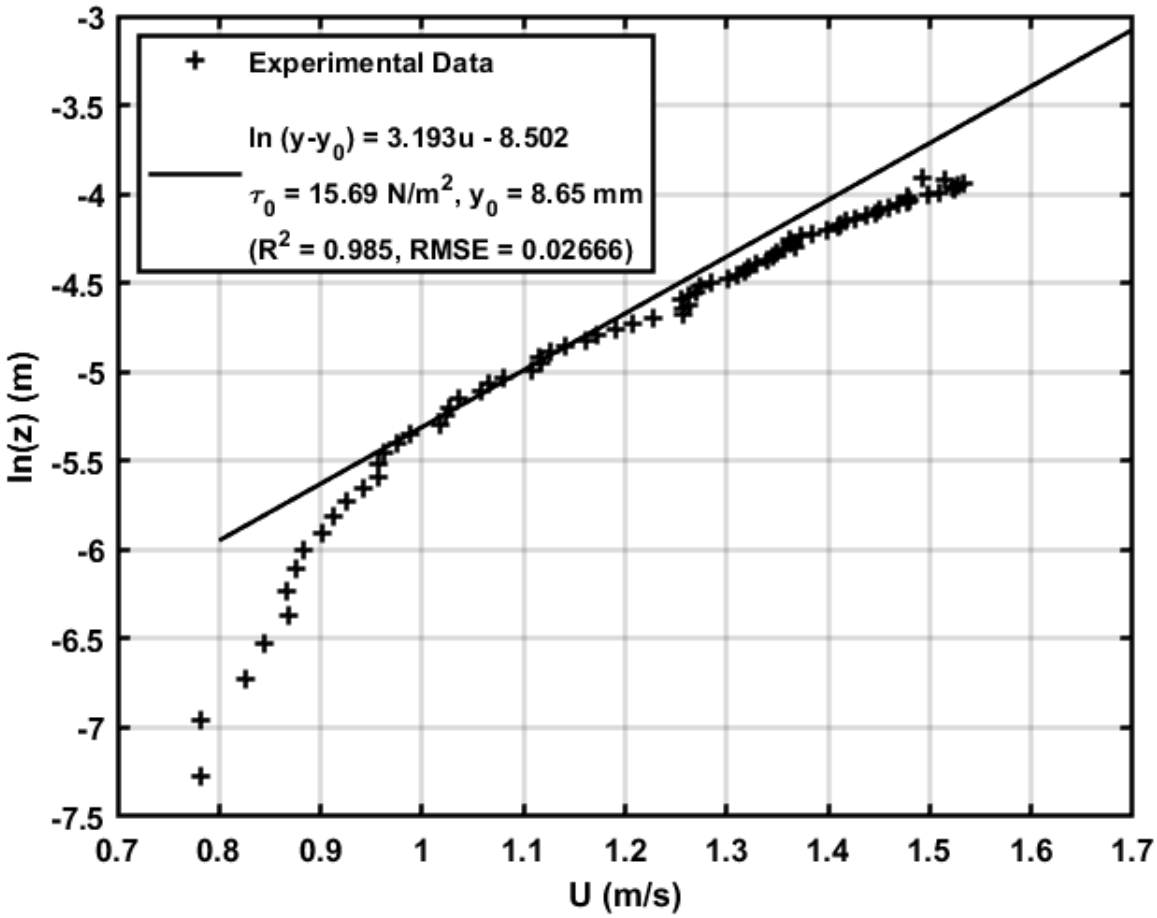

Figure 4.46 Test 8 result 1.6 mm erosion depth

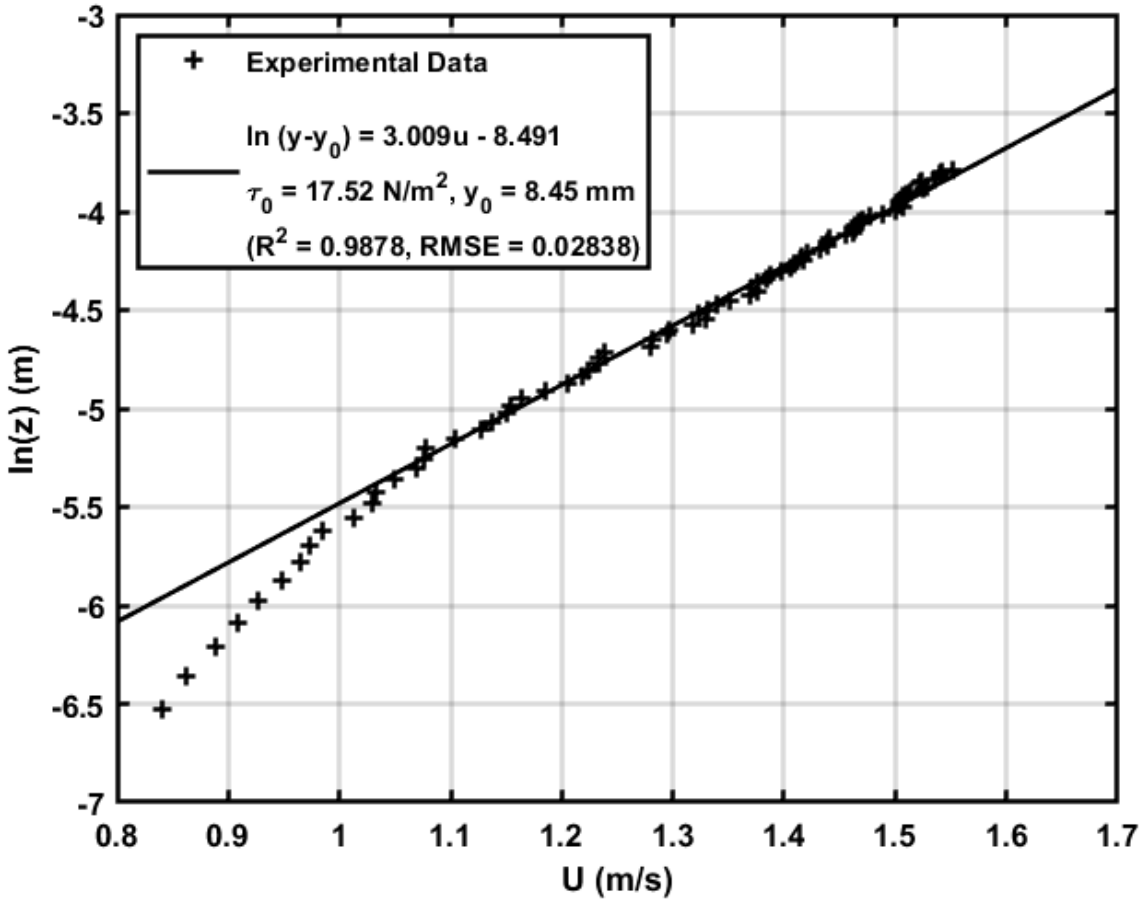

Figure 4.47 Test 9 results for 2.5 mm erosion depth

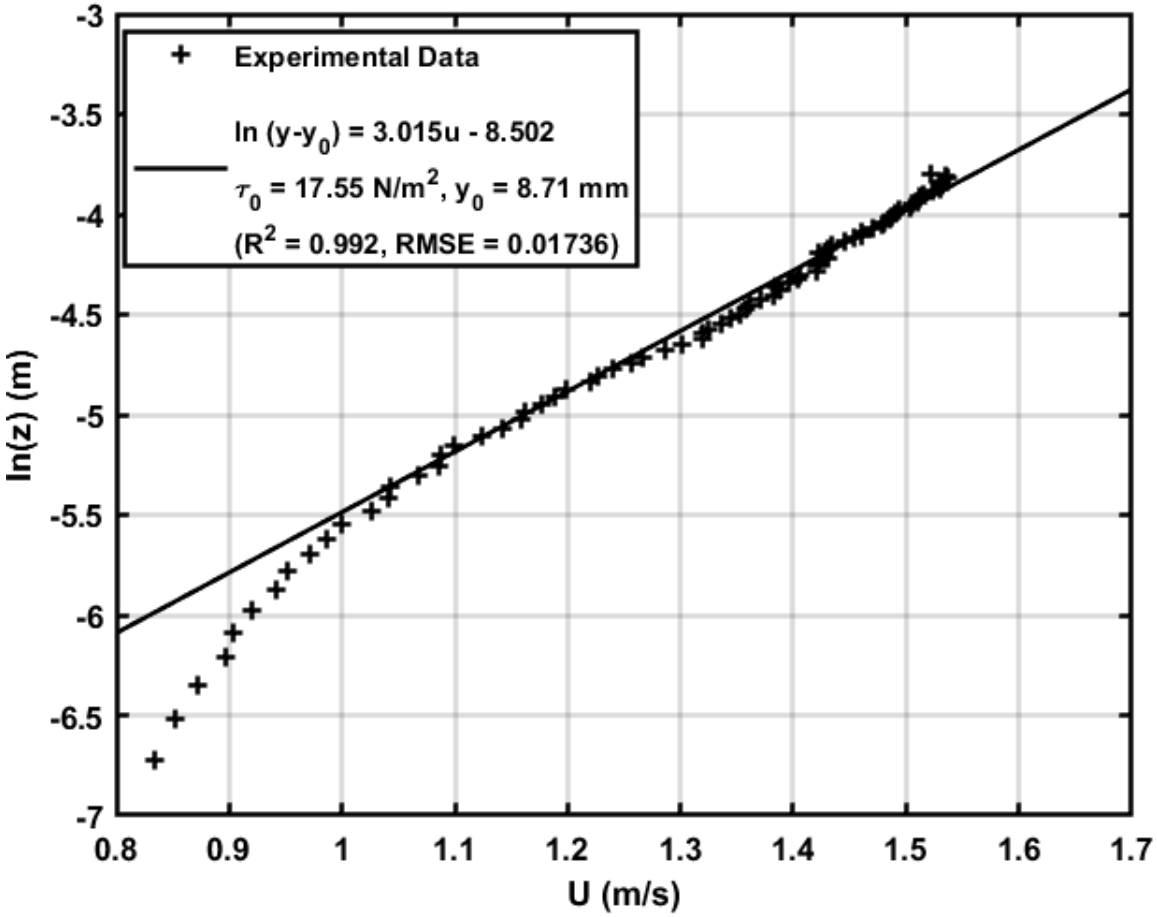

Figure 4.48 Test 10 results for 2.5 mm erosion depth

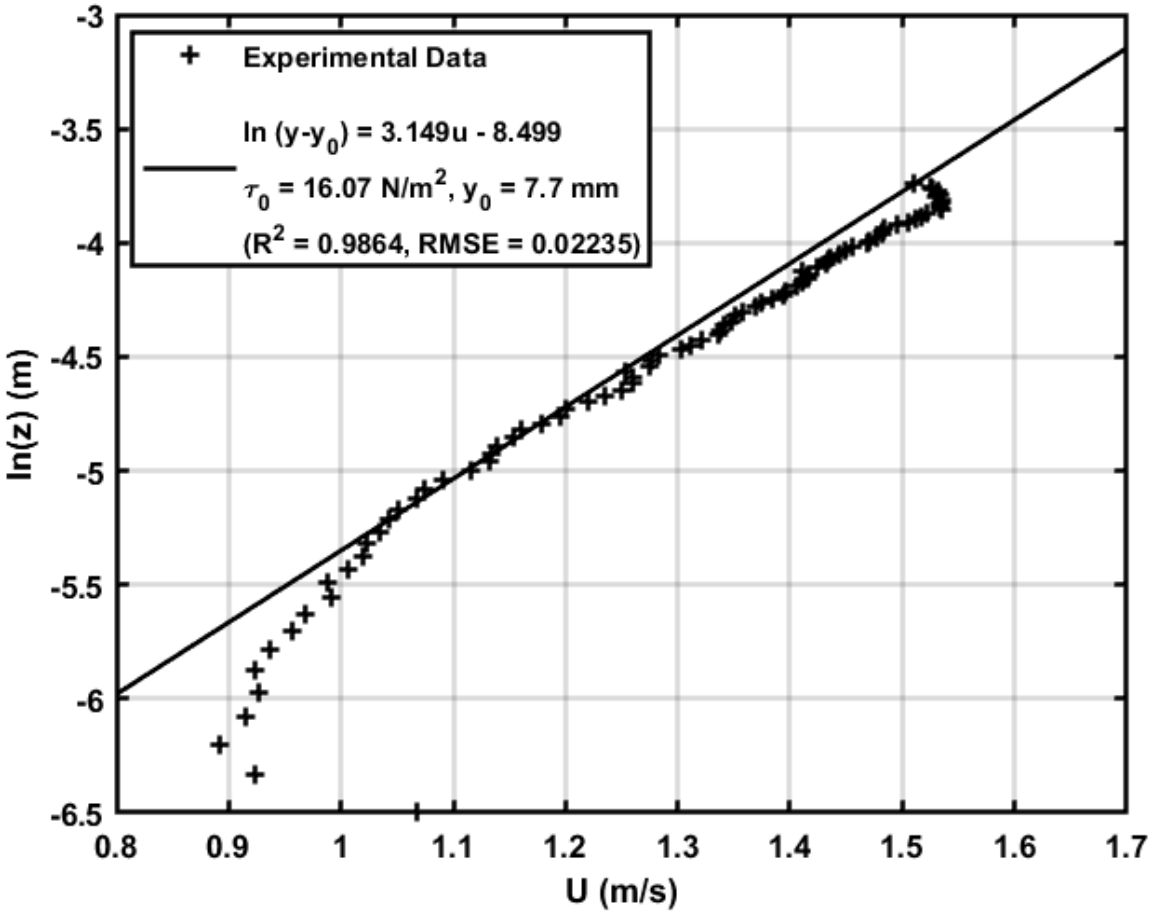

Figure 4.49 Test 11 results for 3 mm erosion depth

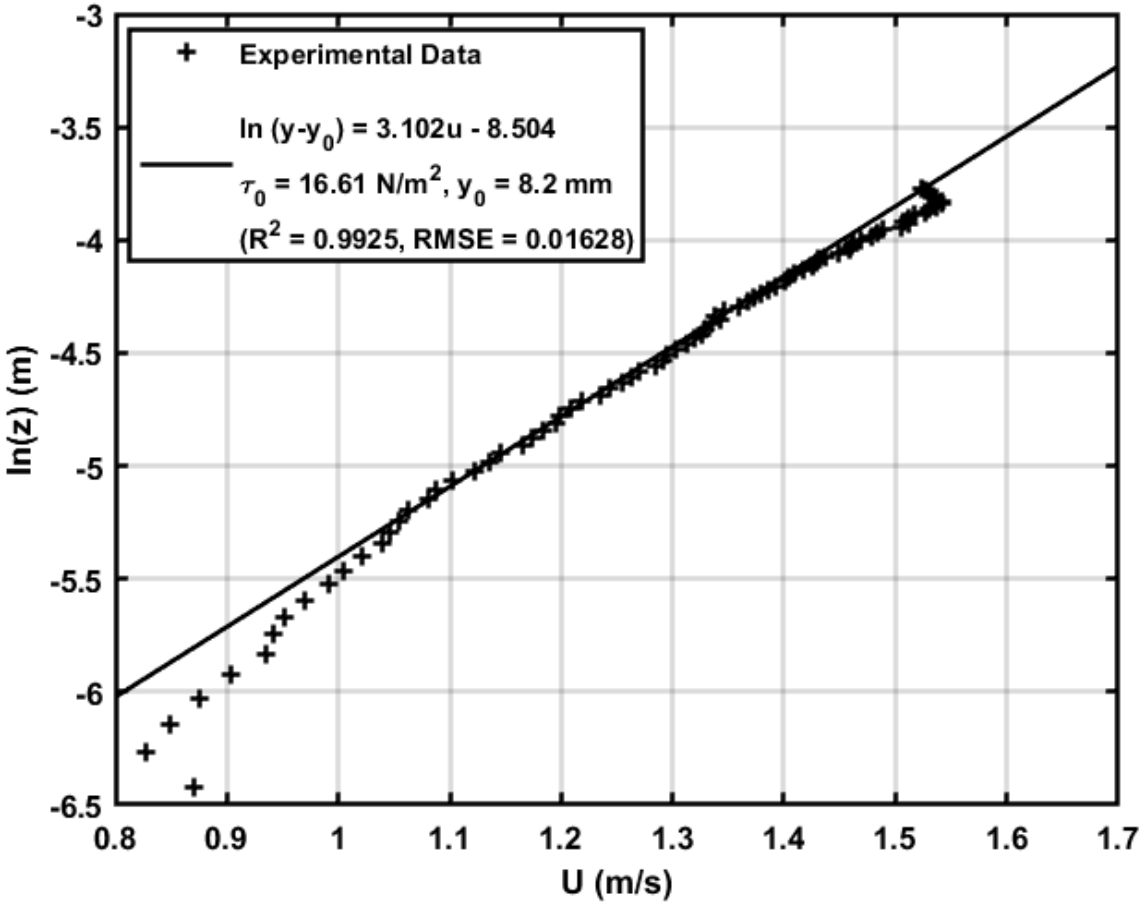

Figure 4.50 Test 12 results for 3 mm erosion depth

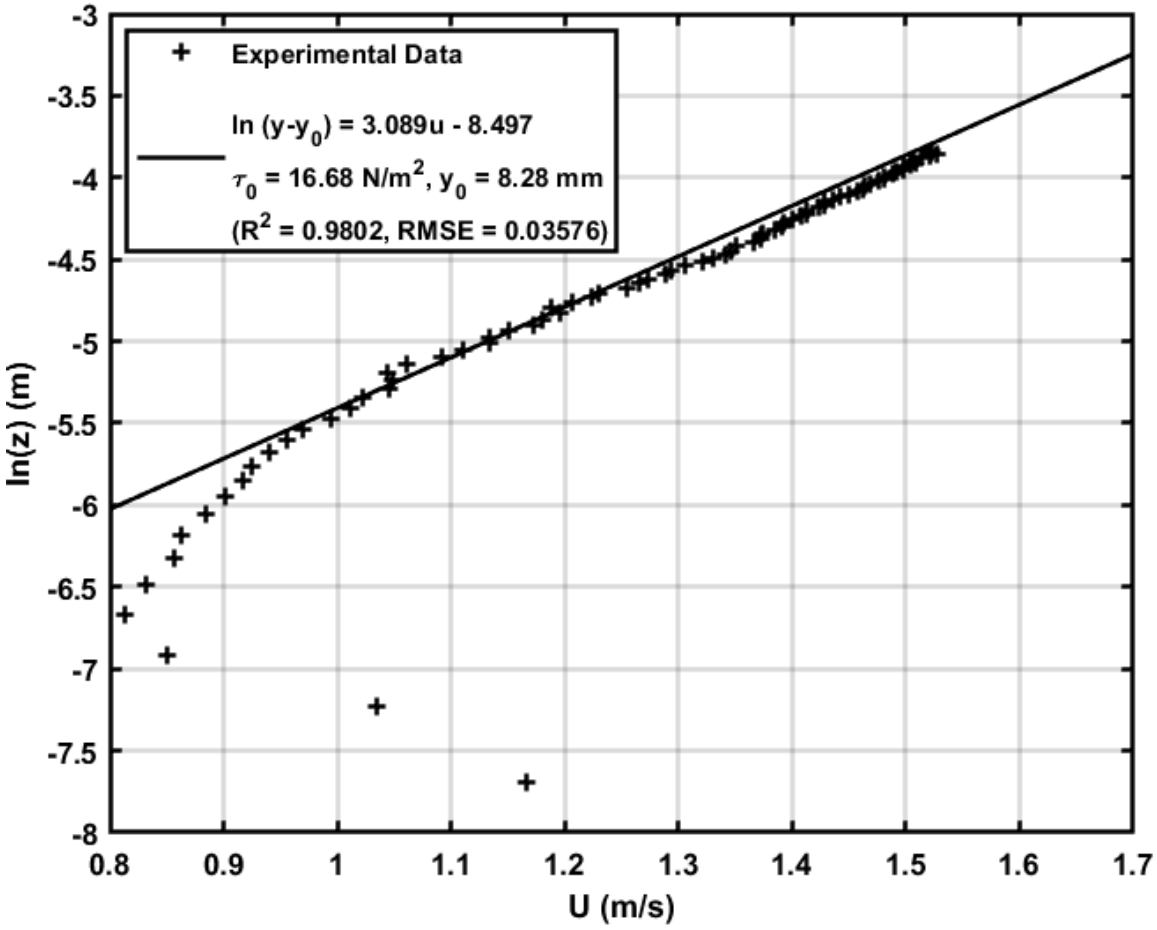

Figure 4.51 Test 13 results for 4 mm erosion depth

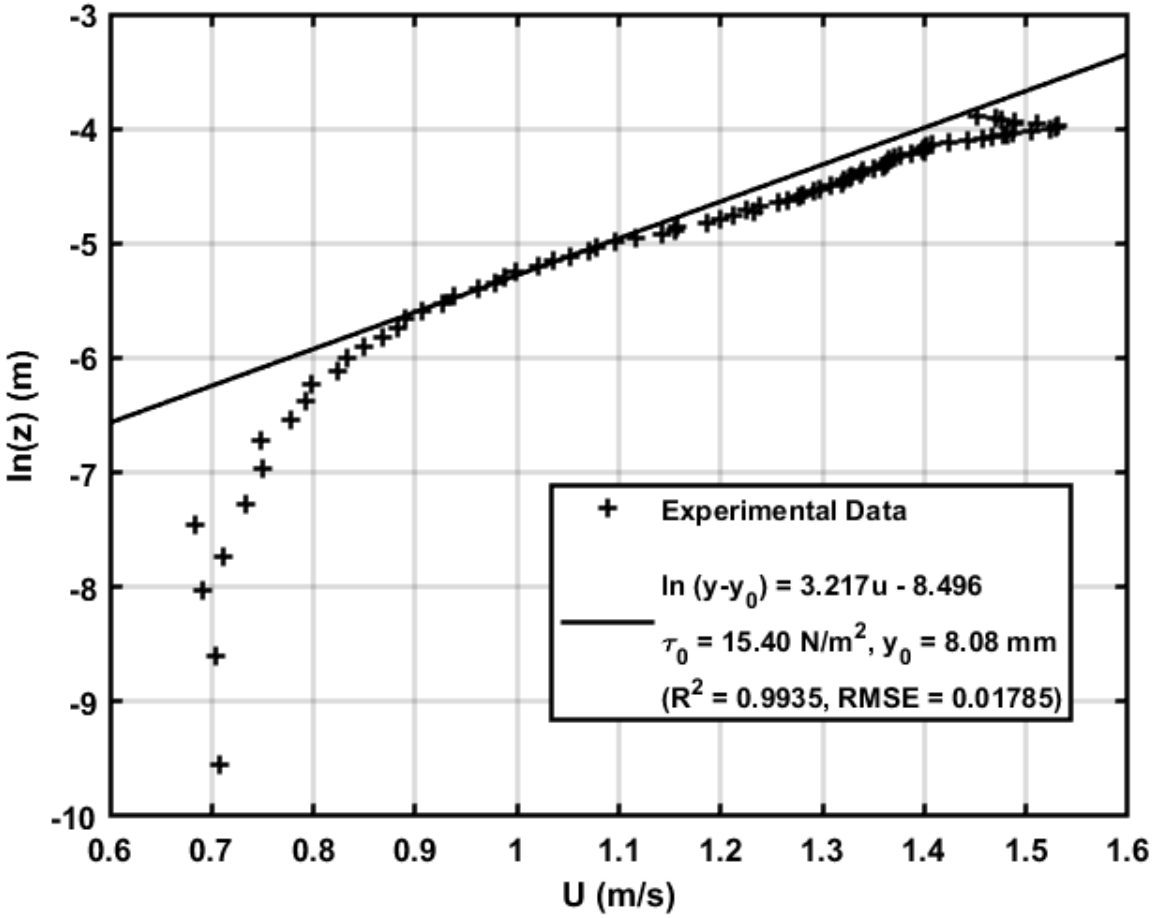

Figure 4.52 Test 14 results for 4 mm erosion depth

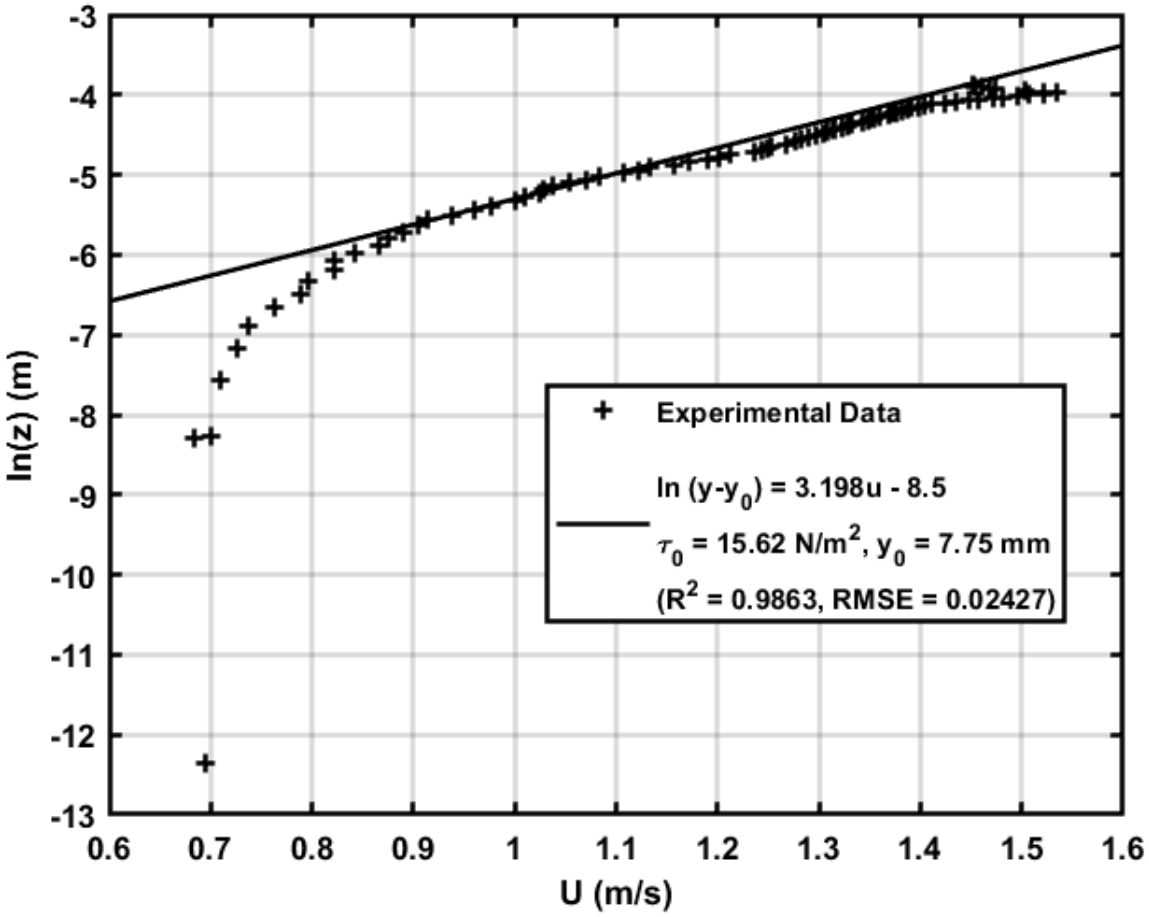

Figure 4.53 Test 15 results for 5 mm erosion depth

(1) Test	(2) Erosion Depth (mm)	(3) h (mm)	(4) h_e (mm)	(5) y_0, y_1, y_2 (mm)	(6) V (m/s)	(7) V_1 (m/s)	**(8) τ_{b1} (N/m^2)**	**(9) τ_{b2} log-law (N/m^2)**	(10) τ_{b2} [95% CI]	(11) Percent Difference
1 (4)	0	26.80	24.00	9.05, 11.4, 26.8	1.22	1.22	**17.40**	**16.70**	14.22 - 19.73	4.0%
2 (4)	0	26.80	24.00	9.14, 9.5, 26.8	1.22	1.22	**17.40**	**16.81**	13.44 - 21.02	3.4%
3 (4)	0	26.80	24.00	9.27, 9.5, 26.8	1.22	1.23	**17.40**	**17.11**	13.26 - 22.07	1.6%
4 (3)	1.5	26.92	24.12	8.7, 9.5, 26.92	1.22	1.22	**17.50**	**16.58**	12.75 - 21.52	5.3%
5 (3)	1.5	26.80	24.00	9.09, 10.25, 26.8	1.22	1.24	**17.40**	**17.23**	14.28 - 20.77	1.0%
6 (4)	1.6	26.92	24.12	8.17, 9.3, 26.92	1.22	1.21	**17.50**	**16.30**	13.60 - 19.52	6.9%
7 (4)	1.6	26.67	23.87	8.65, 8.7, 26.67	1.23	1.18	**17.30**	**15.62**	12.23 - 19.95	9.7%
8 (4)	1.6	26.67	23.87	8.65, 8.7, 26.67	1.23	1.18	**17.30**	**15.69**	11.94 - 20.63	9.3%
9 (3)	2.5	26.80	24.00	8.45, 9.1, 26.8	1.22	1.25	**17.40**	**17.52**	14.17 - 21.63	-0.7%
10 (3)	2.5	26.67	23.87	8.71, 9.1, 26.67	1.23	1.25	**17.30**	**17.56**	14.12 - 21.81	-1.5%
11 (4)	3	26.80	24.00	7.7, 8.1, 26.8	1.22	1.20	**17.40**	**16.07**	12.22 - 21.13	7.7%
12 (6)	3	26.80	24.00	8.2, 8.1, 26.8	1.22	1.22	**17.40**	**16.61**	13.56 - 20.34	4.6%
13 (4)	4	26.92	24.12	8.28, 8.4, 26.924	1.22	1.22	**17.51**	**16.68**	12.45 - 22.32	4.7%
14 (6)	4	26.67	23.87	8.08, 6.1, 26.67	1.23	1.17	**17.30**	**15.40**	12.64 - 18.77	11.0%
15 (6)	5	26.67	23.87	7.75, 5.7, 26.67	1.23	1.18	**17.30**	**15.62**	11.67 - 20.91	9.7%

Table 4.5 Cohesive sediment PIV erosion test results

Table 4.5 shows a summary of all the PIV experiment results over a cohesive sediment sample. τ_{b1}, whose calculation procedure can be found in Section 3.6, has low percent difference when compared to τ_{b2} for zero erosion depth (Tests 1-3). This result indicates that the bed shear stress did not change significantly when the water flowed over the smooth bed for only a short distance within the rough bed. This suggests the bed shear stress on the clay bed may be increased by embedding the soil sample in a rough bed and increasing the channel slope.

The percent difference between τ_{b1} and τ_{b2} are not large and they are within the uncertainties of the bed shear stress measurements. As seen in Table 4.5, Column (10), the bed shear stress differences are within the 95% confidence interval of the measurements.

Tests 11, 12, 13, 14, and 15 have a 3 to 5 mm erosion depth. The results show the τ_{b2} is consistently smaller than τ_{b1}. This may be expected as the erosion depth increases, as with the bed shear stress at the bottom of a deepening scour hole. Larger erosion depth may result in a lower τ_{b2} because the turbulence intensity in the sediment recess decreases. Tests 14 and 15 results in the lowest τ_{b2} values and the highest percent difference, compared to τ_{b1}.

It can also be seen in Table 4.5 that the velocity, V, calculated using the measured discharge and flow depth is close to the depth-averaged velocity, V_1, obtained from the velocity profile for those tests that have similar τ_{b1} & τ_{b2} values.

Chapter 5

Discussion

There were two related research problems that were investigated in this laboratory study. The first was to study the correlations of unconfined compressive strength with the soil critical shear stress and erosion rate. The second was to test a different experimental setup for an EFA type device to determine the bed shear stress and measure the soil erosion rate. The velocity profiles over a rough bed and an embedded soil sample were measured to estimate the bed shear stress using the logarithmic law (log-law). An improved procedure was developed to determine the displacement height that would reduce the uncertainty in the bed shear stress estimates.

An A-8 Hydraulic Channel with a rough bed was used to measure the erosion rate of a prepared clay sample. The EFA devices developed by Briaud et al. (2001a) and improved by Shan et al. (2012) measure the soil erosion rate and bed shear stress of a clay sample in a water tunnel with smooth walls. The device used in the present study was a tilting flume with a rough bed made of a single layer of gravel. The motivation for using a rough bed was to increase the bed shear stress, and thus, the measurable soil erosion rates. In addition, the bed shear stress in a tilting flume may be determined relatively accurately using the measured flow depth and channel slope or the velocity profile.

The flow over the sediment recess involves a step change in surface roughness (from rough-to-smooth-to-rough). Flow over a sudden change in surface roughness has been studied extensively in both external (e.g., atmospheric boundary layer) and internal (e.g., channel) flows. A recent literature review of this subject can be found in Kadivar et

al. (2021). When a flow encounters a sudden change in surface roughness, an internal boundary layer will start at the roughness transition and grows outwards from the wall with distance downstream. If the surface downstream is of sufficient length a new fully developed turbulent boundary layer will be established eventually. Previous studies have shown that the wall shear stress would attain its new equilibrium value almost immediately, but flow quantities outside the internal boundary layer are determined by conditions before the transition and change only gradually with distance downstream. For a rough-to-smooth (RTS) transition, experimental and numerical studies have found that the wall shear stress would be underestimated if obtained from the mean velocity profile measured outside the internal layer (e.g., Antonia and Luxton, 1972; Loureiro et al. 2010; Li et al. 2019). Therefore, the log-law may be applied with the mean velocity profile to provide a conservative estimate of the bed shear stress on the soil surface in the sediment recess.

In addition to the bed shear stress associated with the mean flow described above, the soil surface was also subject to strong near-bed turbulence. The time it took for the flowing water to pass over the sediment recess was very short (< 0.1 seconds). Consequently, the structure of turbulence over the soil sample, which determines the vertical turbulent transport of streamwise fluid momentum and shear stress distribution, would be controlled primarily by the boundary-layer turbulence generated on the gravel bed upstream. The “external” turbulence then impinges on the soil surface resulting in an increase in the instantaneous bed shear stress and erosion rate. On a smooth bed, this effect may be parameterized using an “apparent roughness” in analogous to the equivalent roughness on a rough bed (see Fredsøe et al., 2003). By fitting the log-law to

the measured velocity profiles over the sediment recess, we found that the “apparent roughness” was comparable to the equivalent roughness of the gravel bed.

In previous EFA studies, the soil sample was protruded into the flow by a piston system. The faster the piston is advanced, the faster the erosion rate may occur. Consequently, there were high uncertainties in the measured erosion rates. In the present study, the soil sample was set at a fixed height and eroded for a specific amount of time to minimize subjectivity that could cause error from a human deciding when to advance the sample. The erosion rate was determined by weighing the soil sample before and after the test. The disadvantage of this method is that only one erosion rate can be measured from each sample tested, and the same procedure must be repeated many times to establish the erosion-rate-versus-shear-stress curve. The results from these tests showed that as the bed shear stress increased, so did the measured average erosion rate.

The erosion rate of cohesive soil was found to be related to the unconfined compressive strength in previous studies. Similar results were found in this study. The results show that as the soil unconfined compressive strength increased, the erosion rate decreased. Although there was much scatter in the measured data, the resulting trend was like those found in previous studies. Because the unconfined compressive strength was varied in this study by changing the water content only, our results suggest that water content may be a more fundamental parameter than unconfined compressive strength for measuring soil erodibility.

The erosion pattern of cohesive soils is unpredictable, and the soil surface developed a rough texture as chunks eroded from the specimen. Crowley et al. (2012) and (2014) showed that the shear stress over a cohesive soil increases as the soil surface

erodes. This could make measuring the shear stress accurately very difficult using formulae for pipe flow, unless the shear stress is measured directly over the eroding sample. A rough bed was installed in a tilting flume to determine if the bed shear stress acting on a clay bed could be controlled more carefully in open channel flow. The rough bed results, presented in Section 4.2 and 4.3, show no significant differences between the estimated bed shear stress on the eroding clay sample and surrounding gravel bed. This suggests that the bed shear stress acting on a clay sample can be controlled, by changing the channel slope and roughness of the surrounding rough bed and measured more accurately using methods developed for open channel flow.

It is well known that the soil erodes in a flowing channel until the bed shear stress (τ_b) is equal to the soil's critical shear stress (τ_c). This implies that the time-rate-of-scour decreases as the surface of the soil sample recedes deeper into the surrounding bed. This was studied by Shan et al. (2012). His results show, using direct force measurements, that the measured shear stress decreases with erosion depth. Similar results were found in this present study. Velocity profile over the soil sample was measured using the PIV technique, and the log-law was used to find bed shear stress. Table 4.5 shows that there were no significant changes in the resulting bed shear stress until the erosion depth was greater than about 3 to 4 mm. This is an improvement over existing EFA devices with smooth side walls where the bed shear stress over the soil sample could be significantly underestimated.

The logarithmic law method used in this study to find the bed shear stress produced more consistent results than the traditional method. The alternative method assumes that the equivalent roughness, k_s, of the channel bottom is known, and remains

constant for a given flow-depth-to-grain-diameter ratio. Various k_s values for the gravel bed were tested. The resulting bed shear stress shows that a k_s-value of $d_{84} = 7$ mm produced the best agreement with bed shear stress calculated using the measured flow depth and channel slope (τ_{b1}), in most cases, while the d_{65} may be a better choice for the equivalent roughness height at smaller flow-depth-to-grain-diameter-ratios.

The method adopted in this study to find the bed shear stress from the measured velocity profile assumes that the k_s value is known. The correct k_s value can then be found by comparing the results with the bed shear stress calculated from the measured flow depth and channel slope in open channel flow. Kamphuis (1973) used this approach to determine the equivalent roughness for a wide range of h/d_{90} ratio values. His results show that the ratio of k_s/d_{90} may be taken as 2.5 when the h/d_{90} ratio is greater than 20. The ratio decreases rapidly when the h/d_{90} value is less than 10. These results indicate that the flow depth is an important factor at small h/d_{90} values. In this study, new experiments were performed to determine the k_s/d_{90} value over a range of h/d_{90} values between 3.6 and 5.6. The results show that at the low end of the h/d_{90} ratio, the k_s/d_{90} ratio is around 0.76. These results are in good agreement with the findings by Kamphuis (1973).

Chapter 6

Major Conclusions

This study has examined several improvements to the existing EFA type devices and presented an alternative method for finding the bed shear stress from a measured velocity profile. The main conclusions of the study are given below.

Several EFA type devices had been developed by researchers to measure soil erosion rates. These devices use a water tunnel, or open channel with smooth side walls, that may not simulate the actual turbulent flow conditions over an eroding soil surface in rivers and streams. The hydraulic channel in the present study used a fixed gravel bed to simulate the turbulent flow environment on a more natural channel bottom. The flow measurements conducted in this study showed that the bed shear stress increased substantially when bed roughness was introduced. Two different methods were used to find the bed shear stress and the estimated results were compared; the sidewall correction method, described in Section 3.6, and the log-law method described in Sections 4.2 and 4.3. The study found that bed shear stress did not decrease substantially over a short transition created by a 2.75-inch diameter clay sample for erosion depth comparable to the grainsize of the surrounding gravel bed. This suggests that the bed shear stress acting on a clay sample may be controlled using artificial roughness in an open channel flume and increased by increasing the channel slope.

The soil property found in previous studies to have a significant effect on erosion rate was the unconfined compressive strength, Q_u. This study focused on varying this parameter while holding other soil properties constant. The results showed much scatter, but the trend showed that as Q_u decreased the average rate of the soil increased. Since the

unconfined compressive strength is closely related to the water content, the latter is an important parameter in determining the erodibility of cohesive soils.

The alternative method developed for finding bed shear stress from the measured velocity profile assumes the von Kármán constant (k-value) is a universal constant with a value around 0.4 and the equivalent grain roughness (k_s) is known. Using the PIV technique, the time-averaged velocity profile was measured and graphed on a plot of $\ln(y-y_0)$ versus u. The displacement height, y_0, was varied until the k-value obtained from the y-intercept of the best straight-line fit was equal to 0.4. The friction velocity, u*, was then found from the slope of the best-fit line. This method significantly reduces the variations in bed shear stress produced by varying y_0 and k_s simultaneously. The traditional method of optimizing the log-law fitting by trial and error can produce a wide variation of bed shear stress and equivalent roughness heights when there are many velocity points. The alternative method converges rapidly, with a smaller range of bed shear stress values. The method was applied to a steady, uniform flow over a fixed gravel bed where the h/d_{90} ratio was between 3 and 6. It was found that the log-law represented the measured velocity profile through almost the entire flow depth. The bed shear stress values obtained from the log-law and the values calculated from the measured flow depth and channel slope were compared, and it was found that k_s can be approximated by d_{84} or smaller diameter (d_{65}) for small values of the h/d_{90} ratio.

The alternative method was used to estimate the bed shear stress on a sudden, short transition of bed roughness created by placing a clay sample in a sediment recess in the fixed gravel bed. The same procedure was followed, and the results showed that the bed shear stress did not change significantly as the flow traveled along a short distance

over a clay sample. This result suggests that the bed shear stress on a clay sample may be increased by installing the test sample within a rough bed.

PIV measurements were conducted over recessed clay samples trimmed to a specified depth. It was found that the bed shear stress on the clay sample was about 5% to 10% smaller than the bed shear stress on the gravel bed upstream for a soil recess depth up to about 5.6 mm, or d_{50}, of the fixed gravel bed.

Chapter 7

Recommendations for Future Research

The present study has developed the experimental methods and procedures for finding the erosion rate and bed shear stress using an open channel flume with a rough bed. The experimental setup was tested using soil samples prepared from Nora Moody Clay. Future work may include testing actual soil samples collected from bridge sites and use the measured soil erosion functions to evaluate bridges for scour. A wide range of bed shear stresses can be produced to induce soil erosion by adjusting the flow discharge and slope of the hydraulic channel.

The bed shear stress in the sediment recess should be measured directly using a shear stress sensor to validate the bed shear stress estimates obtained from PIV measurements. This can be done by flush mounting a hot-film probe in the surface of a soil sample. The experiment should be conducted with the soil surface at different recess depths below the top of the surrounding gravel bed.

The effects of grain size and grain size distribution of the gravel on bed shear stress should be investigated further to produce an optimal design for the erosion test facility. The equivalent roughness height can be determined for different flow conditions using the method employed in this study.

LIST OF REFERENCES

Antonia, R. A. and Luxton, R. E. (1972). "The response of a turbulent boundary layer to a step change in surface roughness. Part 2. Rough-to-smooth." *J. Fluid Mech*., 63(4), 737-757.

ASTM (1997). "ASTM D422 – 63: "Standard Test Method for Particle Size Analysis of Soils." *American Society of Testing Materials* (ASTM), 1997.

ASTM (1997). "ASTM D698 – 91: "Test Method for laboratory Compaction Characteristics of Soil Using Standard Effort (12,400 ft-lbf/ft^3 (600kN-m/m^3))." *American Society of Testing Materials* (ASTM), 1997.

ASTM (1997). "ASTM D2166 – 91: "Standard Test Method for Unconfined Compressive Strength of Cohesive Soil." *American Society of Testing Materials* (ASTM), 1997.

ASTM (1997). "ASTM D1140 – 92: Standard Test Method for Amount of Material in Soils Finer than the No. 200 (75μm) Sieve." *American Society of Testing Materials* (ASTM), 1997.

Briaud, J.-L., Ting, F., Chen, H.C., Cao, Y., Han, S.W., Kwak, K.W, (2001a) "Erosion Function Apparatus for Scour Rate Predictions." *Journal of Geotechnical and Environmental Engineering*, ASCE Vol 127, No.2, 105-113.

Briaud, J.-L., Chen, H.C., Kwak K., Han, S.W., Ting, F.C.K, (2001b) "Multiflood and Multilayer Method for Scour Rate Predictions at Bridge Piers." *Journal of Geotechnical and Environmental Engineering*, ASCE Vol 127, No.2, 105-113.

Briaud, J.-L., Chen, H. C., Li, Y., Nurtjahyo, P. and Wang, J. (2005). "SRICOS-EFA method for contraction scour in fine-grained soils." J. *Geotechnical and Geoenvironmental Eng*., 10.1061/(ASCE)1090-0241(2005)131:10(1283).

Cheng, N-S (2011). "Revisited Vanoni-Brooks sidewall correction." *Int. J. Sediment Res*., 26, 524-528.

Chow, V. T.(1959). *Open-Channel Hydraulics*. McGraw-Hill Book Company, New York.

Crowley, R. W., Bloomquist, D. B., Hayne, J. R., Holst, C. M., and Shah, F. D. (2012a). "Estimation and measurement of bed material shear stresses in erosion rate testing devices." *J. Hydraul. Eng.,* 10.1061/(ASCE)HY.1943-7900.0000608, 990–994.

Crowley, R. W., Bloomquist, D. B., Shah, F. D., and Holst, C. M. (2012b)."The sediment erosion rate flume (SERF): A new testing device for measuring erosion rate and shear stress." *Geotech. Test. J*., 35(4),649–659.

Crowley, R. W., Robeck, C., and Thieke, R. J. (2014)."Computational Modeling of Bed Material Shear Stresses in Piston-Type Erosion Testing Devices." *J. Hydraulic Eng.*, American Society of Civil Engineers, Reston, VA.

Fredsøe, J, Sumer, B. M., Kozakiewicz, A., Chua, L. H. C., and Deigaard, R. (2003). "Effect of externally generated turbulence on wave boundary layer." *Coastal Eng.*, 49, 155-183.

Frings, R. M., Schüttrumpf, H., and Vollmer, S. (2011). "Verification of porosity for fluvial and sand-gravel deposits." *Water Resour. Res.,* 47, W07527, doi: 10.1029/2010WR009690.

INSIGHT 4G™ User's Guide (2011). Insight 4G Global Imaging, Acquisition, Analysis and Display Software. TSI Incorporated.

Kamphuis, J. W. (1973). "Determination of sand roughness for fixed beds." *J. Hydraul. Res.*, https://doi.org/10.1080/00221687409499737.

Kadivar, M., Tormey, D. and McGranaghan, G. (2021). "A review on turbulent flow over rough surfaces: Fundamentals and theories." *Int. J. Thermofluids*, 10, 1000777.

Li, M., de Silva, C. N., Rouhi, A., Baidya, R., Chung, D., Marusic, I., and Hutchins, N. (2019). "Recovery of wall-shear stress to equilibrium flow conditions after a rough-to-smooth step change in turbulent boundary layers." *J. Fluid Mech.*, 8 72, 472-491.

Loureiro, J. B. R., Sousa, F. B. C. C., Zotin, J. K. Z., and Silva Freire, A. P. (2010). "The distribution of wall shear stress downstream of a change in roughness." *Int. J. Heat Fluid Flow*, 31, 785-793.

Middleton, G. V. and Southard, J. (1984). Mechanics of Sediment Movement. *SEPM for Sedimentary Geology Short Course Number 3*, 2nd edition.

Nikuradse, J. (1933). "Strömungsgesetze in rauhen Rohren." *VDI-Forschungsheft*; English trans., NACA Tech. Mem. 1292.

Shan H., Kerenyi K., Guo J., Shen J., Wagner A., and Xie. Z., (2012). "An ex-situ scour testing device for characterizing erosion of cohesive soils." *6th International Conference on Scour and Erosion (ICSE-6).*

Shan H., Shen J., Kilgoe R., Kerenyi K., (2015). "Scour in Cohesive Soils." *U.S. Department of Transportation Federal Highway Administration.* McLean, VA.

Straub, T.D., and T.M. Over. 2010. Pier and Contraction Scour Prediction in Cohesive Soils at Selected Bridges in Illinois. *Illinois Center for Transportation, Research Report* ICT-10-074. Rantoul, IL.

Ting, F. C. K. and Kern, G. (2021). "Find the bed shear stress on a rough bed using the log law." Submitted to *J. Waterw. Port, Coast. Ocean Eng.*

Validyne Engineering Corp. "Differential Pressure Transducer User Manual."

Appendix A

Procedure for finding the Flow Rate in the A-8 Hydraulic Channel

The discharge rate in the A-8 Hydraulic Channel with a gravel bed installed was measured using a 7.62-cm diameter orifice that had been calibrated in the factory using a V-Notch weir. The flow discharge is related to the differential pressure head:

$$Q = k\sqrt{\Delta h}$$

where *k* is the discharge coefficient (= 0.2887); Δh is the differential pressure head, ft; and Q is the discharge rate, ft^3/s.

Figure A.1 A-8 Hydraulic Channel

The differential pressure across the orifice was measured using a low range differential pressure transducer manufactured by Validyne with a pressure range of 5.5-inch H_2O (0.2 psi)

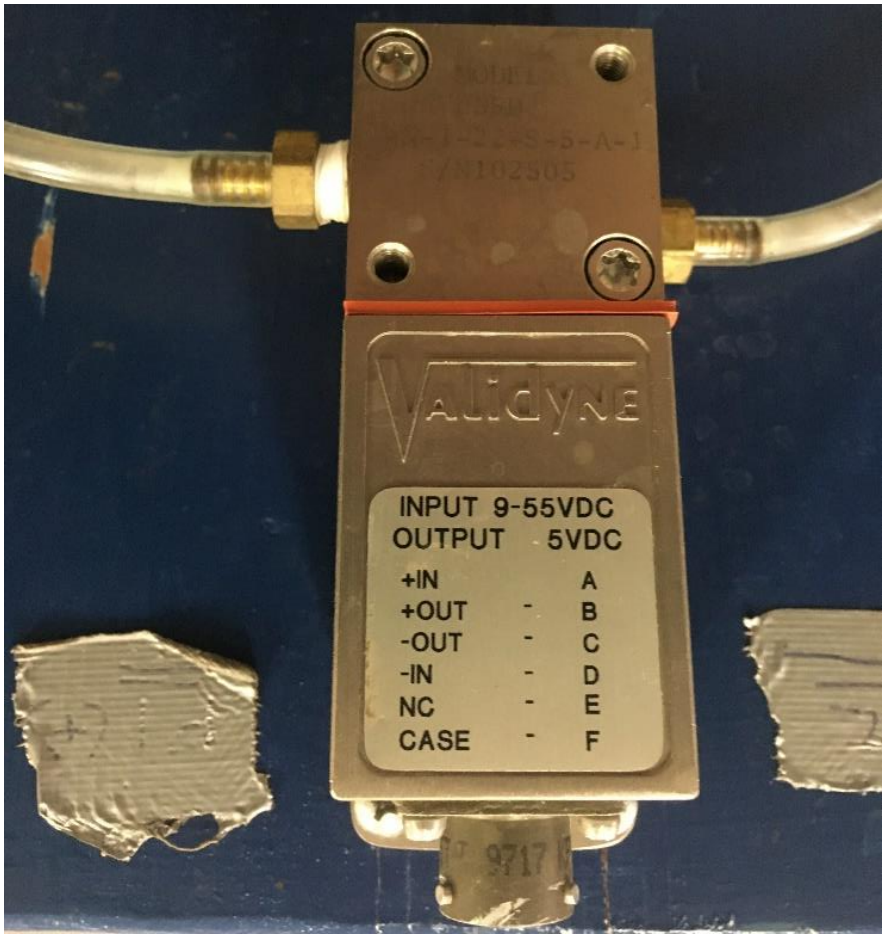

Figure A.2 Validyne Engineering Co. Differential Pressure Transducer

The differential pressure transducer was calibrated using two static manometer columns to obtain a calibration curve between the differential pressure head (Δh) and the measured voltage (volt). The calibration procedure is described below.

Figure A.3 Static Manometer set up

1. The differential pressure transducer was connected to pressure taps on the manometer using a valve system.

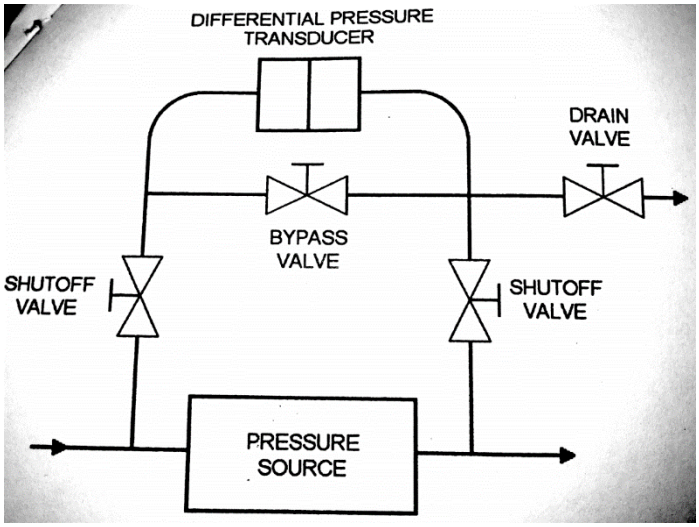

Figure A.4 Typical Valve arrangement (Validyne Engineering Corp.)

2. The tubing was then fully flooded with water and trapped air was bled from the system through two bleed holes in the transducer.
3. Once water completely flooded the tubing system connected to the differential pressure transducer, the water levels in both manometer tubes were filled to the same height.
4. A voltage output from the differential pressure transducer was sampled at 50Hz for 1 minute (3000 data points) using a data acquisition system and averaged. The procedure was repeated with different differential pressure heights, Δh, over the full range of the pressure transducer to establish a calibration curve

$$\Delta h\ (ft) = 0.1003 * (volt) + 0.00710$$

5. The differential pressure transducer tubes were disconnected from the manometer tubes and connected to pressure taps on each side of the large orifice in the A-8 Hydraulic Channel.

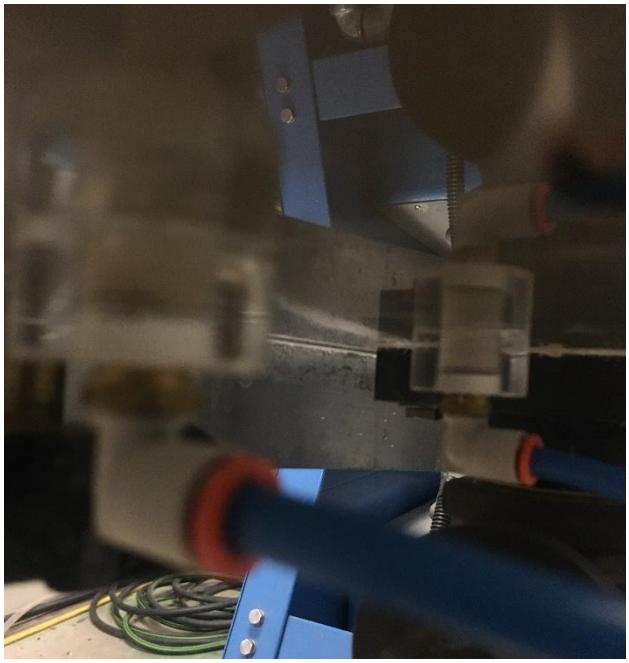

Figure A.5 Pressure taps on each side of Orifice in hydraulic channel (bottom view)

6. The hydraulic channel was set to a 1% slope and the water pump was turned on at the maximum discharge.
7. After a uniform flow was established in the hydraulic channel, voltage readings were taken over a one-minute period at a sample rate of 50 Hz and averaged. Two water depth measurements were also taken using a point gauge, at $^2/_3$ and ¾ length along the flume, and averaged.
8. The averaged voltage reading was then used with the calibration curve to find a Δh. The measured Δh was corrected for the difference in the elevation of the pressure taps due to the slope of the flume.
9. The corrected Δh was used in the factory calibrated orifice equation to calculate the discharge rate.

$$Q = 0.2887\sqrt{\Delta h}$$

10. Steps 9-12 were then repeated at slopes 2% through 12%.

Slope	Measured Q (ft^3/s)	Measured Water Depth (in)
0.01	0.1585	1.815
0.02	0.1580	1.545
0.03	0.1607	1.395
0.04	0.1599	1.270
0.05	0.1569	1.215
0.06	0.1566	1.16
0.07	0.1567	1.115
0.08	0.1563	1.065
0.09	0.1585	1.03
0.1	0.1594	1.005
0.11	0.1578	0.985
0.12	0.1576	0.96

Table A.1 Measured flow depth and discharge over a fixed gravel bed at different slopes in A-8 Hydraulic Channel

Appendix B

Soil Erosion Test Results

Slope (%)	Initial w (%)	Final w (%)	Time (min)	SA (in^2)	H_0 (in)	$M_{0, wet}$ (g)	$M_{f, wet}$ (g)	$M_{0,dry}$ (g)	$M_{f, dry}$ (g)	Y US sample (in)	Y at Sample (in)	Y DS Sample (in)	Avg. Water Depth (in)	Difference (g)	Percent of sample	Erosion Rate (in/min)	**Erosion Rate (mm/hr)**	T_{b1} (N/m^2)	Qu (psi)
1	19.45%	21.44%	250	2.16	1.625	281.51	284.12	235.67	233.96	2.00	1.96	1.81	1.923	1.71	0.7%	4.7E-05	**0.07**	3.8034	33.137
2	19.45%	20.93%	250	2.16	1.75	311.61	313.74	260.87	259.43	1.56	1.66	1.39	1.537	1.44	0.6%	3.9E-05	**0.06**	6.2041	33.137
4	24.23%	29.27%	249	2.16	1.375	270.89	280.50	218.06	216.98	1.24	1.35	1.17	1.253	1.08	0.5%	2.72E-05	**0.04**	10.2461	14.977
5	24.96%	28.10%	540	2.16	1.4375	280.94	227.82	224.82	177.84	1.21	1.16	1.20	1.190	46.98	20.9%	5.56E-04	**0.85**	12.2264	9.975
5	20.69%	25.01%	374	2.16	1.375	265.13	262.60	219.679	210.07	1.21	1.20	1.21	1.207	9.61	4.4%	1.61E-04	**0.25**	12.4457	21.756
5	25.64%	28.26%	120	2.16	1.625	318.49	316.96	253.49	247.12	1.16	1.31	1.16	1.210	6.37	2.5%	3.41E-04	**0.52**	12.4844	9.223
5	24.63%	26.18%	420	2.16	1.4375	283.05	236.33	227.11	187.3	1.23	1.25	1.23	1.237	39.81	17.5%	6.00E-04	**0.91**	12.8322	15.389
6	24.63%	28.29%	235	2.16	1.4375	270.47	218.72	217.02	170.49	1.16	1.15	1.15	1.153	46.53	21.4%	1.31E-03	**2.00**	14.2976	15.389
6	24.57%	26.78%	185	2.16	1.375	262.99	249.68	211.12	196.94	1.17	1.13	1.17	1.153	14.18	6.7%	4.99E-04	**0.76**	14.2976	15.796
7	24.23%	27.56%	280	2.16	1.375	265.66	269.16	213.85	211.01	1.00	1.12	1.01	1.043	2.84	1.3%	6.51E-05	**0.10**	14.8744	14.977
7	24.96%	29.03%	240	2.16	1.5	275.14	191.15	220.18	148.14	1.05	1.04	1.07	1.052	72.04	32.7%	2.04E-03	**3.12**	15.0366	9.975

Table B.1 Hydraulic channel erosion test results for bed shear stress < 16 N/m^2

Green highlighted rows tests conducted in parallel with PIV measurements

Slope (%)	Initial w (%)	Final w (%)	Time (min)	SA (in^2)	H_0 (in)	$M_{0, wet}$ (g)	$M_{f, wet}$ (g)	$M_{0,dry}$ (g)	$M_{f, dry}$ (g)	Y US sample (in)	Y at Sample (in)	Y DS Sample (in)	Avg. Water Depth (in)	Difference (g)	Percent of sample	Erosion Rate (in/min)	**Erosion Rate (mm/hr)**	T_{b1} (N/m^2)	Qu (psi)
7	24.06%	26.83%	180	2.16	1.375	254.38	220.66	205.05	173.98	1.12	1.10	1.11	1.108	31.07	15.2%	1.16E-03	**1.76**	16.0443	15.046
7	20.69%	24.02%	335	2.16	1.5625	307.38	289.68	254.686	233.58	1.10	1.14	1.11	1.115	21.11	8.3%	3.87E-04	**0.59**	16.1700	21.756
7	24.17%	27.47%	160	2.16	1.4375	293.75	243.73	236.57	191.2	1.13	1.12	1.12	1.123	45.37	19.2%	1.72E-03	**2.63**	16.3136	15.321
8	25.64%	31.00%	79	2.16	1.5	300.53	260.04	239.20	198.51	1.02	1.06	1.00	1.027	40.69	17.0%	3.23E-03	**4.92**	16.8295	9.223
7	19.01%	20.87%	280	2.16	1.5	315.07	288.45	264.74	238.64	1.17	1.18	1.17	1.173	26.10	9.9%	5.3E-04	**0.80**	17.2100	34.918
8	23.64%	26.71%	370	2.16	1.4375	284.79	223.66	230.34	176.51	1.07	1.02	1.05	1.047	53.83	23.4%	9.08E-04	**1.38**	17.2402	16.187
8	22.85%	24.66%	210	2.16	1.625	326.08	273.20	265.43	219.15	1.07	1.04	1.03	1.047	46.28	17.4%	1.35E-03	**2.06**	17.2402	18.3
8	22.40%	31.37%	300	2.16	1.3750	257.81	230.17	210.63	175.21	1.05	1.07	1.05	1.053	35.42	16.8%	7.71E-04	**1.17**	17.3633	16.812
8	24.96%	28.08%	276	2.16	1.4375	251.61	209.20	201.35	163.33	1.06	1.06	1.05	1.057	38.02	18.9%	9.84E-04	**1.50**	17.4454	9.975
8	23.64%	25.41%	310	2.16	1.4375	277.37	213.67	224.34	170.38	1.06	1.06	1.06	1.057	53.96	24.1%	1.12E-03	**1.70**	17.4454	16.187
8	24.06%	25.04%	160	2.16	1.4375	270.42	188.59	217.98	150.82	1.07	1.07	1.06	1.063	67.16	30.81%	2.77E-03	**4.22**	17.5684	15.046
8.2	20.02%	22.50%	302	2.16	1.5	264.28	266.36	220.197	217.43	1.06	1.05	1.06	1.053	2.77	1.3%	6.24E-05	**0.10**	17.8254	27.423
8	20.69%	25.76%	340	2.16	1.5625	297.39	278.60	246.408	221.53	1.07	1.11	1.08	1.083	24.88	10.1%	4.64E-04	**0.71**	17.9783	21.756
8	19.01%	20.80%	285	2.16	1.75	359.47	362.37	302.05	299.97	1.10	1.12	1.10	1.107	2.08	0.7%	4.2E-05	**0.06**	18.4696	34.918
9	24.06%	26.36%	120	2.16	1.375	268.15	248.76	216.15	196.87	1.03	1.02	1.02	1.023	19.28	8.92%	1.02E-03	**1.56**	18.9842	15.046
9	21.93%	21.71%	314	2.16	1.625	335.85	302.08	275.445	240.3	1.03	1.02	1.03	1.027	35.14	12.8%	6.60E-04	**1.01**	19.0764	21.725
9	24.63%	26.83%	185	2.16	1.4375	281.23	239.97	225.65	189.2	1.04	1.05	1.04	1.043	36.45	16.2%	1.26E-03	**1.91**	19.4448	15.389

Table B.2 Hydraulic channel erosion test results for bed shear stress 16 N/m^2 – 19.5 N/m^2

Green highlighted rows tests conducted in parallel with PIV measurements

Slope (%)	Initial w (%)	Final w (%)	Time (min)	SA (in^2)	H_0 (in)	$M_{0, wet}$ (g)	$M_{f, wet}$ (g)	$M_{0,dry}$ (g)	$M_{f, dry}$ (g)	Y US sample (in)	Y at Sample (in)	Y DS Sample (in)	Avg. Water Depth (in)	Difference (g)	Percent of sample	Erosion Rate (in/min)	**Erosion Rate (mm/hr)**	T_{b1} (N/m^2)	Qu (psi)
10	23.33%	27.09%	246	2.16	1.625	326.26	259.13	264.54	203.9	0.95	0.95	0.99	0.963	60.64	22.9%	1.51E-03	**2.31**	19.6889	16.145
9	22.85%	24.72%	180	2.16	1.625	324.48	301.76	264.13	241.95	1.06	1.07	1.04	1.057	22.18	8.4%	7.58E-04	**1.16**	19.7670	18.3
9	18.93%	21.94%	375	2.16	1.625	315.04	316.22	264.895	259.33	1.06	1.09	1.05	1.067	5.57	2.1%	9.10E-05	**0.14**	19.9970	25.54
10	22.85%	27.31%	153	2.16	1.625	320.02	256.74	260.50	201.66	1.03	0.93	0.97	0.977	58.84	22.6%	2.40E-03	**3.66**	20.0475	18.3
9	19.01%	22.88%	212	2.16	1.375	277.96	241.11	233.56	196.22	1.08	1.06	1.07	1.070	37.34	16.0%	1.0E-03	**1.58**	20.066	34.918
10	24.17%	27.15%	165	2.16	1.375	262.31	185.06	211.25	145.55	1.01	1.00	1.01	1.005	65.70	31.1%	2.59E-03	**3.95**	20.7637	15.321
10	24.57%	27.27%	160	2.16	1.375	253.17	205.55	203.24	161.51	1.02	1.01	1.01	1.012	41.73	20.5%	1.76E-03	**2.69**	20.9426	15.796
11	23.33%	27.87%	230	2.16	1.625	327.44	256.47	265.50	200.57	0.95	0.94	0.96	0.950	64.93	24.5%	1.73E-03	**2.63**	21.4152	16.145
10	24.18%	25.84%	120	2.16	1.625	321.23	269.34	258.68	214.04	1.05	0.98	1.06	1.030	44.64	17.3%	2.34E-03	**3.56**	21.4023	11.901
11	23.64%	28.05%	165	2.16	1.4375	290.06	225.99	234.60	176.46	0.99	0.96	0.99	0.980	58.14	24.8%	2.16E-03	**3.29**	22.2586	16.187
11	24.17%	29.38%	136	2.16	1.375	267.37	208.82	215.33	161.4	0.98	0.99	0.98	0.982	53.93	25.0%	2.53E-03	**3.86**	22.2147	15.321
11	20.36%	25.13%	271	2.16	1.5625	309.26	248.49	256.95	198.58	0.99	0.97	1.01	0.990	58.37	22.7%	1.3E-03	**2.00**	22.5394	25.763
11	18.93%	23.92%	242	2.16	1.5	308.48	223.32	259.38	180.21	1.04	0.92	1.02	0.993	79.17	30.5%	1.89E-03	**2.88**	22.6236	25.54
11	19.91%	21.06%	330	2.16	1.625	330.44	324.64	275.57	268.16	0.99	1.01	0.99	0.997	7.41	2.7%	1.3E-04	**0.20**	22.7358	29.924
12	20.36%	26.24%	300	2.16	1.625	330.73	226.23	274.78	179.2	0.96	1.01	0.93	0.967	95.58	34.8%	1.9E-03	**2.87**	23.997	25.763
12	18.76%	21.08%	317	2.16	1.5	305.95	307.37	257.62	253.85	0.97	1.00	0.96	0.977	3.77	1.5%	6.9E-05	**0.11**	24.3029	37.667
12	18.93%	22.04%	240	2.16	1.625	326.16	306.23	274.245	250.92	0.98	1.03	0.98	0.997	23.33	8.5%	5.76E-04	**0.88**	24.9143	25.54
12	18.76%	21.17%	247	2.16	1.625	349.92	311.47	294.64	256.78	0.98	1.04	0.97	0.997	37.86	12.9%	8.5E-04	**1.29**	24.9143	37.667

Table B.3 Hydraulic channel erosion test results for bed shear stress > 19.5 N/m^2

Appendix C

Raw PIV images Over Cohesive Soil Bed

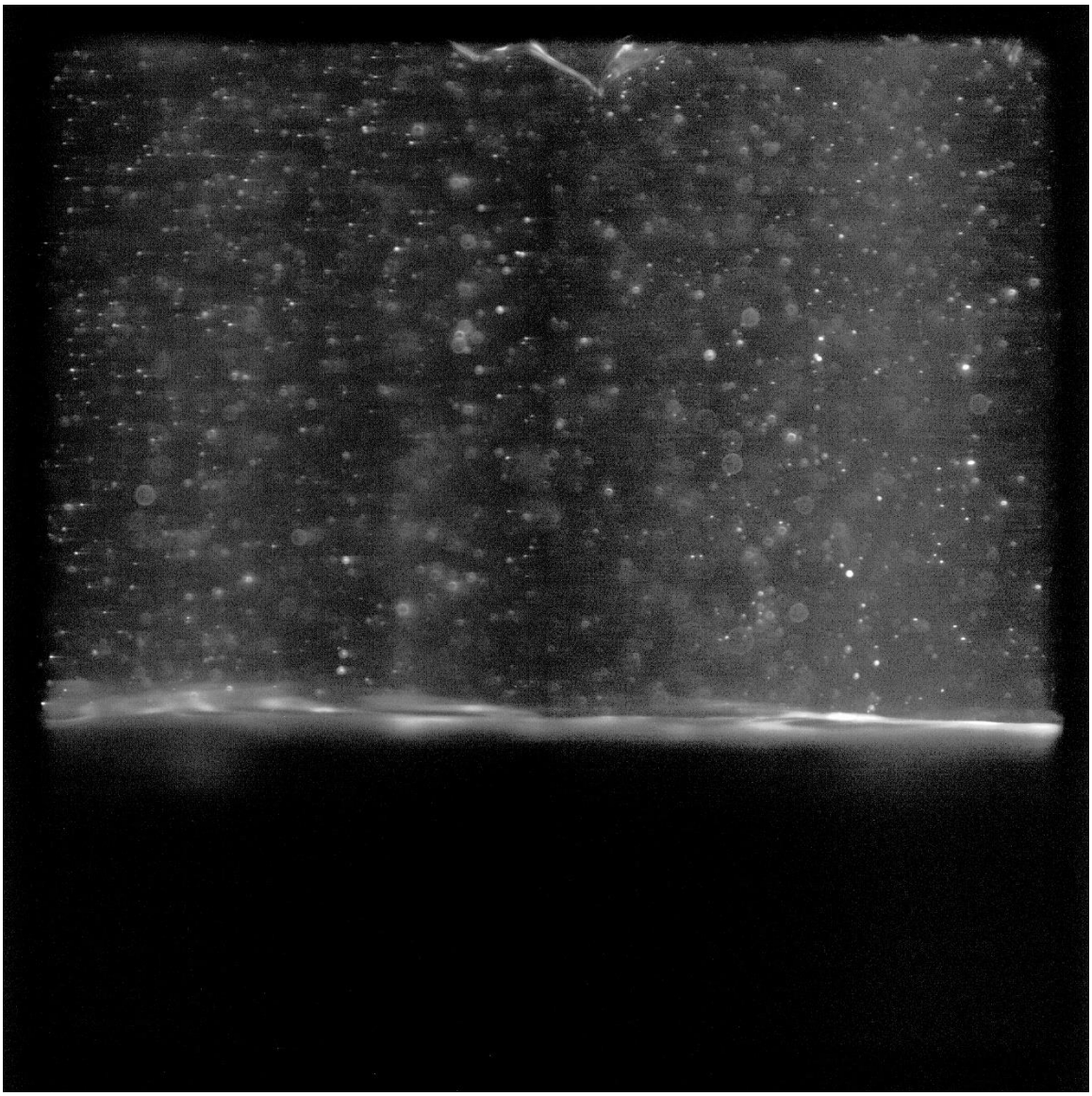

Figure C.1 Raw PIV image for Test 2

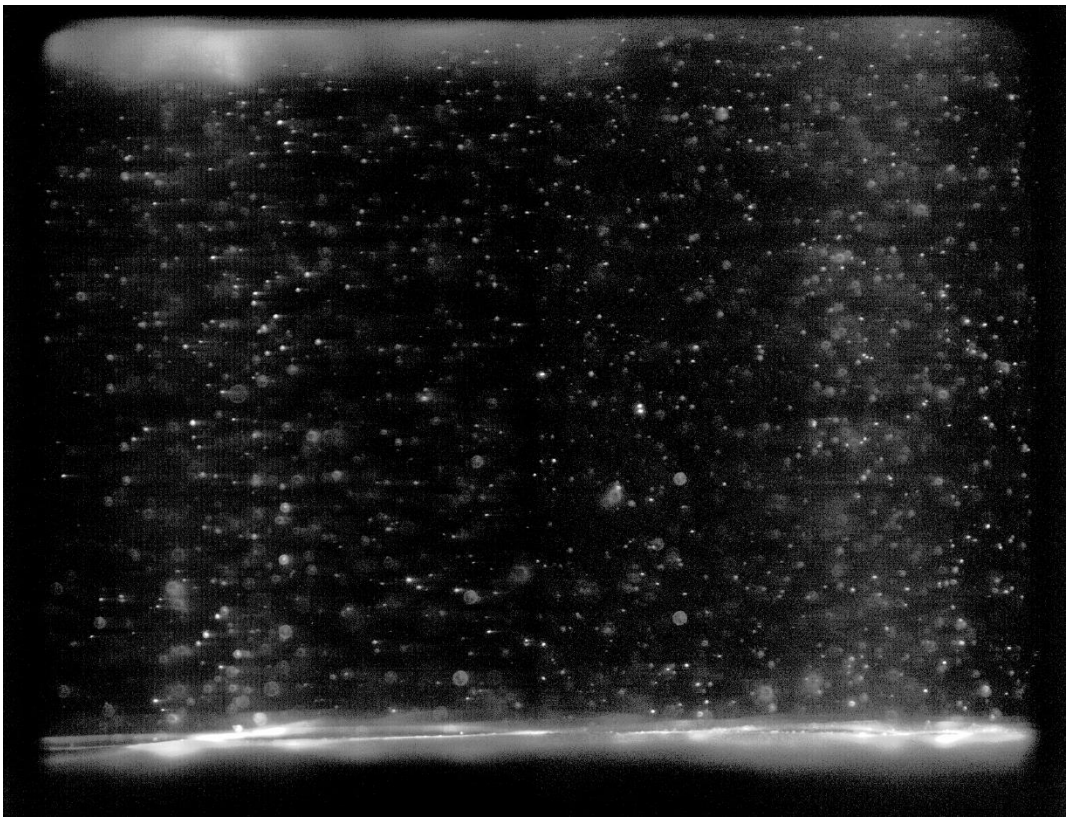

Figure C.2 Raw PIV image for Test 3

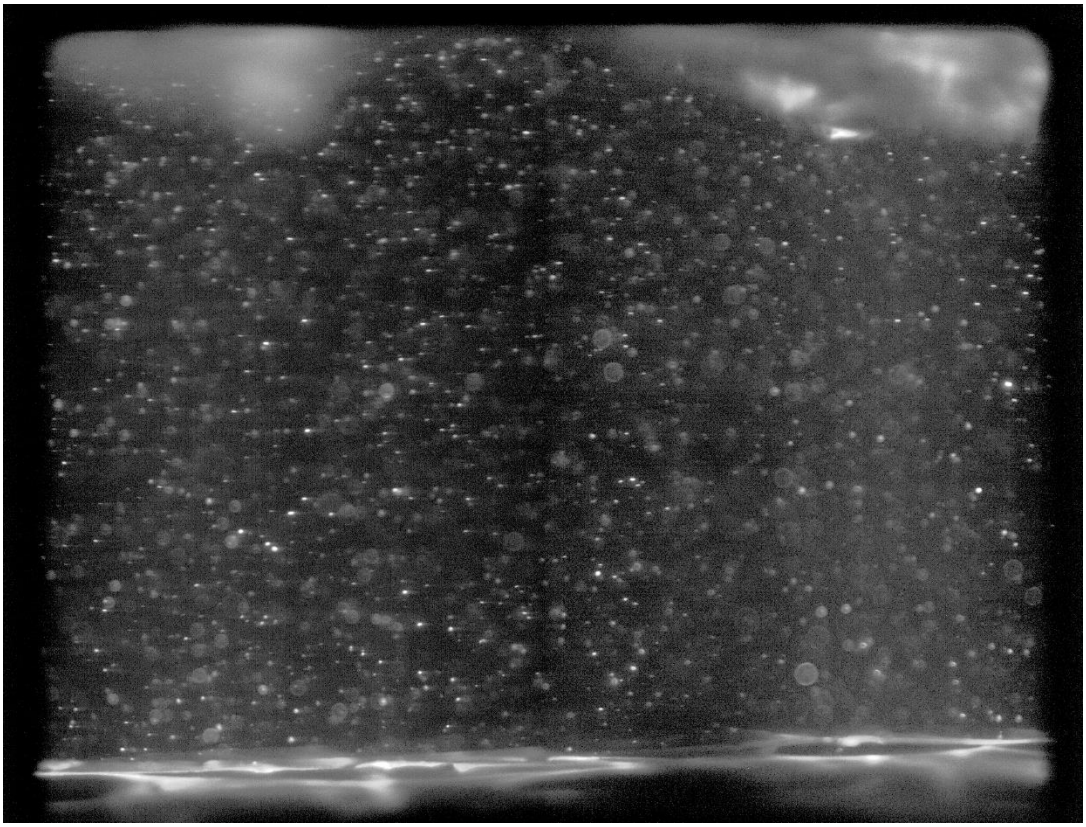

Figure C.3 Raw PIV image for Test 4

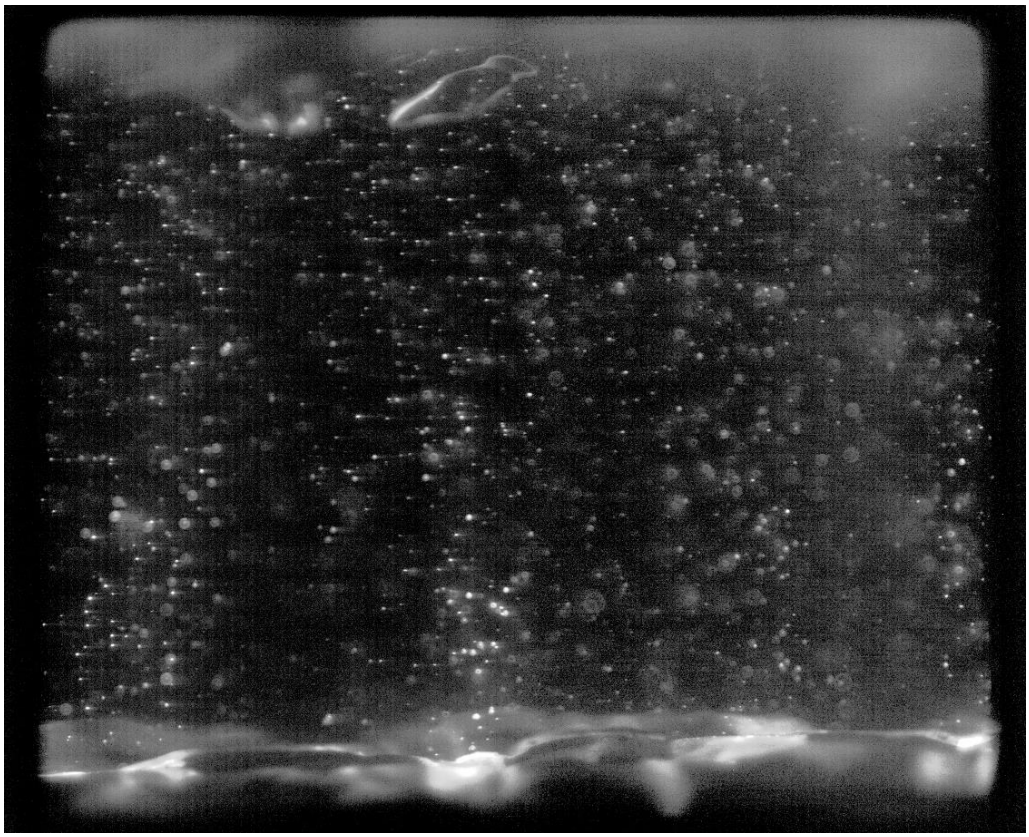

Figure C.4 Raw PIV image for Test 5

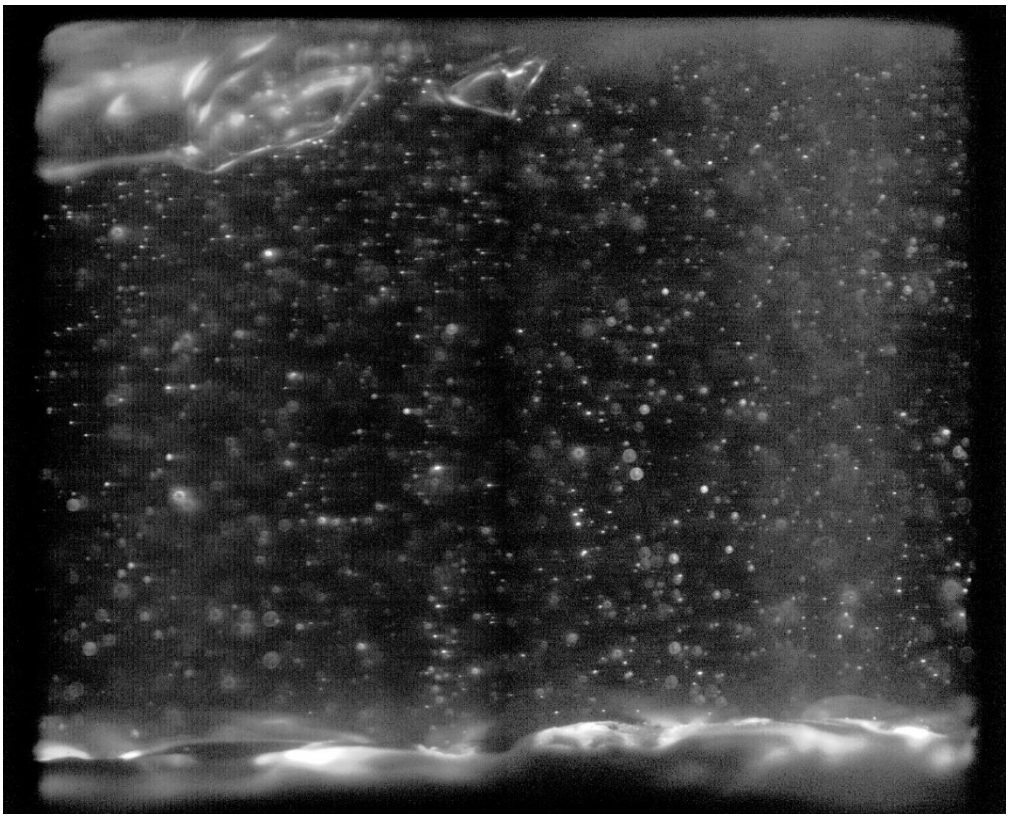

Figure C.5 Raw PIV image for Test 6

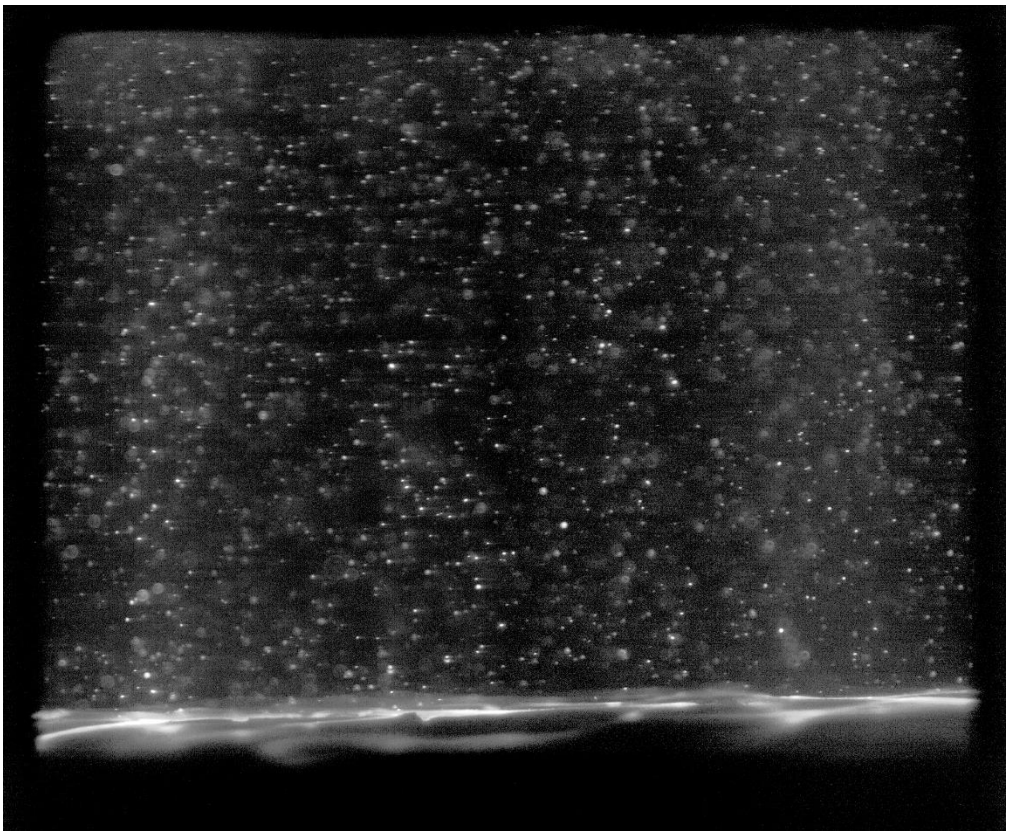

Figure C.6 Raw PIV image for Test 7

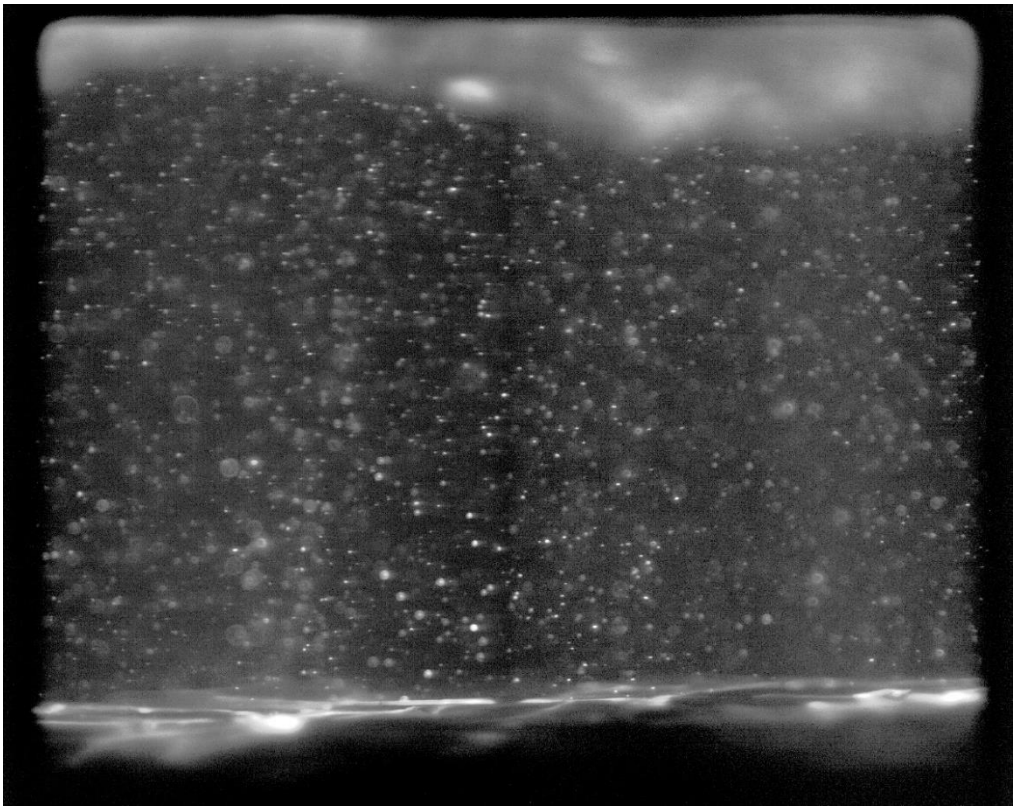

Figure C.7 Raw PIV images for Test 8

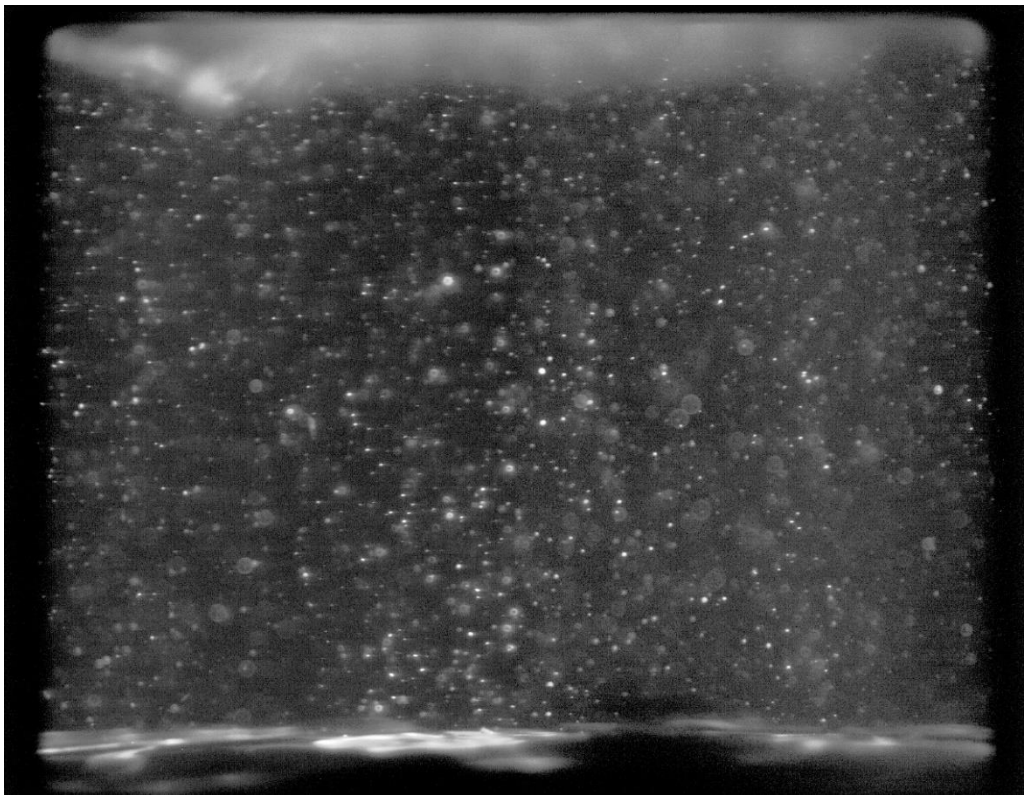

Figure C.8 Raw PIV image for Test 9

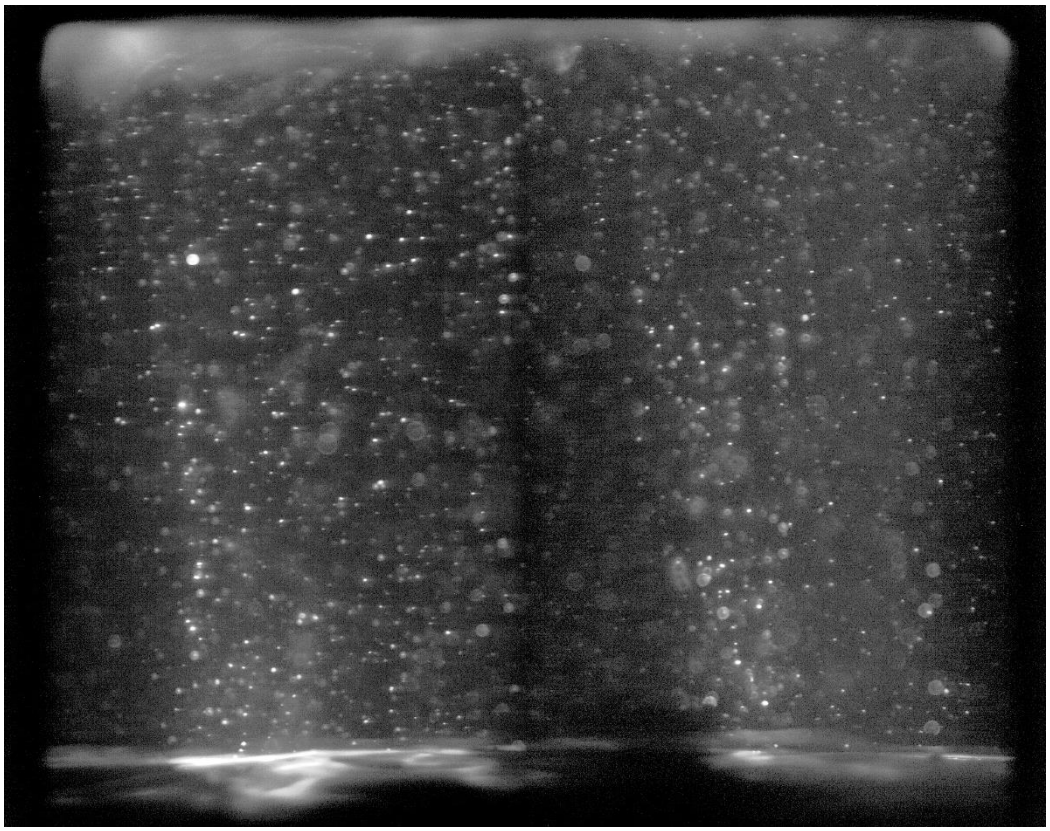

Figure C.9 Raw PIV image for Test 10

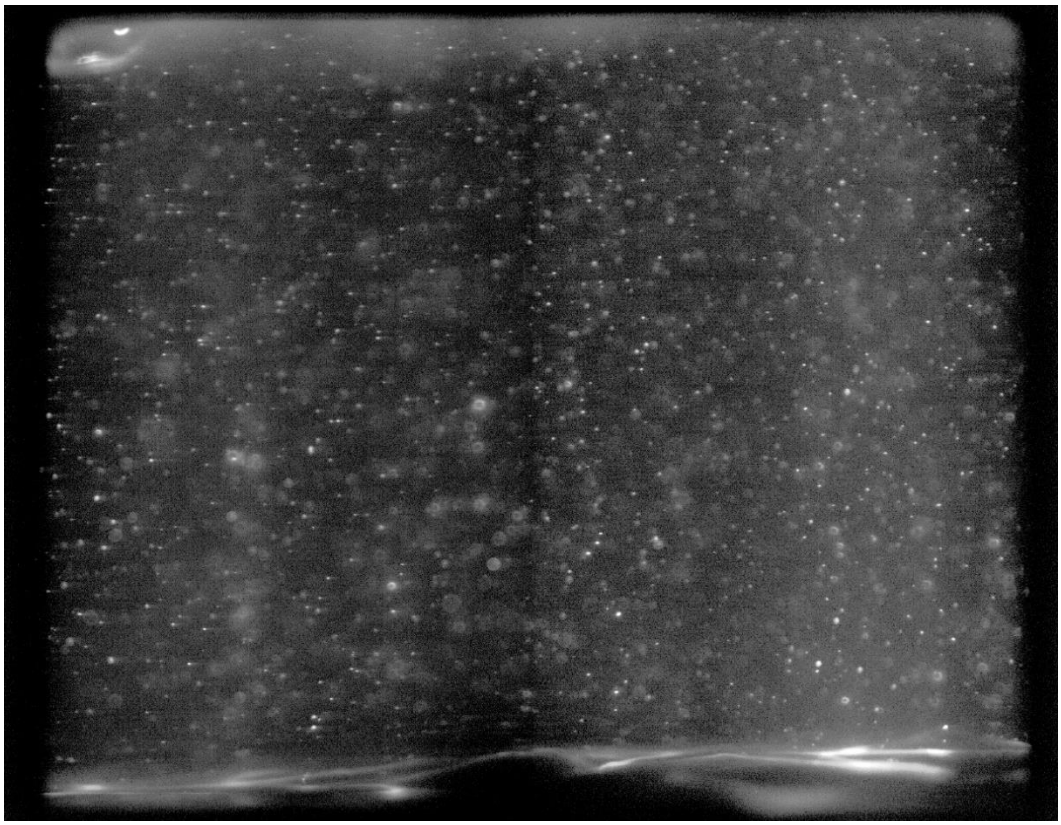

Figure C.10 Raw PIV image for Test 11

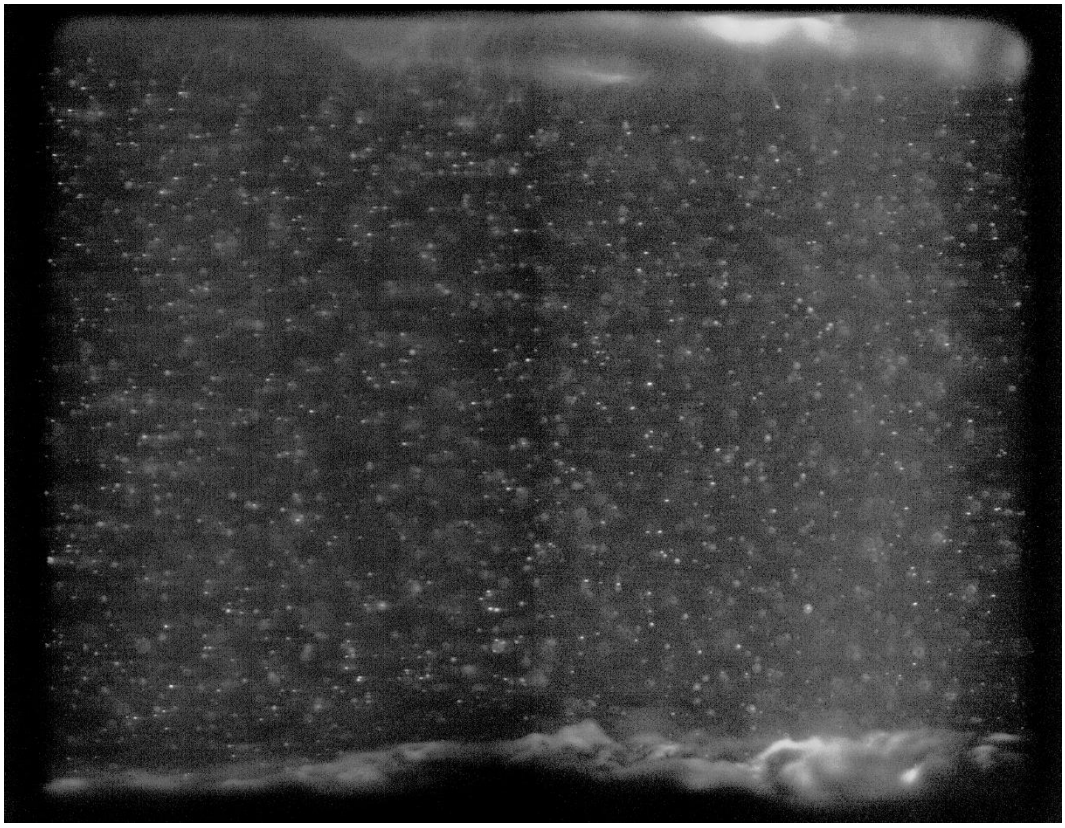

Figure C.11 Raw PIV image for Test 12

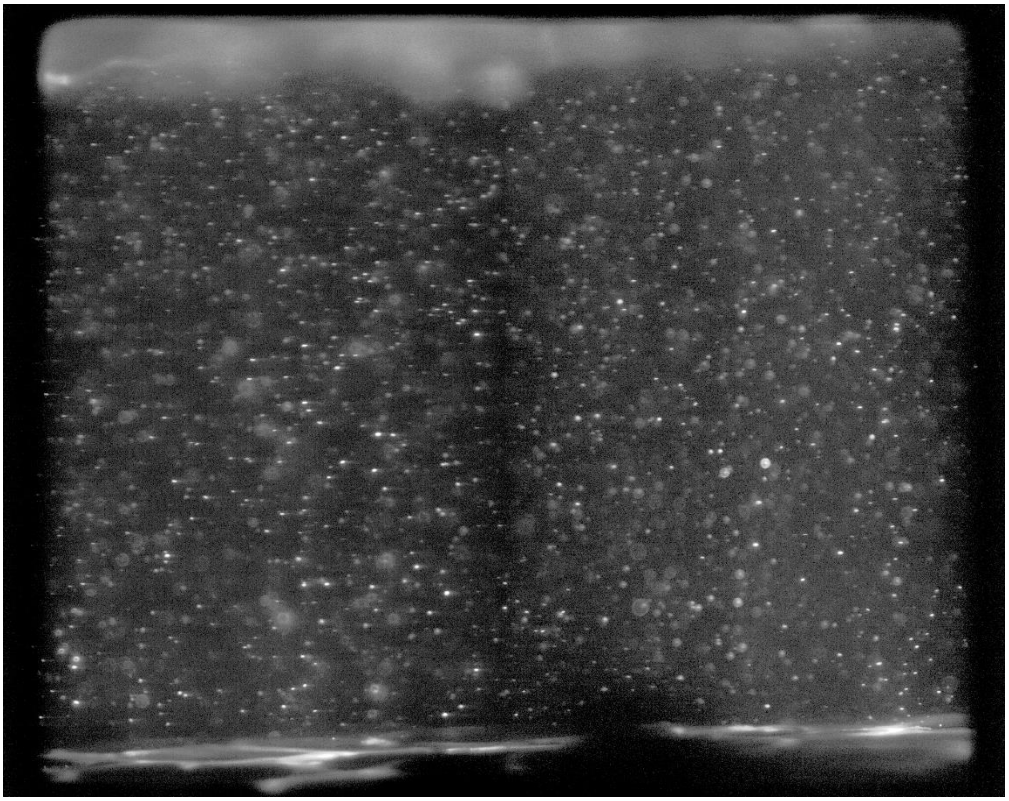

Figure C.12 Raw PIV image for Test 13

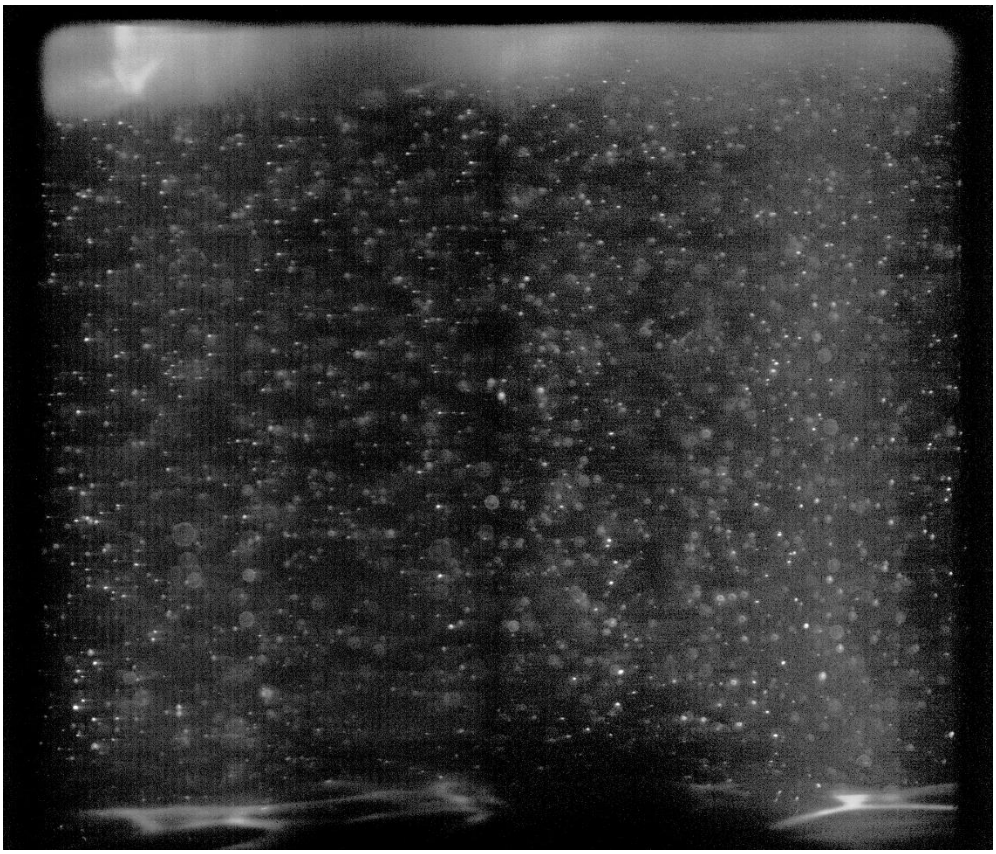

Figure C.13 Raw PIV image for Test 14

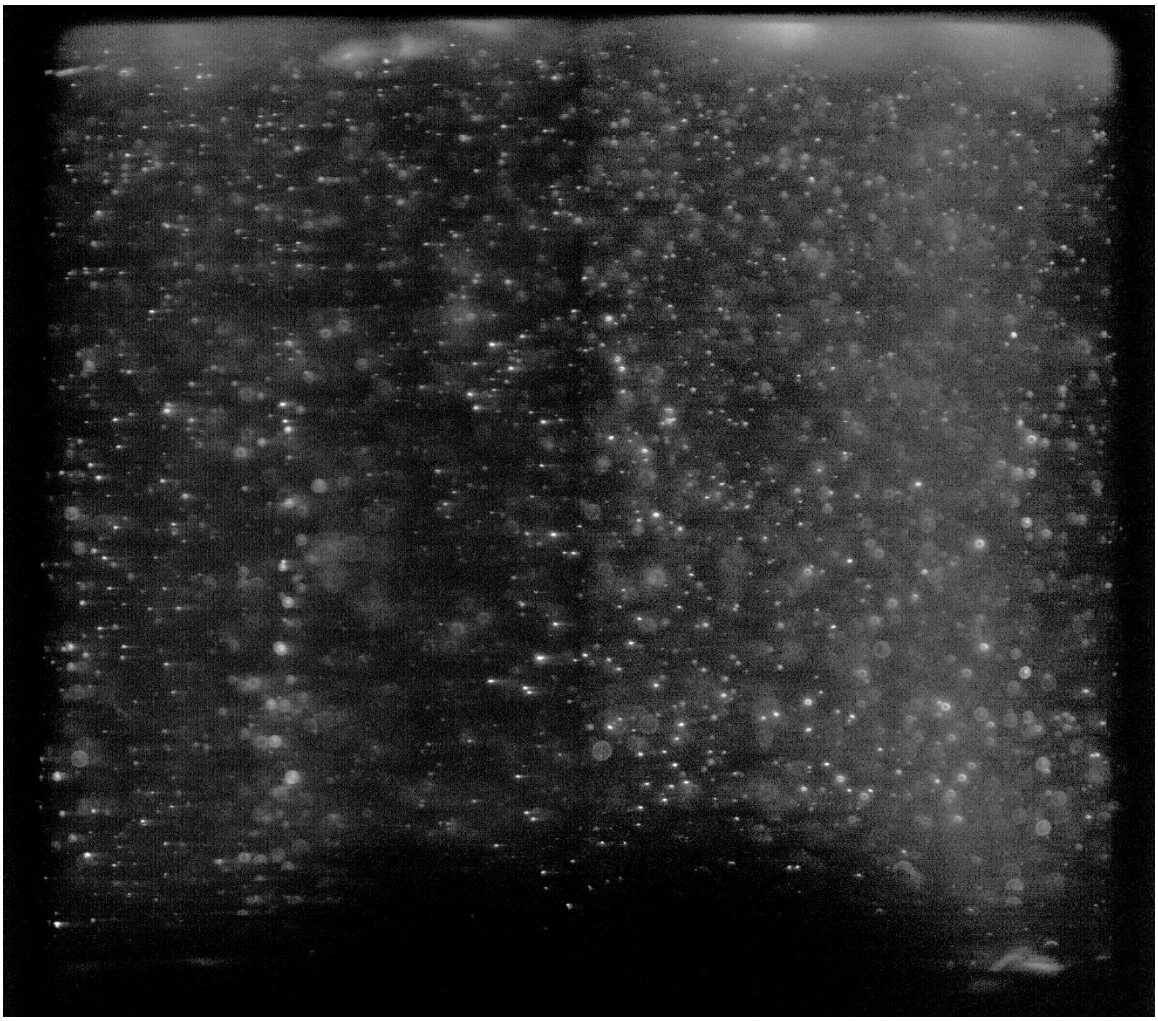

Figure C.14 Raw PIV image for Test 15

Appendix D

Time-Average Velocity Profiles for PIV tests

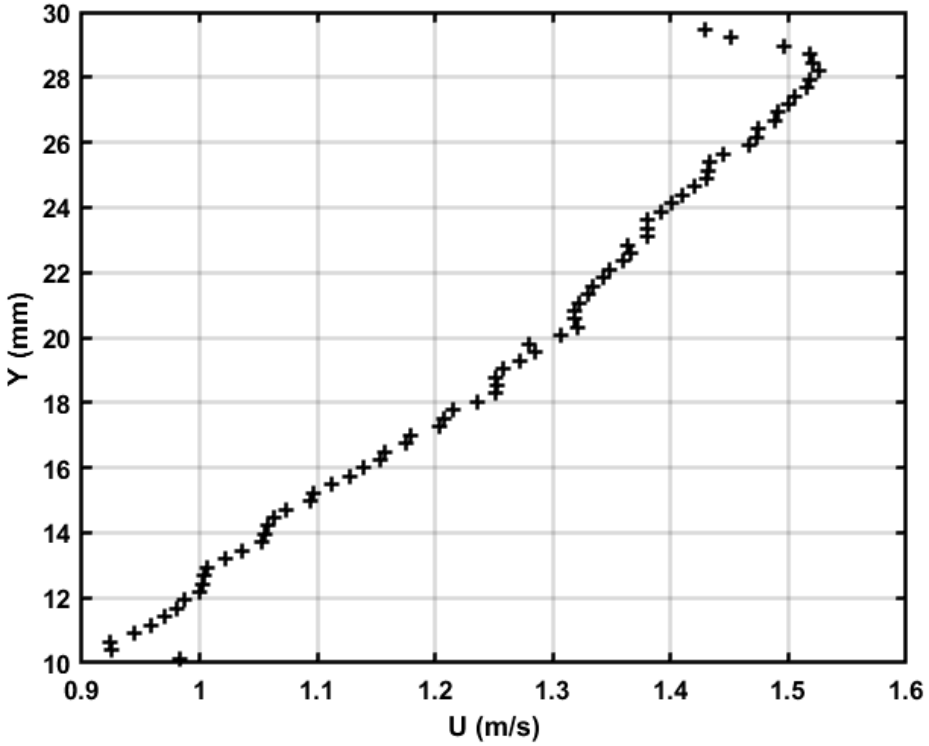

Figure D.1 Test 2 time-average velocity profile (No erosion depth)

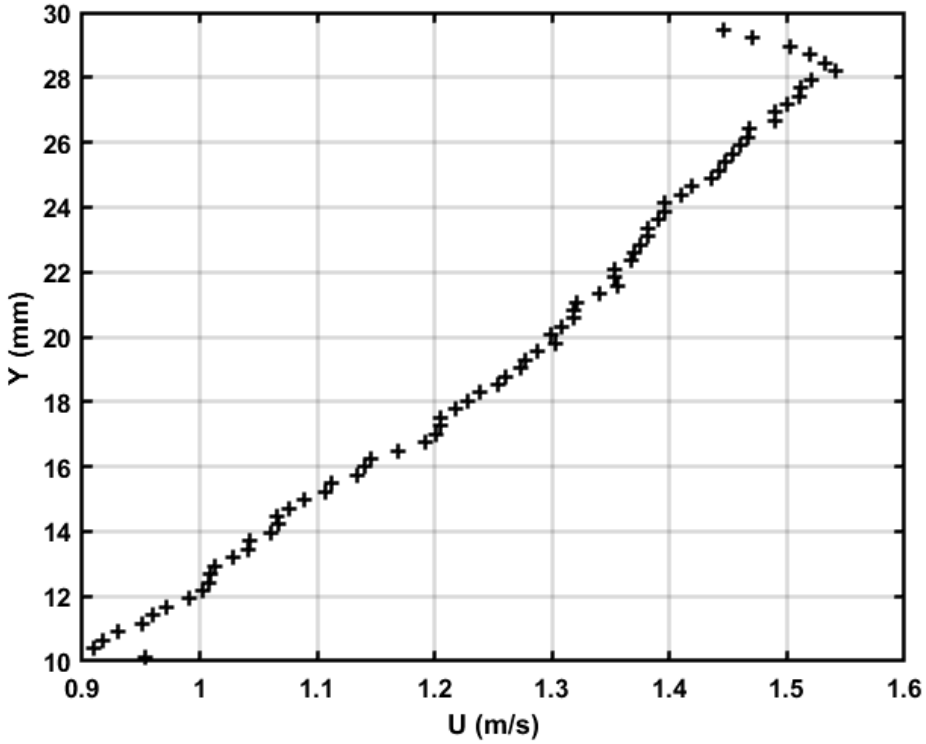

Figure D.2 Test 3 time-average velocity profile (No erosion depth)

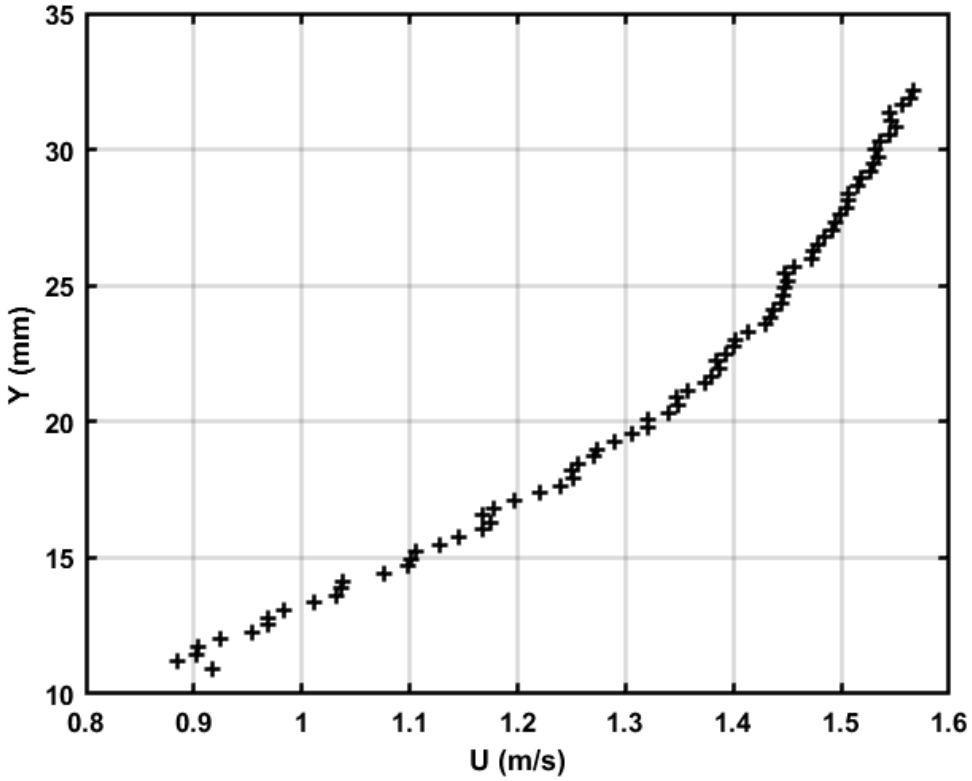

Figure D.3 Test 5 time-average velocity profile (1.5 mm erosion depth)

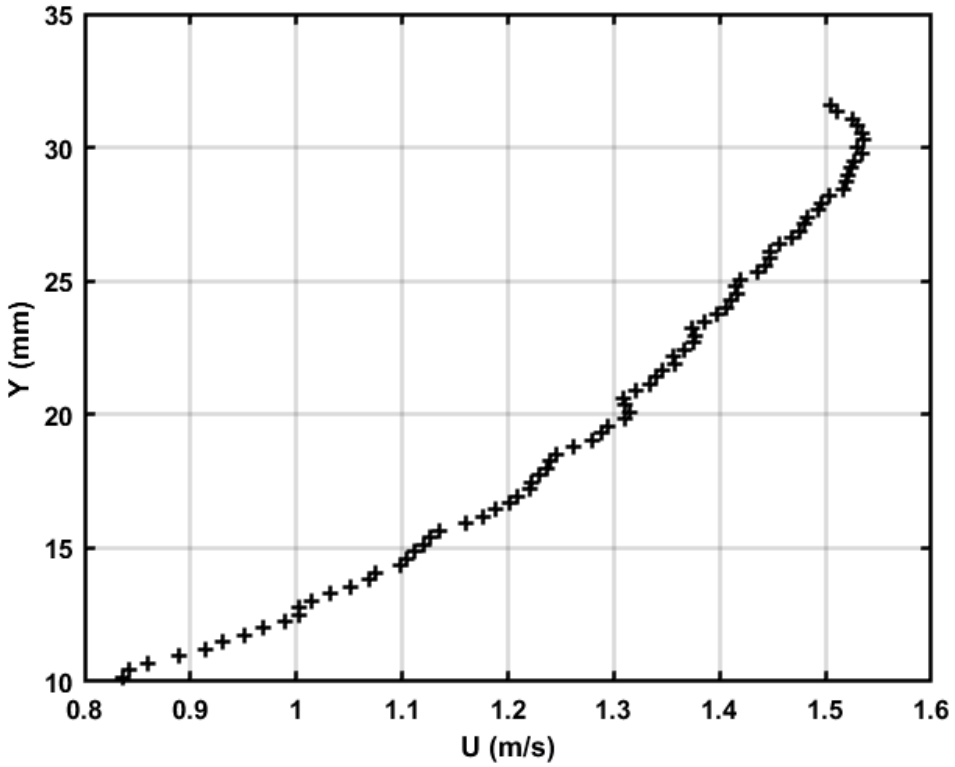

Figure D.4 Test 6 time-average velocity profile (1.6 mm erosion depth)

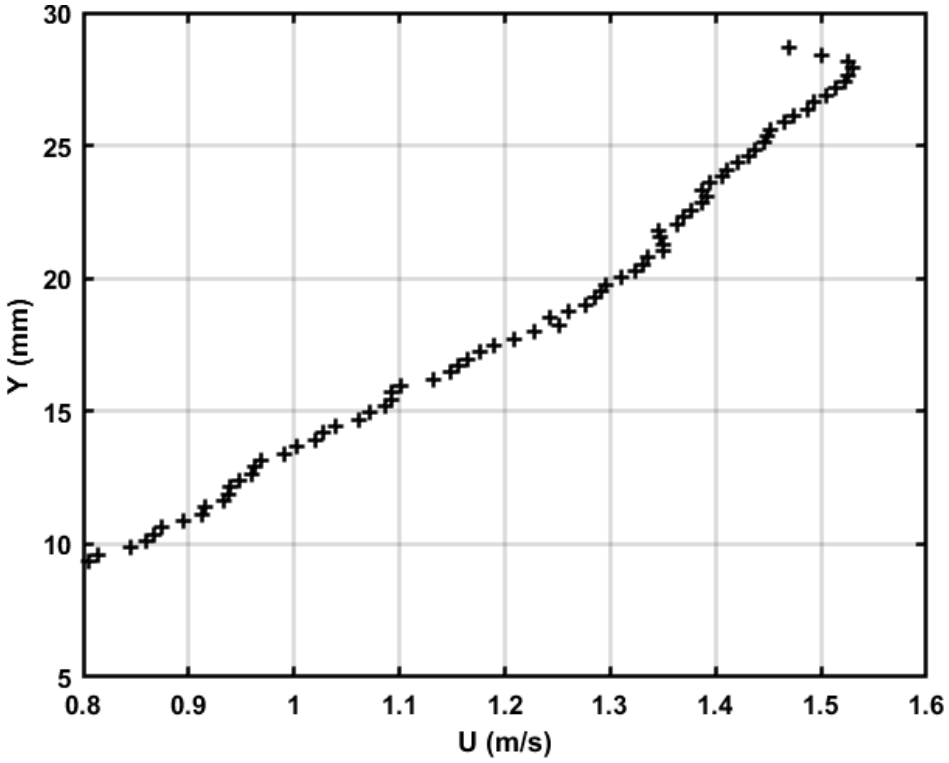

Figure D.5 Test 7 time-average velocity profile (1.6 mm erosion depth)

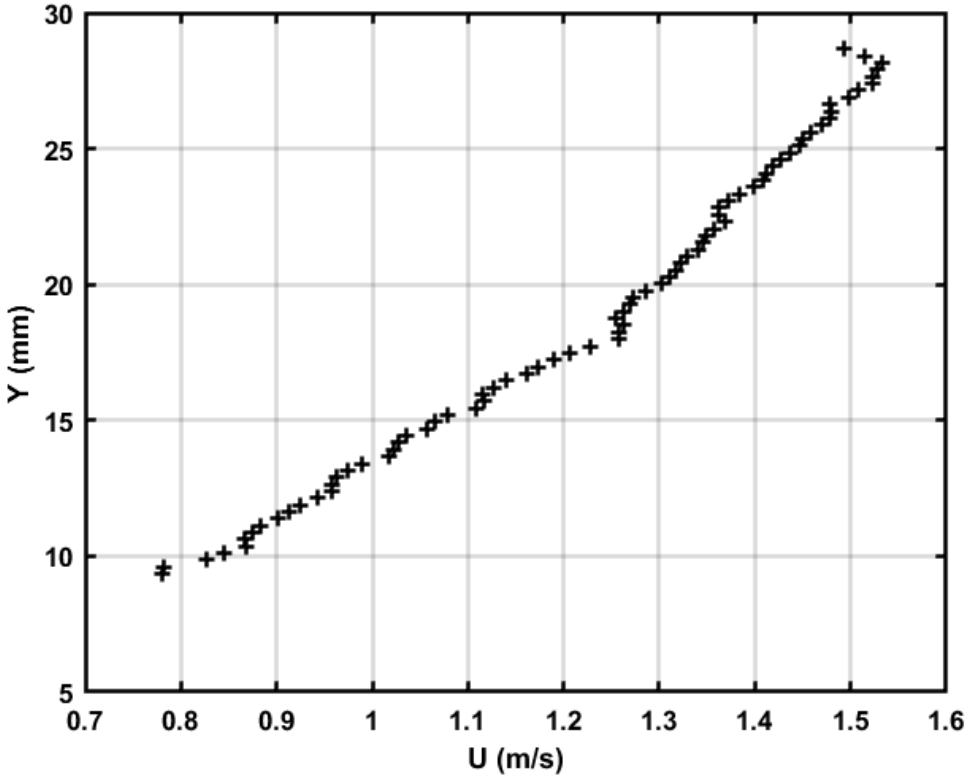

Figure D.6 Test 8 time-average velocity profile (1.6 mm erosion depth)

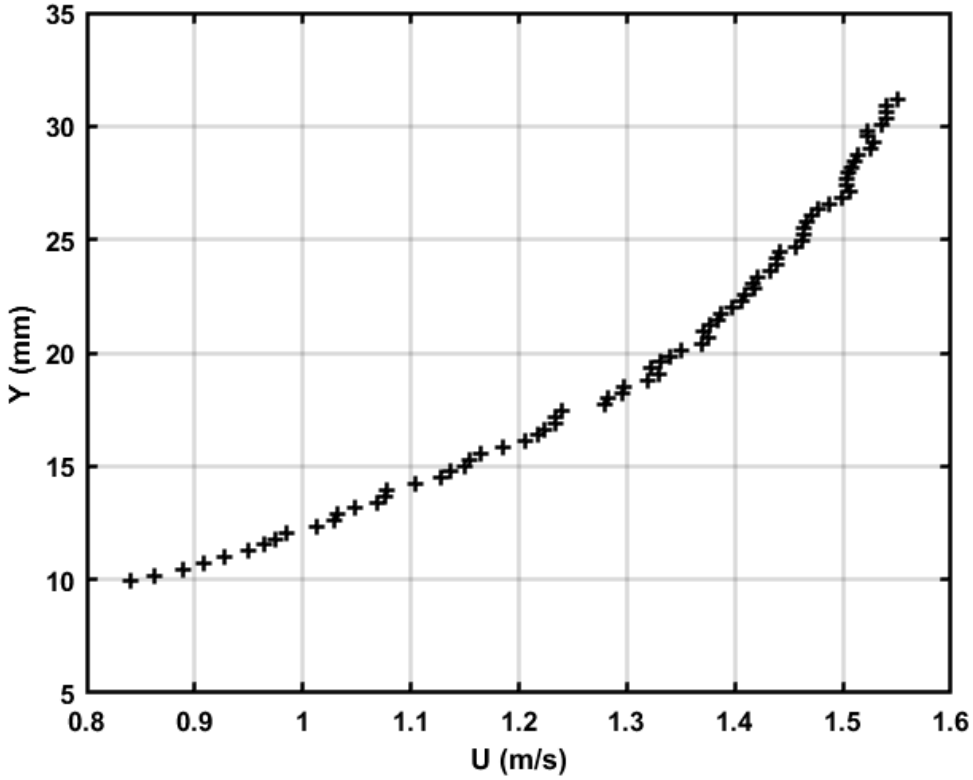

Figure D.7 Test 9 time-average velocity profile (2.5 mm erosion depth)

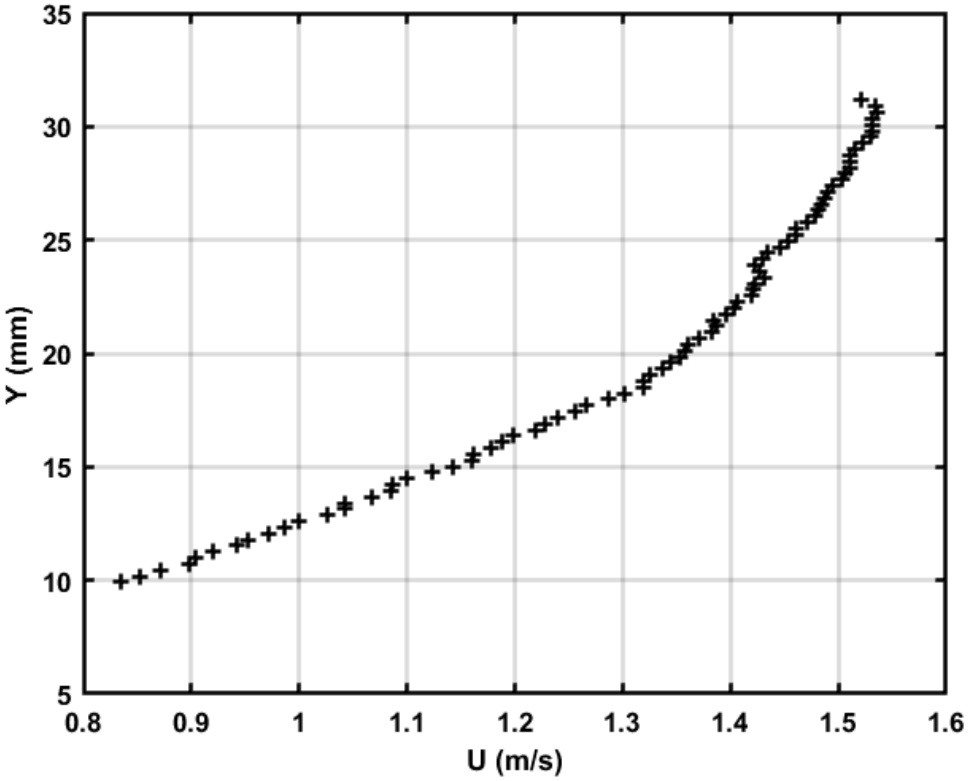

Figure D.8 Test 10 time-average velocity profile (2.5 mm erosion depth)

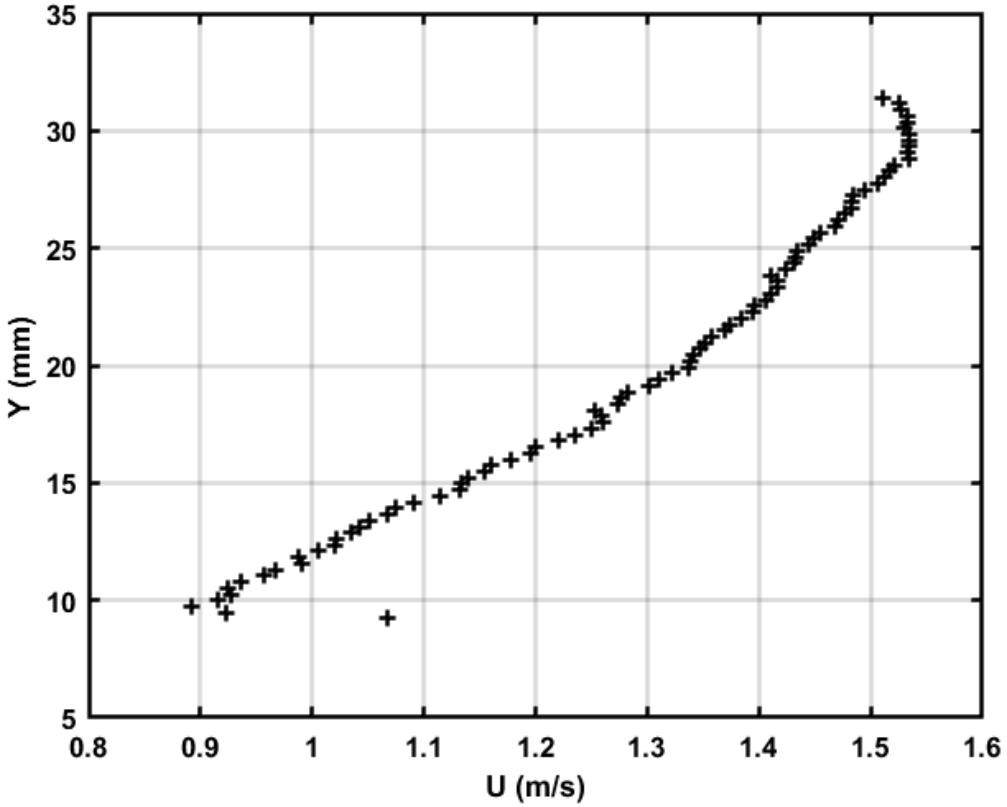

Figure D.9 Test 11 time-average velocity profile (3 mm erosion depth)

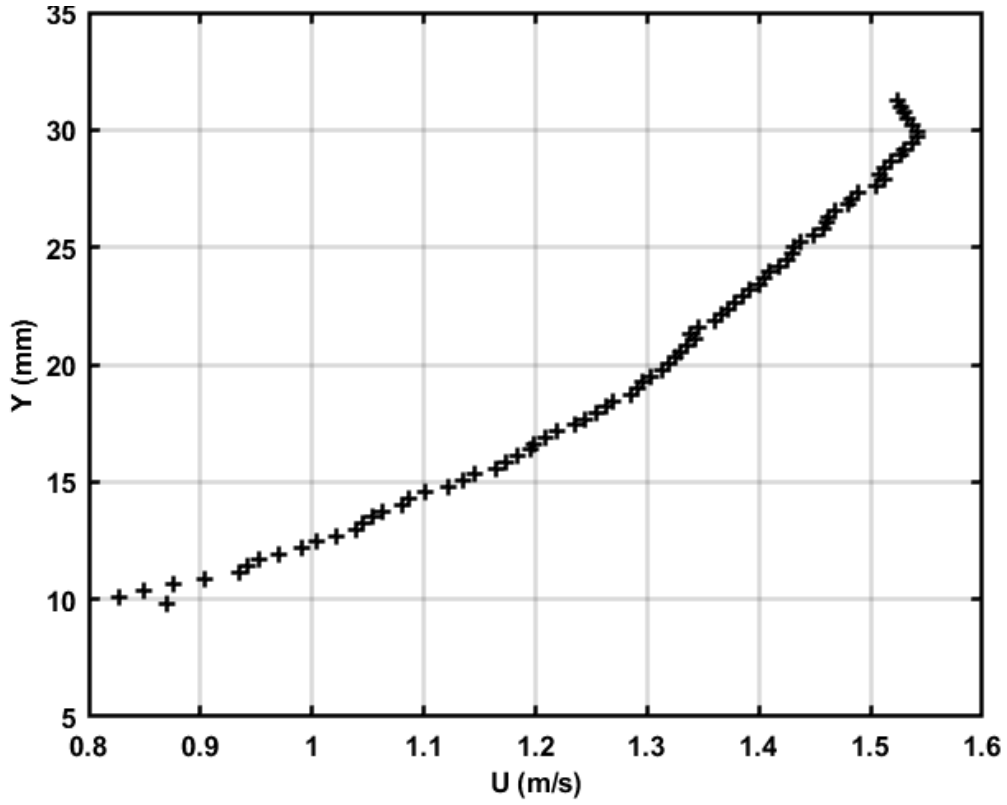

Figure D.10 Test 12 time-average velocity profile (3 mm erosion depth)

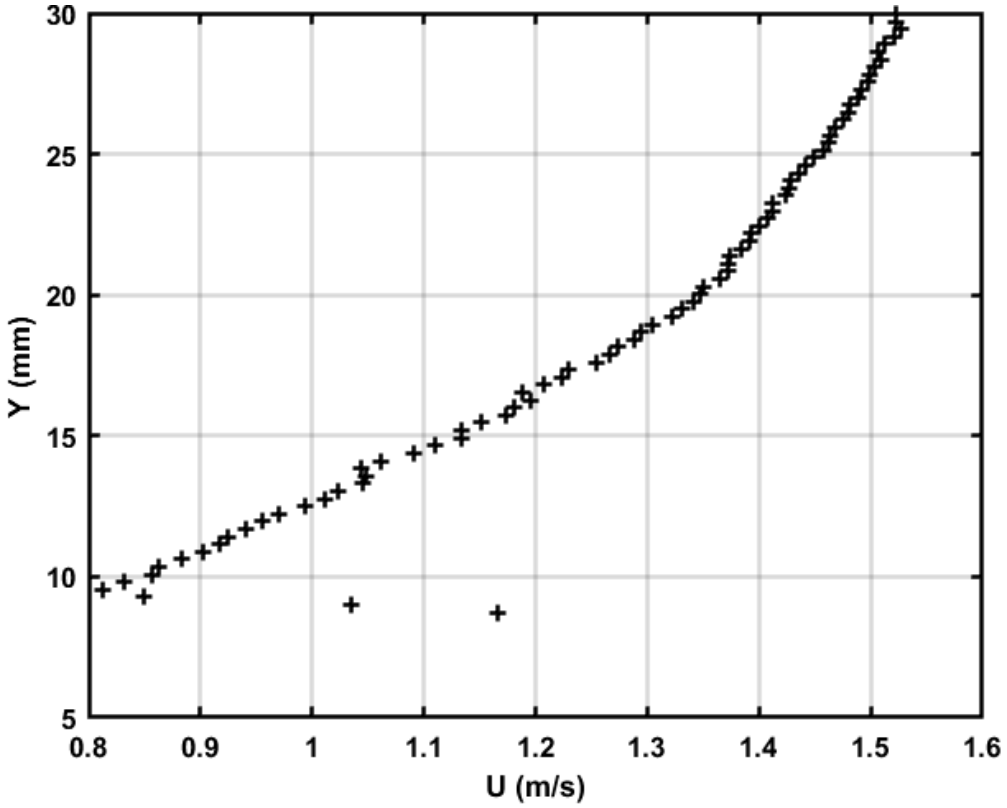

Figure D.11 Test 13 time-average velocity profile (4 mm erosion depth)

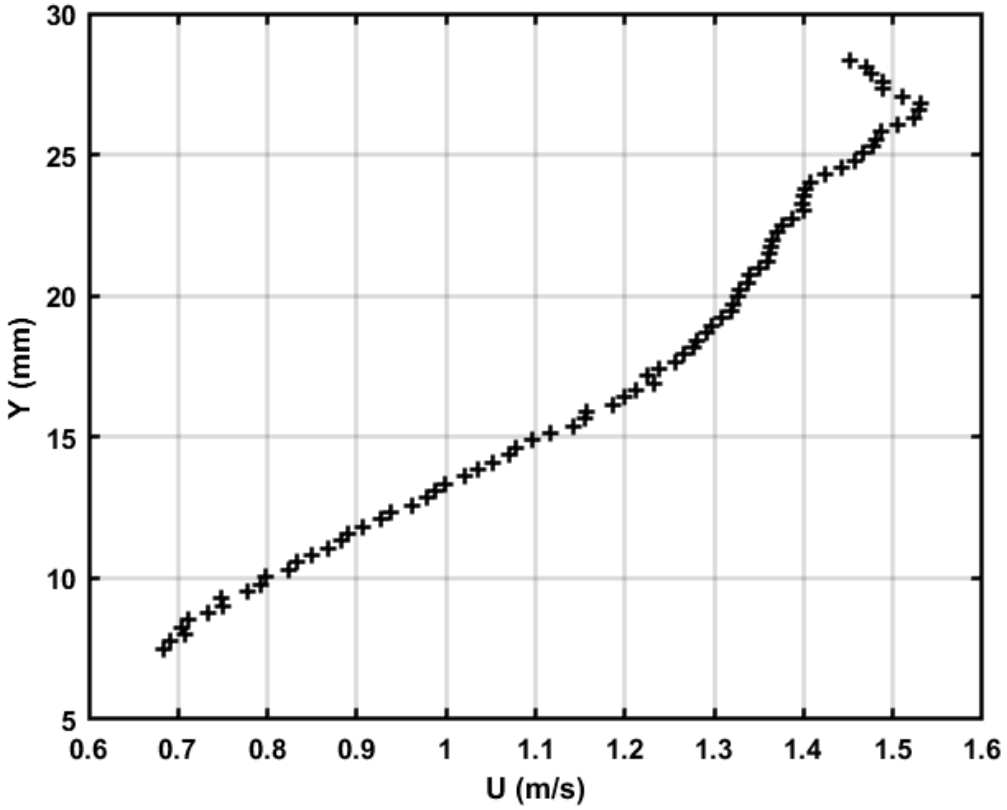

Figure D.12 Test 14 time-average velocity profile (4 mm erosion depth)

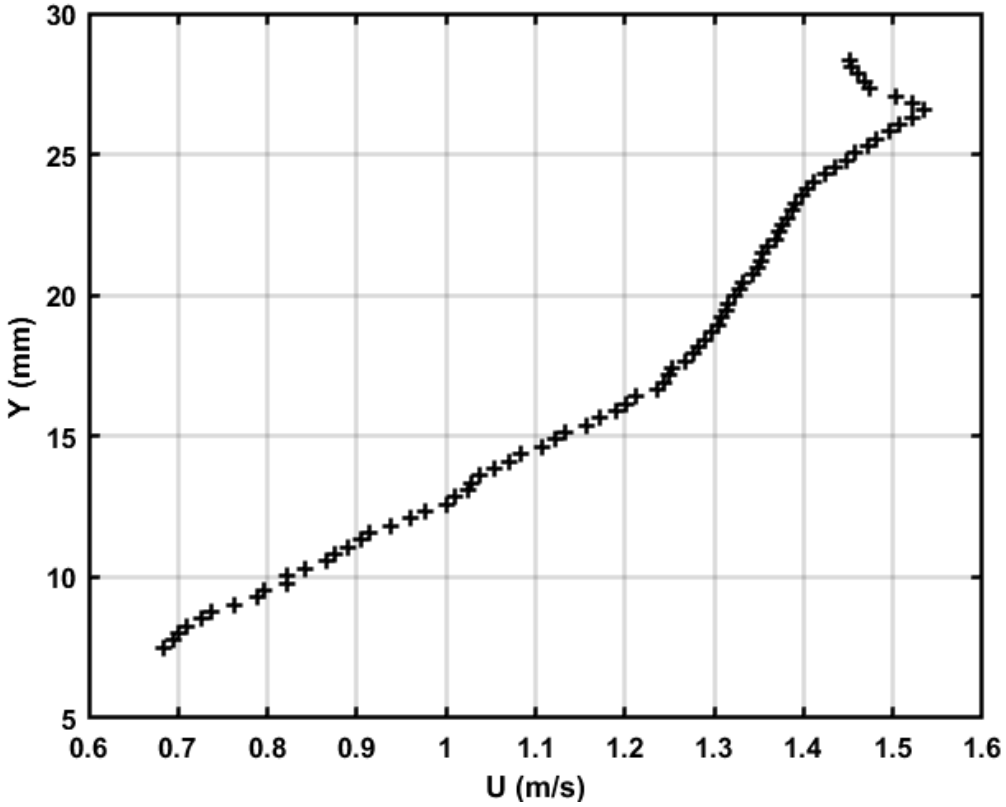

Figure D.13 Test 15 time-average velocity profile (5 mm erosion depth)